EFFECTS OF PRE-MONSOON BIOMASS BURNING AEROSOLS ON RAINFALL CHARACTERISTICS OVER WEST AFRICA

BY

NJIE TEEDA

B.Sc., M.Sc. (Mathematics)

(MET/19/3754)

A Thesis of the Doctoral Research Programme of the West Africa Climate Systems, under the West Africa Science Service Centre on Climate Change and Adapted Land Use, in the Department of Meteorology and Climate Science submitted to the School of Postgraduate Studies in partial fulfilment of the requirements for the award of the degree of Doctor of Philosophy in Meteorology and Climate Science of the Federal University of Technology, Akure, Nigeria.

May, 2023.

DECLARATION

I hereby declare that this Thesis was written by me and is a correct record of my own research work. It has not been presented in any previous application for any degree of this or any University.

All citations and sources of information are clearly acknowledged by means of references.

Candidate's Name: NJIE Teeda

Signature: Date

CERTIFICATION

We certify that this Dissertation entitled "Weather for Survival" is the outcome of the research carried out by John Stone under the WASCAL DRP-WACS in the Department of Meteorology and Climate Science of the Federal University of Technology, Akure.

Prof. O. O. Jegede **……..**

(Major Surpervisor) Signature Date

Department of Physics & Engineering Physics

Obafemi Awolowo University

Ile-Ife, 220005 Osun State, Nigeria.

Prof. A. Oluleye **……..**

(Co-Surpervisor) Signature Date

Department of Meteorology and Climate Science,
Federal University of Technology,
Akure, Nigeria.

Prof. Zachariah Debo Adeyewa **……..**

(Director) Signature Date

Doctoral Research Program – West African Climate Systems
West African Science Service Center on Climate Change and
Adapted Land Use (DRP-WACS, WASCAL),
Federal University of Technology,
Akure, Nigeria.

ABSTRACT

This study investigate the effects of pre-monsoon biomass burning aerosols (BBA) on rainfall characteristics over West Africa. The specific objectives aimed to be achieved are; estimating the distribution of pre-monsoon biomass burning aerosols (BBA) over the study area; analyzing rainfall characteristics over the study area; evaluating the capability of the regional climate model (WRF-Chem) on capturing BBA effect on monsoon rainfall and determining the influence of BBA on rainfall characteristics and cloud formation. AERONET Aerosol Optical Depth (AOD) and Angstrom Exponent (AE) data were used to estimate the temporal distribution of AOD and AE and classification of aerosol types over the five selected AERONET sites namely; Agoufou, Banizoumbou, Dakar, IER_Cinzana and Ilorin. Rainfall data from ERA5 for the period of 1998-2021 was used to evaluate rainfall characteristics such as distribution, variability, normal, wet and dry (drought) condition and rainfall trend over the five selected sites. Simulations were also run using WRF-Chem model to evaluate the capability of the model in capturing BBA and to investigate the effect of BBA on rainfall and cloud formation. The study found out that AOD peaks in March-June in all the sites except Ilorin were AOD peaks in January. The maximum values of AE were in December-January for all the sites except Ilorin were maximum AE value was in August. This shows the presences of fine mode aerosols. It has been found that desert dust aerosol was the dominant aerosol in all the sites throughout the study period. The normal and wet climatic condition were dominant for both annual and seasonal rainfall in all the sites during the study period. High rainfall variability throughout the study period and all the seasons with no trend for annual and negative trend for MAM and JJA season. This means that it is easier to use mean to predict rainfall performance for the annual rainfall but difficult the seasonal rainfall performance in the study area. Lastly, the study found out that the WRF-Chem model overestimated the rainfall characteristics and the effect of BBA radiation

can increase or decrease rainfall amount depending on the period/season over West Africa. The WRF-Chem model also underestimate the values of OLR. But the effect BBA radiative has increased the rate of convective cloud formation over West Africa

DEDICATION

In loving memory of Mr. Momodou N. Samateh, you are not here to witness the completion of the foundation you have laid. I know you will be proud and happy wherever you are. May Allah continue to have mercy on your soul. Ameen

To my Father, my role model and my lovely Husband, my source of strength and encouragement. Thank you for your endless sacrifices and support for me and for always believing in me.

ACKNOWLEDGEMENTS

I want appreciate God for His grace to successfully complete my Ph. D Degree Programme.

Many thanks to the Federal Ministry of Education and Research (BMBF), Germany for sponsoring the WASCAL programme at the Federal University of Technology, Akure (FUTA DRP-WACS).

My sincere gratitude goes to my team of supervisors, the major Supervisor, Prof. O.O. Jegede and Co-Supervisor Prof. Ayodeji Oluleye. Thank you for always motivating me, for the invaluable advice, encouragement, constructive criticism, insightful suggestions and comments throughout the conduct of this research.

To my host university, the Federal University of Technology Akure, Nigeria through the Doctoral Research Program West African Climate Systems (DRP-WACS) under the Directorship of Professor Z.D. Adeyewa for the coordination and efforts toward the successful completion of the program.

I would like to show my gratitude to the University of The Gambia for granting me study leave with salary throughout the program and the director of WASCAL Gambia for his words of encouragements.

My profound gratitude goes to my wonderful, caring and loving husband Mr. Kebba Sillah his restless support, words of encoragement and always been with me throughout the program. My beautiful kids Suaibu and Fatimah for your love, understanding and prayers. To my wonderful and encouraging parents Mr. Lamin J Njie and Mrs. Fatou Njie Ceesay for the prayers, my siblings, and my in-laws

My sincere appreciation to Mr. Akinyoola Julius for his technical support and giving me space in a cluster to used high-performance computing to compute the WRF-Chem model and Dr. Gbode, Imoleayo Ezekiel for his moral support.

My gratitude also goes to my all my fellow WASCAL comrades, especially Nimo Pouwereou, Ochie M.C, Peace Awoleye, Peter Odum, Assa Tapily, Modou Pouye, Idealbert, Meminvegni, Laouali Ibrahim and Boubcar Doumbia.

TABLE OF CONTENTS

LIST OF FIGURES

LIST OF TABLES

LIST OF EQUATIONS

CHAPTER ONE

1.0 INTRODUCTION

1.1 BACKGROUND

Biomass burning (BB) is the second major sources of aerosols in Africa after Saharan dust. It happens in both natural fire and anthropogenic fire, such as forest, burning of wood and agricultural waste to clear land, manage forests, and generate residential heating (Jacobson, 2012; Reid *et al.*, 2013; Chen *et al.*, 2016). Therefore, emissions from BB have characteristics of both natural and anthropogenic sources. BB mainly emits gases, such as carbon dioxide (CO2), carbon monoxide (CO), and oxynitrides (NO*x*), and aerosol particles, such as black carbon (BC) and organic carbon (OC) (Jacobson and Mark, 2012; Wang *et al.*, 2015; Chen *et al.*, 2016). Biomass burning is a major source of BC and OC aerosols and normally takes place during the dry season.

BC in BB aerosols absorb solar shortwave radiation, this heats the local atmosphere and inhibiting cloud formation (Ackerman *et al.*, 2000; Lau *et al.*, 2006; Meehl *et al.*, 2006; Wu *et al.*, 2011; Ding *et al.*, 2016). It modifies the cloud properties by serving as cloud condensation nuclei (CCN) or ice nuclei (IN). This process is called the "semi-direct effect" (Hansen *et al.*, 1997). Through atmospheric and surface energy budget change, the hydrological cycle can be affected by BC (Hodnebrog *et al.*, 2015). Unlike greenhouse gases, BC is removed from the atmosphere after a few days (Boucher *et al.*, 2013; Samset *et al.*, 2014; Hodnebrog *et al.*, 2015).

Scattering aerosols, like OC in BB, scatter solar radiation and prevent it from reaching the ground through the "aerosol direct effect" (Charlson *et al.*, 1992; Wang *et al.*, 2007; Zhang *et*

al., 2009; Wu *et al.*, 2011; Pani *et al.*, 2018). Under this effect, both ground and near-surface atmospheric temperatures decrease.

Changes in precipitation patterns had been revealed from the observational data as far back in the 19th century, with increased precipitation in some regions in the world while other regions are experiencing less precipitation (Hartmann *et al.*, 2013; Greve *et al.*, 2014). Generally, on a global scale, increases in anthropogenic emissions have led to more precipitation due to surface temperature warming (Knutti *et al.*, 2013).

Martins *et al.*, (2009) studied the role of aerosols in modifying clouds and precipitation using the numerical atmospheric model in the Amazon. They found increases or decreases in total precipitation cause by high CCN concentrations on typical of polluted days, depending on the level of pollution used as a reference. The results also show that on the grids evaluated, higher CCN concentrations reduced low-to-moderate rainfall rates and increased high rainfall rates. The aerosol absorption of radiation in the lower layers of the atmosphere was also found to delayed convective evolution but produced higher maximum rainfall rates due to increased instability.

Several studies have investigated the effects of BBA on Weather and Climate. Walter *et al.*, (2016) did a modeling study to investigate the impact of Canadian forest fires on shortwave (SW) radiation and temperature using the regional climate model, COSMO-ART, and found that downwelling surface SW radiation reduces below the biomass plume under cloudless conditions due to absorption in dense smoke layers, which leads to a decrease of temperature. Surface cooling and warming in elevated layers led to increased atmospheric stability, which induced a decrease in precipitation. Thornhill *et al.*, (2018) did a simulation to assess the impact

of BB on the South American regional climate. The simulation found a decrease in mean precipitation by 14.5% in the peak region of BB.

Huang *et al.,* (2013) investigated the impact of the direct radiative forcing of BC on West African Monsoon (WAM) precipitation during the dry season. The result concluded that there was a reduction in precipitation in the WAM region due to the radiative effect of BC. It was demonstrated that aerosols from the southern African hemisphere significantly reduced convective precipitation, particularly during the boreal cold season, when BB smoke was prevalent. The result also highlighted that BB can affect local weather and climate in West Africa. These results suggest that cloud amount reductions, top height, and surface precipitation are due to a high BC aerosol load in the atmosphere.

Modeling the biomass burning (BB) in Amazonia using large eddy simulation, (Feingold *et al.*, 2005) shows that where BBA was at the cloud formation layer, it acts to reduce cloud fraction but at lower levels, it tends to either increase or decrease cloudiness. However, they also found that surface sensible and latent heat fluxes are sufficient in themselves to reduce cloudiness. Effects of BBA on convection and could formation characteristics can result in changes in precipitation (Goncalves *et al.*, 2015; Thornhill *et al.*, 2018).

1.3 AIM AND OBJECTIVES

This study aims to determine the impact of pre-monsoon biomass burning aerosols (BBA) on rainfall characteristics over West Africa

The specific objectives of the work are to:

1.) estimate the distribution of pre-monsoon biomass burning aerosols (BBA) over the study area;

2.) analyze rainfall characteristics over the study area;

3.) evaluate the capability of the regional climate model on capturing the BBA effect on monsoon rainfall; and

4.) determine the influence of BBA on rainfall characteristics and cloud formation

1.4 JUSTIFICATION

Most of the agricultural practices take off at the onset of the rainy season. Over West Africa, the onset varies between the months of March, April, and May (MAM) depending on the latitudinal position of the location. This onset is characterized by heavy rainfall which is companied by thunder and lightning (it can be referred to as convective systems e.g. thunderstorms and squall lines). The precipitation during this period can be referred to as pre-monsoon rainfall. This is the period when farmers start land preparation for the planting season by burning farm residuals. Several scenarios can take place within this period, which ranges from the false onset, dry spell, increase and decrease in rainfall amount, etc., which can lead to loss of seedlings and other financial involvement on the part of the farmer. There will be a

longer planting season/period in the event of early onset and late cessation, but late onset and early cessation cause a shorter planting season/period.

In other to minimize the impact of some of the above-stated scenarios on the part of the farmer, which can lead to low crop yield and/or total loss of crops, there is a need to study and understand the effect of pre-monsoon biomass burning on rainfall characteristics.

1.5 THE CONTRIBUTION OF THE RESEARCH TO KNOWLEDGE

The research has shown that the most predominant aerosol found in the study area during the pre-monsoon was dust and not biomass-burning aerosols. This will enlighten the model developers to modify the model input for a better output or prediction.

CHAPTER TWO

2.0 LITERATURE REVIEW

2.1 AEROSOLS IN THE ATMOSPHERE

Atmospheric aerosols are suspensions of liquid, solid, or mixed particles with highly variable concentrations, chemical composition, and size distribution (Putaud *et al.*, 2010). Aerosols play a crucial role in the dynamics of the climate system of Earth as well as environmental change (Tiwari *et al.*, 2015; Al-Taie *et al.*, 2020). Photochemical smog, global warming, stratospheric ozone depletion, and poor air quality are some the environmental problems caused by aerosols (Colbeck *et al.*, 2014; Al-Taie *et al.*, 2020). Also, aerosols may affect hydrologic cycles, ecosystems, visibility, and precipitation significantly and exert a great influence over human health and economic activity (Saikia *et al.*, 2018; Hofmann *et al.*, 2020; Al-Taie *et al.*, 2020). Aerosol particles that are directly emitted into the atmosphere are known as primary aerosols and are quite distinct from those that are produced in the atmosphere from precursor gases regarded as secondary aerosols.

Primary aerosols are generated from a wide range of natural and anthropogenic sources such. These natural ways are the emission of sea spray, release of soil and rock debris (as mineral dust), biomass burning smoke, biogenic aerosols and injection of volcanic ash. The anthropogenic primary aerosols are mainly due to fuel combustion as vehicular emissions from transportation (roads, seaway corridors, and air traffic), traffic dust, deforestation fires, and biomass burning. Other notable emissions are from industrial processes, non-industrial fugitive sources such as roadway dust (from paved and unpaved roads), wind erosion of cropland, and construction.

Due to the rapid increase of population, industrialization, and urbanization in the last few decades, the production of anthropogenic aerosols has increased which is affecting regional air quality, atmospheric visibility, and agricultural crop production, and has a significant potential to affect the global climate. Urban areas of fast-developing countries (like India, China, Brazil, etc.) are the major source regions of these anthropogenic emissions and are heavily polluted throughout the year. Under suitable meteorological conditions, these pollutants can also trigger pollution events that reduce the local air quality, and atmospheric visibility and are hazardous for human health.

Anthropogenic aerosols also have significant potential to perturb the hydrological cycle by affecting monsoonal circulation patterns. Aerosols also affect the biogeochemical processes of the oceanic region through the supply of macro and micronutrients. Thus, they can modulate the food chain and eventually our marine bio-resources and hence, the country's economy. Aerosols are usually dispersed and distributed in the atmosphere by turbulence movement of air masses; but are being removed from the atmosphere by ice, dew, and precipitation as well as dry sedimentation (Demott *et al.*, 2003; Jones and Harrison, 2004; Ayanlade *et al.*, 2019). The chemical, physical and optical properties of aerosols significantly affect radiation capacity and can directly influence the forecast and evaluation of climate change (Zhao *et al.*, 2016; Al-Taie *et al.*, 2020).

Aerosols in the atmosphere have mitigated some of the impacts of global warming in the short term in the past by reflecting some of the sun's heat into space. This has masked some of the effects of rising greenhouse gas concentrations, but just for the short term because most of the aerosols fall back to the ground (earth) after a few days. They are unlike greenhouse gasses eg. Carbon dioxide, which stays in the atmosphere for centuries (Persad *et al.*, 2022).

Major source regions of dust aerosols across the globe includes all the dry lands such as the Middle East, central and eastern Asia, Sahara, and long-range transport enable dust from these source region to reach other parts of the world (Middleton 2017; Ayanlade *et al.,* 2019). The annual cycles are mainly related to Sahara dust and biomass-burning aerosols in the southern hemisphere with major sources in South America and West Africa (Strong *et al.,* 2015). Aerosol sources locally are mainly from domestic wood burning, vehicular emissions, and industrial gas flaring giving rise to urban air pollution (Ravindra *et al.,* 2008). Aerosols diffuse from regions where emissions are high to regions with a relatively clean atmosphere (Zhang *et al.,* 2012; Ayanlade *et al.,* 2019).

2.2 MAJOR SOURCES OF AEROSOLS IN THE ATMOSPHERE

There are many sources of atmospheric aerosols. The Intergovernmental Panel for Climate Change, IPCC reported in its 2001 assessment concerning aerosol sources, soil dust, sea salt, sulfate aerosols, biogenic aerosols, and biomass burning are some of the major sources of aerosol (IPCC, 2007). The picture of some of the major sources of these aerosols is shown in figure 2.1. From the top is the large-scale air pollution from (bottom, counterclockwise) volcanic eruptions, sea spray, desert storms, savannah biomass burning, and road transport. In the center are the electron microscope images of (A) sulfates, (B) soot, (C) fly ash a product of coal combustion (Posfai *et al.,* 1999; Myhre *et al.,* 2013).

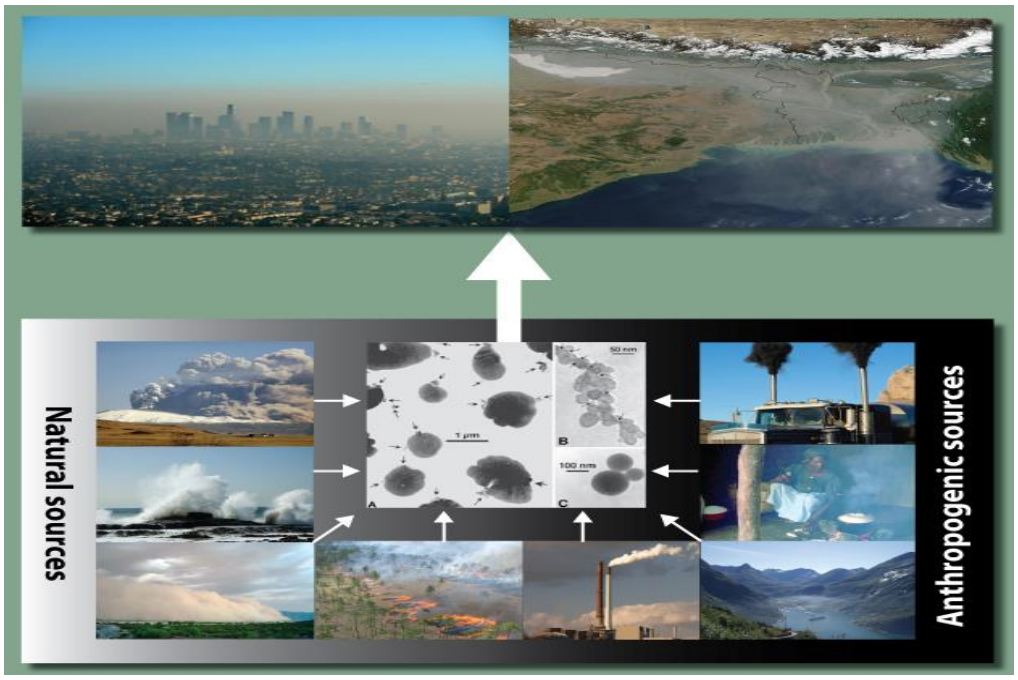

Figure 2.1: Natural and anthropogenic atmospheric aerosol source by Myhre et al. (2013)

2.2.1 Fumigative Soil Dust

Mineral dust mainly originates from the desert and semiarid land surfaces. This is as a result of the wind forces that mobilize the soil particles. The main dust source regions include the Sahara Desert and other desert regions that constitute the dust belt, a chain of arid regions extending not only over North Africa but also over South Africa and Middle East Asia, and China (Gobi Desert), besides the desert regions in South America. Dry lakes and lakebeds and other once-wet areas also act as particularly efficient sources of atmospheric dust (Prospero, 1999).

Dust particles are the major components of the atmospheric aerosols in the subtropical regions of the planet. This is because all the above-mentioned arid and semiarid regions of the Earth (dust source areas) occupy about one-third of the global land areas. Desert dust is also the dominant particle type in air masses thousands of kilometers away from the source. The annual emission flux of mineral dust was estimated over the global scale (Duce, 1995; Tomasi *et al.*, 2017).

During the transport of mineral dust, the composition of the original aerosol can substantially change due to particles reaction and internal mixing with other aerosols, such as mineral particles become internally mixed with sea-salt components through cloud processing (Trochkine *et al.*, 2003). In other cases, dust particles mixed with Saharan minerals with sulfate, particles transported from both urban and agricultural pollution areas (Falkovich *et al.*, 2001) and mixing with organics contained in combustion smoke and anthropogenic particulate matter (Gao, Anderson, and Hua, 2007). Meteorology also plays a key role in the seasonality of dust emissions and transport in Africa. Large-scale atmospheric circulations such as intertropical convergence zone (ITCZ) and the African monsoon, shift the location of

maximum dust activity and transport of dust northward (~5°N to ~20°N) from winter through summer (Jankowiak and Tanre, 1992; Moulin *et al.*, 1997; Prospero *et al.*, 2002; Schepanski *et al.*, 2009; Leon *et al.*, 2009).

In addition to its local and regional impact, Saharan dust is exported over the Atlantic Ocean and contributes to the cooling of tropical North Atlantic and influencing Atlantic climate variability (Evan *et al.*, 2011; Doherty and Evan, 2014). Climate change may reduce future dust emissions, which may lead to positive warming feedback over the North Atlantic (Evan *et al.*, 2016). Saharan dust significantly increases nutrient transport to other regions like the Amazon rainforest, which may also feedback on climate (e.g., Bristow *et al.*, 2010; Yu *et al.*, 2015).

2.2.2 Sea Salt Spray

Sea salt spray are aerosol particles, which originate predominantly from the oceans. Through various physical processes, the bursting of entrained air bubbles at the air-sea interface during whitecap formation generates sea salt spray particles (Lewis et al., 2004). Sea spray contains both organic and inorganic matter, which is termed sea salt aerosols (SSA) (see Gantt *et al.*, 2013). Due to its hygroscopic nature, SSA can form cloud condensation nuclei (CCN) and remove anthropogenic aerosol pollutants from the atmosphere (Rosenfeld *et al.*, 2002). They are mainly dominant in the regions near the marine atmosphere and contributor to both light scattering and cloud nuclei.

Seaspray affect the global climate patterns and tropical storm intensity (Andreas *et al.*, 1992). It is directly and indirectly responsible for a significant degree of the heat and moisture fluxes between the atmosphere and the ocean (Andreas *et al.*, 1995), influences plant growth

(Andreas *et al.,* 2001), species distribution in coastal ecosystems (Malloch *et al.*, 1972) and increases corrosion of building materials in coastal areas (Schindelholz *et al.,* 2014). Sea spray aerosol contributes to atmospheric cooling because they scatter incoming solar radiation.

Although the sea spray aerosol number concentrations are not very high compared to those of anthropogenic but their role is significant considering the oceans cover 70% of the Earth's surface. Particularly, anthropogenic aerosols are produced locally over limited periods.

Sea salt contributes 44% to the global aerosol optical depth. Estimates for top-of-atmosphere global annual radiative forcing are -1.51 and -5.03 Wm^{-2} for low and high emission values, respectively (IPCC, 2001). Seaspray not only affects climate by scattering solar radiation, but it also acts as cloud condensation nuclei and thus contributes to the indirect aerosol effect (IAE). This effect accounts for the perturbation of the hydrological cycle due to the abundance of aerosol particles. The main contribution to the IAE, the most uncertain forcing mechanism in the prediction of climate change, comes from marine stratocumulus clouds. Boers *et al.*, (1998) report an example of IAE related to changes in the distributions of natural cloud condensation nuclei (CCN) over the ocean. And it is also important in atmospheric chemistry.

2.2.3 Sulphate Aerosols

Sulphate is a primary anthropogenic aerosol and also has natural origins in the atmosphere. Sulfur dioxide (SO_2) are the main precursor gases of sulfate aerosols, of which volcanoes and fossil fuels are the major natural and anthropogenic sources, respectively. Dimethyl sulfide (DMS), which is emitted from oceanic phytoplankton and land vegetation are the natural sources. SO_2 is also emitted by biomass burning, which is currently dominated by anthropogenic causes. Sulfate aerosols alter the atmospheric solar radiation budget. They

affect climate through aerosol-radiation interactions by scattering radiation and through aerosol-cloud interactions by changing the microphysical properties of water clouds as they act as cloud condensation nuclei.

Several studies have estimated the effects of anthropogenic sulfate aerosols on radiative forcing (i.e., changes in the radiation budget). The latest Assessment Report of the Intergovernmental Panel on Climate Change (IPCC AR5) evaluated the instantaneous radiative forcing of anthropogenic sulfate aerosols due to aerosol–radiation interactions to be -0.40 W m^{-2}, with uncertainty levels of -0.20 to -0.60 W m^{-2} in the global and annual means. The global and annual mean radiative forcing of total anthropogenic aerosols due to aerosol–cloud interactions was estimated as -0.45 W m^{-2} (IPCC AR5) with great uncertainty from 0 to -1.2 W m^{-2}. Aerosol–cloud interactions include changes in radiation scattering and absorption via changes in cloud particle size, as well as meteorological field perturbations, i.e., changes in the amount of clouds; thus, the values estimated by the IPCC AR5 represent effective radiative forcing.

2.2.4 Biogenic Aerosols

Solid and liquid particles released into the atmosphere from plants and animals are primary biogenic aerosols. They consist of plant debris (cuticular waxes, leaf fragments), insects, humic matter, microbial particles (living and dead viruses, bacterial cells, fungi, spores, pollens, algae, seeds, etc.) and other biogenic debris, such as marine colloids and pieces of animal skins. Biological aerosol particles exhibit a large variety of shapes due to their highly different origins and has size range from less than $0.1\ \mu m$ to at least $250\ \mu m$. For example, the sizes of fungal spores ranges from 1 to $30\ \mu m$, pollens varies from 20 to $60\ \mu m$, while

bacteria, algae, protozoa, fungi, and viruses have sizes generally smaller than a few micrometers

In the remote tropical continental areas covered by pluvial forests, biogenic aerosols can contribute up to 30% of the total atmospheric volume and in remote oceanic regions; its contribution can be at least three times lower concentrations (Elbert *et al.*, 2007). Biogenic aerosols can travel thousands of kilometers from their origin area due to their low density. Such long-range transport episodes are commonly used to identify the origin of a certain airmass at a given location (Mandrioli *et al.*, 1980). Biogenic aerosols are widely spread out and occupy the whole of troposphere, presenting highly variable number concentrations with altitude. For instance, several molds of spores were identified at 11 km altitude in the atmosphere. Cadle (1966) reported that the primary biological particles can efficiently participate in the cloud and ice nucleation processes. The primary biological particles contributes to the problems in atmospheric science, the spread of pathogens and the roles of microorganisms in cloud and ice nucleation (Morris et al., 2011). These aerosols can easily penetrate the respiratory systems of animals and humans and cause serious allergologic pathologies (pollens) affecting various biological functions of humans. Some bacteria are also suspected to be active in cloud droplets, governing the biological activities occurring inside these droplets (Sattler, Puxbaum, and Psenner, 2001).

Biogenic aerosols also have humic-like substances present in them which makes the aerosol particles light absorbing, especially in the ultraviolet (UV)-B wavelength range (Havers *et al.*, 1998). These particles not only absorb and scatter light but can also fluoresce when zapped with a beam of UV light. Due to their relatively low background number concentrations, however, biological particles are consider to produce low direct radiative effects on the

Earth's climatic system and can also act as cloud droplets and ice nuclei (Schnell and Vali, 1976). Thus, biogenic particles are expected to play a role in inducing indirect climatic effects.

2.2.5 Biomass Burning (BB)

Biomass burning is the burning of organic matters such as living and dead vegetation. This consists of burning of forests and savanna grasslands for land clearing and agricultureal use, burning of agricultural waste and biomass for fuel (wood, charcoal, pellets and sawdust). Biomass burning can be natural or anthropogenic (man-made). Anthropogenic fires includes burning of vegetation for land clearing and land-use and burning of fuel. The natural fires includes lightning-induced fires. Anthropogenic fires contributes 90% of the fires on the planet, with little contribution from natural fires (Yadav *et al.*, 2018).

Biomass burning emits both aerosols and gases. It emits elemental carbon (EC) and organic carbon (OC) and other particulate substances as aerosols and CO_2, CO, NO_x, CH_4, and non-methane hydrocarbons (NMHCs) as gases. Elemental Carbon (EC) refers to the most refractory part of the carbonaceous aerosol particles often called black carbon (BC). BC is a combustion product capable of strongly absorbing the incoming solar radiation over the completely visible wavelength range. The gaseous emissions from biomass burning affect the atmospheric chemistry and climate. Biomass burning is one of the major sources of atmospheric aerosols, mainly consisting of small smoke particles. These smoke particles can easily penetrate the respiratory system of humans causing various health problems. They have major effects on air quality, biogeochemical distribution of nutrients, and climate as they are quickly uplifted to high altitudes and transported over long distances. The particles from BB affect the climate by decreasing the surface reflectance and single scattering albedo, which

both causes local warming effects in the atmosphere. These aerosols may also cause several spectacular optical atmospheric effects, such as the blue moon and the Sun.

2.3 AEROSOL OPTICAL DEPTH (AOD) AND ANGSTROM EXPONENT (AE)

Aerosol optical depth (AOD) and Angstrom Exponent (AE) are the main parameters often used for studying optical properties due to aerosol particles in the atmosphere. AOD which is sometimes referred to as Aerosol Optical Thickness (AOT), is the aerosol extinction coefficient integrated over the whole depth of the atmosphere and it is related to aerosol concentration (Al-Taie *et al.*, 2020, Liu 2005). AOD can be described as the section of light removed from a beam due to scattering and absorption in its path through an environment (Kannel 2016; Al-Taie *et al.*, 2020). It is also a measure of opacity (turbidity) of a medium (environment). It is a parameter that can be associated with the aerosol concentration and it is a dimensionless quantity (Liu, 2005; Al-Taie *et al.*, 2020). Its value depends on the size, shape, number, concentration, and refraction index of the particles. AOD was used to detect the presence of atmospheric aerosols. A sudden and constant increase in the observed AOD can indicate the arrival of an aerosol layer, e.g., volcanic ash (Papagiannopoulos *et al.*, 2016). It is an important parameter for the observation of visibility degradation due to atmospheric pollution, solar radiation extinction, and other climate effects. The wavelength dependence of AOD varies between different aerosol types because of their different physical and chemical characteristic. AODs are usually found to be higher during hazy days, moderate during partially clear days, and low on clear-sky days.

Angstrom Exponent (AE) depends mainly on the size distribution and the refractive index of aerosols (Kannemadugu *et al.*, 2015; Al-Taie *et al.*, 2020). The parameter is significant in the

study of aerosol forcing on the climate system (Devara *et al.*, 1995; Eshet and Raju, 2021). It is treated as an indirect measurement of the aerosol size in a given column of air since it is inversely proportional to the average size of aerosols. It is utilized to obtain main information on the aerosol size distribution in the solar spectrum (Al-Dabbagh *et al*,.2015; Al-Taie *et al.*, 2020).

Angstrom Exponent is a commonly used parameter that represented the wavelength dependence of AOD and it is a significant indicator of aerosol size and its variation. By fitting a power law to the aerosol optical depth and wavelength, the spectral dependence of AOD at a particular wavelength is typically approximated using AE (Angstrom 1964; Eck *et al.*, 1999). The Angstrom empirical for approximating aerosol extinction can therefore be expressed as:

$$AOD_{\lambda} = \beta\lambda^{-\mathrm{AE}} \qquad (2.1)$$

Where λ is the wavelength and is expressed in micrometers of the corresponding AOD value. β is the Angstrom turbidity coefficient, which is related to the amount of aerosol present in the atmosphere and is used to characterize the degree of air pollution or turbidity. The wavelength exponent AE describes the spectral behavior of the optical depth, which is a good indicator of their size or the fraction of the fine-mode aerosols in the atmosphere (Praseed *et al.*, 2012). AE is calculated from the values of the aerosol optical depth at 440 and 675nm of wavelength with the following expression:

$$AE_{\_440-670} = \frac{ln(\frac{AOD_{440}}{AOD_{675}})}{ln(\frac{675}{440})} \qquad (2.2)$$

In general, AE is found to reduce with the enhancement in particle size. For AE values greater than 1 are mainly determined by fine mode, submicron aerosols while AE less than 1 are largely determined by coarse, super micron particles (Kaufman *et al.*, 1994). The magnitude of AE depends strongly on the wavelength region selected for its determination. Angstrom Exponent is commonly employed in operational sun photometry. The joint use of these two parameters is widely employed for classifying various aerosol types and sizes.

2.4 IMPACTS OF AEROSOLS ON THE ATMOSPHERE

2.4.1 Cloud Condensation Nuclei and Ice Nuclei

Atmospheric aerosols are associated with the formation of cloud droplets and cloud ice crystals. These aerosols are produce by natural and anthropogenic processes. Without such aerosols, the conversion of water vapor into liquid water or ice crystals requires conditions with higher relative humidity concerning a flat surface of H_2O. This process is called as homogenous nucleation, which occurs only in a controlled laboratory environment. Aerosols serve as the starters for the condensation or deposition of water vapor in the atmosphere. With a surface of discrete sizes, aerosols reduce the amount of super-saturation required for water vapor to change its phase to form what is called cloud condensation nuclei (CCN).

Different types of atmospheric particulates such as dust or clay, soot or black carbon, sea salt, etc., and secondary organic matter can act as CCN. Their ability to form cloud droplets varies according to their size and composition since the hygroscopic properties of these different components are very different. Sulfate and sea salt, for instance, readily absorb water whereas soot, organic carbon, and mineral particles do not. Many of the chemical species may be mixed within the particles (in particular the sulfate and organic carbon), that made it even more

complicated. However, as some particles such as soot and minerals cannot make very good CCN, they do act as ice nuclei in colder parts of the atmosphere. Ice nuclei can be defined as aerosols that are good for changing water vapor to ice crystals. Unlike cloud condensation nuclei, the most effective ice nuclei are having a low liking for water with molecular spacing and a crystallographic structure close to that of ice. The examples of cloud condensation nuclei include sodium chloride (NaCl) and ammonium sulfate ($[NH4]_2\ SO_2$), whereas the clay mineral kaolinite is an example of ice nuclei. In addition, naturally occurring bacteria found in decayed leaf litter can serve as ice nuclei at temperatures of less than about −4 °C (24.8 °F). In a process called cloud seeding, silver iodide, with effective ice-nucleating temperatures of less than −4 °C, has been used for years in attempts to convert super-cooled water to ice crystals in regions with a scarcity of natural ice nuclei.

Studies like (Lynn *et al.,* 2007; Rosenfeld and Givati, 2006; Jirak and Cotton, 2006) have shown that by reducing the efficiency of cloud droplets conversion into raindrops, CCN can reduce warm rain from orographic clouds and CCN can reduce warm rain from orographic clouds snowfall precipitation can be reduce (Lowenthal *et al.,* 2011; Rosenfeld *et al.,* 2008). Nevertheless, some recent studies show a possibility of increased precipitation by CCN in orographic mixed-phase clouds (Fan *et al.,* 2014; Xiao *et al.,* 2015). While other studies have shown that CCN may not have a significant effect on the total precipitation, but rather shift precipitation from the windward to leeward slope; (spillover effect) (Saleeby *et al.,* 2011; 2013). Aerosols can enhance ice growth processes such as deposition and riming and thereby significantly increase snow precipitation as they act as IN (Fan *et al.,* 2014). Both observational and modeling studies have shown that long-range transported dust particles can

enhance orographic precipitation in California by serving as IN (Ault *et al.,* 2011; Creamean *et al.,* 2013; Fan *et al.,* 2014).

Besides precipitation, aerosols may also have significant impacts on the cloud phase and super-cooled water content in the mixed-phase clouds, which directly change cloud radiative forcing and Earth's energy balance. Modeling studies have shown that CCN tends to increase super-cooled water through the processes such as suppressed warm rain and/or reduced riming efficiency (Khain *et al.,* 2009; Ilotoviz *et al.,* 2016; Saleeby *et al.,* 2013). CCN and IN can modify cloud microphysical processes and potentially alter the location, intensity, and type of precipitation (Tao *et al.,* 2012).

2.4.2 Biomass Burning Aerosols (BBA)

Biomass Burning Aerosols (BBA) comprises mainly of submicron particles giving form to an accumulation particle mode (peaked at 0.1 μm). It contains relatively high concentrations of BC and OC. BC in BBA have major light absorption effects while OC have the scattering effects. BBA affects both the local environment and the atmosphere. Aerosols from biomass burning provoked serious diseases in humans, animals, and plants. BBA affect the Earth's albedo and lower the overall single scattering albedo of airborne aerosols, which may consequently induce strong warming effects in the atmosphere, through dry deposition. They caused a decrease in local and regional visibility due to their ability to absorb and scatter light. Acting as effective CCNs, large amount of BBA in the atmosphere may increase the CCN number concentration, which leads to more, but smaller, cloud droplets for fixed liquid water content. This increases the albedo of the cloud, resulting in enhanced reflection and a cooling effect, termed the cloud albedo effect (Twomey, 1977; Myhre *et al.,* 2013).

This is first done by heating their surrounding air and at the same time reducing the amount of solar radiation reaching the ground. This stabilizes the atmosphere and diminishes the convection and thus the potential for cloud formation. Secondly, it is done by increasing the atmospheric temperature, which reduces the relative humidity, inhibits cloud formation and enhances the evaporation of existing clouds. These processes together is referred to as the semi-direct aerosol effect (Hansen *et al.* 1997; Myhre *et al.*, 2013). The net effect is uncertain and highly depends on the vertical profile of BC (Koch and Del Genio 2010).

The BBA direct and indirect radiative effects both combined are responsible for the net radiative forcing that can be compared to the radiative forcing induced by sulfate aerosols.

Ackerman *et al.* (2002) reported that aerosols have impact directly on cloud properties in different ways in the Amazonia area as the study used airborne measurements over human-influenced areas. BBA directly affected the energy balance by diffusing and reflecting solar radiation into space. This is called the direct effect and is caused by natural processes and human activities such as industrial activities, fossil fuel, and biomass burning (Danjuma *et al.*, 2020). Aerosols can modify the microphysics, radiative properties, and cloud lifetime as they serve as cloud condensation nuclei (CCN) (indirect effect). The indirect effects of aerosols involve an increase in aerosol concentrations, which increases droplet concentration and decreases droplet size for fixed liquid water content (Twomey, 1974; Martins *et al.*, 2007). Reduction in cloud droplet size, which affects precipitation efficiency, tending to increase the liquid water content and cloud lifetime is also considered as indirect effect (Albrecht, 1989; Martins *et al.*, 2007; Liu *et al.*, 2020) and both types of indirect effects cool the Earth by reflecting solar radiation into space.

Several studies have reported that the concentration level of biomass burning aerosols (BBA) released into the environment affects rainfall amount (e.g. Peters *et al.,* 2009; Lee *et al.,* 2014). In a study by Martins *et al.* (2009), the amount of rainfall is sensitive to the changes in the concentrations of CCN and cloud size distribution. High CCN concentrations slow the conversion of cloud drops into raindrops by nucleating larger number concentrations of smaller drops, which are slower to coalesce into raindrops or rime onto ice hydrometeors resulting in the suppression of warm-rain formation (Albrecht, 1989; Rosenfeld *et al.,* 2008). In convective rainstorms, the suppression of warm-rain processes and smaller cloud droplet sizes allow more cloud water to be transported higher in the atmosphere, which can result in additional latent heat release due to the freezing of a larger amount of cloud liquid water. As a result, convection could be invigorated by more vigorous cold-rain processes (Rosenfeld *et al.,* 2008) in a polluted environment.

Rotstayn *et al.,* (2007), Wang (2004, 2007) and Huang *et al.* (2009) suggested that aerosols have a remote impact on precipitation by altering the atmospheric large-scale circulation. Model simulations demonstrated that the radiative forcing of anthropogenic aerosols from pre-industrial to present-day conditions has a significant influence on upper tropospheric clouds and water vapor (Liu *et al.,* 2009; Huang *et al,*.2009), and exerts different perturbations in the radiative energy budget of the global climate system (Schulz *et al.*, 2006; Huang *et al.*, 2009). Some researchers have explicitly explained the possible radiative, microphysical, and dynamical mechanisms in the aerosol-monsoon interaction (e.g., Lau *et al.* (2008); Huang *et al.,* 2009). However, in the fourth climate assessment report of the Intergovernmental Panel on Climate Change (IPCC), the modulation of the global change in precipitation due to aerosols is not yet known (Huang *et al.,* 2009; Denman *et al.*, 2007).

2.5 RAINFALL DISTRIBUTION OVER WEST AFRICA

Rainfall is a weather parameter, which shows climatic variability over the African continent and particularly in West Africa. The economic and social development of the African tropical region are strongly dependent on agricultural and water resources and the irregularity of precipitations sometimes leads to disastrous consequences if a given abnormal situation persists.

West Africa is a region in the Tropics that is very sensitive to climatic variability. Strong droughts have raised concerns about the knowledge of the system and predictability (Nicholson 1980; Gounou *et al.*, 2012). This region exhibits three main zonal climatic zones: Guinean, Sudanian, and Sahelian regions (White, 1983). The Guinean region receives the highest amount of rainfall with an average annual rainfall between 1,200 and 5000 mm followed by the Sudanian region with an average annual rainfall between 600 and 1,200 mm. The average annual rainfall in the Sahelian region has great variability in amount and timing in a given year as its amount ranges from 150 to 600mm.

Precipitation variability and amounts have impacts on society, agriculture, and the environment in West Africa. Increase in precipitation variability can reduce agricultural yields (Rowhani *et al.*, 2011). Also, it is strongly connected to extreme wet and dry events, floods, and droughts. It can pose a threat to the environment and society, which can have devastating consequences on ecosystems, food supplies, and economies at the local, regional, and global scale (Easterling *et al.* 2000; Layi-Adigun *et al.*, 2020). The Intergovernmental Panel on Climate Change (IPCC) stresses that there is an increase in the number of extreme weather events in the twenty-first century due to climate change (IPCC, 2014). As temperatures rise, the amount of water vapor in the atmosphere also increases, and the spatiotemporal

distributions of precipitation change, resulting in significant differences in precipitation across the world (Chou and Lan, 2011; Layi-Adigun *et al.,* 2020).

Rainfall over West Africa is mainly related to the West African monsoon (WAM) system (Maranan *et al.,* 2013*;* Gounou *et al.,* 2012). The West African Monsoon (WAM) is a large-scale circulation feature that is characterized by the seasonal the change in wind direction in the lower levels of the atmosphere (Sylla *et al.,* 2013) and is a result of strong scale interaction between different elements of the atmospheric circulation. Within the atmospheric circulation pattern, include several rainfall-producing systems as shown in figure 2.2, such as monsoon flow, African Easterly Jet (AEJ), African Easterly Waves (AEW) Tropical Easterly Jet (TEJ), and Mesoscale Convective Systems (MCS). WAM is seen as complex (Sylla *et al.,* 2013). For example, the African Easterly Jet (AEJ), located in the mid-troposphere is one of the most prominent features of the WAM, with a core around $600-700\ hPa$ and maximum zonal wind reaching $10\ m\ s^{-1}$. The combined baroclinic–barotropic instability of the AEJ gives rise to the African Easterly Waves (AEWs), a phenomenon that has been identified as a key driver of rainfall patterns and convection

(Diedhiou *et al.,* 1998; Akinsanola and Zhou, 2020). Furthermore, most of the convective rainfall over the region follows the displacement of the Intertropical Discontinuity (ITD), with a mean upward motion reaching the upper troposphere around $150\ hPa$ (Nicholson 2009). At this level (i.e., 150 hPa), there is a Tropical Easterly Jet (TEJ) that is associated with the South Asian monsoon outflow and propagates across West Africa during boreal summer. Additionally, the low-level southwesterly monsoon flow at around $850\ hPa$ is the key driver of moisture from the Atlantic Ocean to the continent. Previous studies have shown that the strength and position of all the above-mentioned circulation features influence not only the

amount of rainfall but also its variability (Janicot 1997; Nicholson 2009*;* Akinsanola and Ogunjobi, 2017).

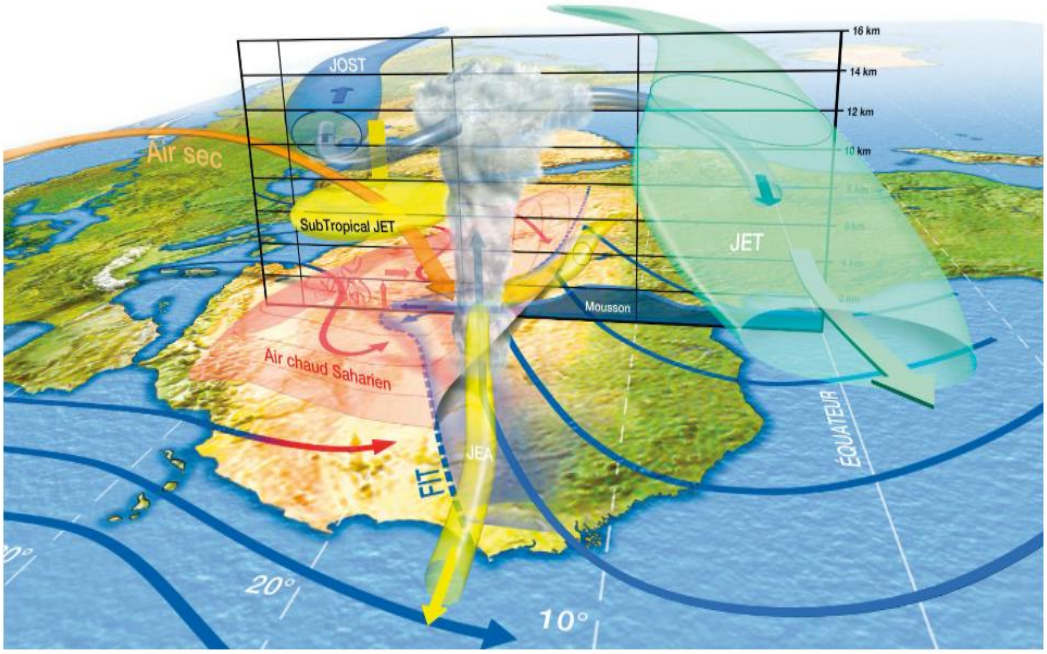

Figure 2.2: Schematic view of the West African Monsoon System adopted from (Laforeet al., (2010); Sylla et al., 2013). FIT stands for ITD (InterTropical Discontinuity) "Air chaud Saharien" stands for 'Warm Saharian Air', JEA stands for AEJ (African Easterly Jet), JET stands for TEJ (tropical Easterly Jet), "Air sec" stands for "Dry Air".

The summer months of June–September are usually the wettest in West Africa, accounting for about 80% of the total annual rainfall (Omotosho and Abiodun, 2007). This period of heavy rainfall was generally referred to as the West African Summer Monsoon (WASM) season, which is an important component of the WAM. Over the years, the West African region has experienced large variability in seasonal rainfall (Nicholson 2000), with pronounced variability across a range of temporal scales. These ranges from inter-seasonal and seasonal variations are critical for water resource management, hydroelectric power generation, and rain-fed agriculture (Lebel *et al.,* 20003). The inter-annual and decadal variability that have strong implications for long-term water availability. Notable is the continuous drought over the Sahel in the 1980s, which is the strongest inter-decadal climate signal among recent observational records in global monsoon regions (Ward, 1998; Trenberth *et al.,* 2007). An increase in annual rainfall has been reported in recent decades (Nicholson 2000), although compared to the long-term mean, a negative anomaly persists. The large scale of impacts that the drought events have on the socioeconomic of the region has led to increased interest in understanding the mechanisms that influence rainfall variability in West Africa (Nicholson 2000; Omotosho and Abiodun 2007). A study by Charney (1975) associated the prolonged drought with changes in surface albedo and land cover along the southern boundary of the Sahara Desert. Folland et al., (1986); Janicot et al., (2001); Sahu et al., (2014) have attributed the event to numerous local and remote forcing including variations in abnormal sea surface temperatures (SSTs) and regional land–atmosphere feedbacks. Wang and Eltahir, (2000); Clark et al., (2001) attribute it to the effect of anthropogenic activities on surface vegetation and continental land surface conditions (Nicholson and Grist 2001; Jenkins et al., 2005) and large-scale patterns of atmospheric circulation. Nevertheless, variation in atmospheric circulation features has been

identified as the most crucial driver of this rainfall variability (Akinsanola and Zhou 2019; Sanogo et al., 2015), as their characteristics differ significantly in typical wet and dry years over the region (Grist and Nicholson, 2001). However, only a few studies have linked the variation of these atmospheric features to the variability of summer monsoon rainfall and the potential of using it as an objective monsoon index.

2.6 WEATHER AND CLIMATE CHANGE OVER WEST AFRICA DUE TO AEROSOL LOADING

The atmospheric aerosols' optical and radiative properties can alter atmospheric and ocean circulation due to their non-uniform distribution (Ming and Ramaswamy, 2011; N'Datchoh et al., 2017). West Africa is one of the most important regions of the world where different types of aerosols exist in large numbers in the atmosphere. These aerosols are mineral dust particles released from arid and semi-arid regions (Sahara and Sahel), biomass burning aerosols (mostly released during dry season), sea salt, and anthropogenic aerosols released from fossil fuel are frequently loaded in the regional atmosphere. Aerosols loaded into the West African atmosphere may likely interact with the regional climate system, especially during the West African Monsoon (WAM) period in the boreal summer. The biomass-burning aerosols are almost-absent during this period due to fire seasonality and high soil moisture as a result of rainfall (N'Datchoh et al., 2015), and dust outbreaks are frequent with Bodélé region being one of the major sources (Prospero et al., 2002; Laurent et al., 2008). Studies have been made to estimate the impacts of dust-aerosol on climate using both direct and indirect approaches. Field *et al.*, (2014) and N'Datchoh *et al.*, (2017) investigated the relationship between the Saharan Air Layer located above the Atlantic Ocean (OSAL) and West African Monsoon features using

the RegCM4 regional model at 30 km grid resolution. The result shows that dust load into the atmosphere greatly influences both the wind and temperature structure at different levels that result in the observed changes in the main features of the WAM system (Monsoon flow, African Easterly Jet (AEJ), and Tropical Easterly Jet (TEJ)) during summer. These changes shift the AEJ core westward with a slight strengthening over the tropical Atlantic and weaken both TEJ and monsoon flux penetration over land.

The aerosols loading in the atmosphere can modulate the radiative balance both at local [Slingo *et al.,* 2009] and regional scales [Grini *et al.,* 2006; Solomon *et al.,* 2008), especially during intense events of dust uplift that regularly occur (Myhre *et al.,* 2003; Heinold *et al.,* 2007; Tulet *et al.,* 2008; Crumeyrolle *et al.,* 2010). Several studies have already investigated the response of the West African climate to the aerosol direct radiative forcing DRF. Although no clear consensus on the net effect of aerosols on West African climate has been achieved. It is clear that the dust DRF has an impact on the hydrological cycle (Malavelle et al 2011) but its link with the development and dynamics of the West African monsoon are suggested in several recent studies such as (Solomon *et al.*, 2008; Konaré *et al.*, 2008; Yoshioka *et al.*, 2007; Perlwitz and Miller, 2010).

CHAPTER THREE

3.0 METHODOLOGY

3.1 DESCRIPTION OF THE STUDY AREA

The West Africa region comprises 16 countries namely; Benin, Burkina Faso, Cape Verde, The Gambia, Ghana, Guinea, Guinea-Bissau, Ivory Coast, Liberia, Mali, Mauritania, Niger, Nigeria, Senegal, Sierra Leone, and Togo. West Africa occupies the approximately one-fifth size of the African continent with an area of 6,140,000 km^2 (Speth *et al.*, 2010). From south to north, West Africa can be subdivided into five broad east-west belts that characterize the climate and the vegetation. The identifiable bioclimatic zones are known as the Guineo-Congolian, Guinean, Saharan, Sudanian, and Sahelian Regions. These zones are strongly influenced by the movement of the West African monsoon, which provides most of the rains for agriculture and other sectors of the economy of countries lying within these zones.

The Guineo-Congolian is located in the southern part of the region and is characterized by a sub-humid climate with an average annual rainfall ranging from about 2200 -500 mm which makes it to be the wettest region in West Africa. The rainfall is distributed across most of the year, with a double peak rainfall season and a “little dry season” between July and August. This region is split geographically into western and eastern blocks, separated by the Dahomey Gap where the savanna reaches the coast. These blocks are often referred to as the Upper Guinean and Lower Guinean Forests, respectively (Church, 1966).

The Guinean Region lies between Guineo-Congolian and Sudanian Regions and is characterized by a sub-humid climate with an average annual rainfall ranging from about 1200 - 2200 mm.

The region has a single peak rainfall season spanning from July to September with a maximum in August. Despite the relatively high rainfall, this region has a distinct dry season of 7 to 8 months, which distinguishes it from the Guineo-Congolian Region.

The Sudanian Region consists of a very large belt immediately north of the Guinean region. It is characterized by a semi-arid climate with an average annual rainfall ranging from about 600 - 1200 mm and is spread over the months of May to October. It is part of savanna ranging from open tree savannas to wooded savannas to open woodlands with tall, perennial grasses, mainly of the genus Andropogon. Fire has been part of the region's ecology for millennia. Both natural and human-induced bushfires sweep through the savanna areas, burning up to 80 percent of their area each year. Gallery forests, with tall tree species more common in the Guinean Region to the south, follow watercourses, penetrating deep into the Sudanian Region. They are generally not affected by bushfires and often act as natural firebreaks.

The Sahelian Region is located between the Sahara Desert to the north and the Sudanian region to the south. It spans 5900km from the Atlantic Ocean in the west to the Red Sea in the east and covers an area of 3053 km^2. The Sahel is characterized by a tropical semi-arid climate (according to Koppen Climate Classification, BSh) which is typically hot, sunny, dry, and somewhat windy all year long. It has a short rainy season and a very long prevailing dry season with low to very low precipitation amounts annually. The region receives about 200 - 700mm of rain annually varying from season to season. The aerosol climate in this region is influenced by the Harmattan, an easterly or northeasterly wind laden with dust transported from the Sahara.

The Saharan Region stretches across the whole northern extent of West Africa, formed by the Sahara Desert, and is characterized by an arid climate with an average annual rainfall ranging from 0 to 150 mm. It consists of a variety of arid landscapes varying from sandy sheets and

dune fields to gravel plains, low plateaus, and rugged mountains. Vegetation cover is sparse to absent, except in depressions, wades, and oases, where water is present at or just below the surface.

This study covers five AERONET sites in West Africa. The choice of these sites was mainly based on the availability of the data on the sites. These sites were Agoufou located in Mali, Banizoumbou located 50 km from Niamey in Niger, Dakar located in Senegal, Ilorin located in Nigeria, and IER_Cinzana located in Mali. The coordinates (latitude and longitude), elevation above sea level, and years of the data used in the study are shown in table 3.1.

The model configuration domain covers the West Africa region with no nested domain is shown in figure 3.2. The coordinates sprang from the lower latitude of 0.00^{o}S to 2^{o}N and spread from 20^{o}W to 20^{o}E covering major land cover, Lakes, and the Ocean revealing the coastal area.

Table 3.1: AERONET site information: Latitude (lat), longitude (Lon), elevation, and years of data used in the study.

Site	Lat (ºN)	Lon (ºE)	Elevation (m)	Years of data used in study
Agoufou	15.34	-1.48	305	2003-2010
Banizoumbou	13.54	2.67	250	2003-2010
Dakar	14.39	-16.96	0	2004-2010
Ilorin	8.32	4.34	350	2004-2009
IER_Cinzana	13.27	-5.93	285	2005-2010

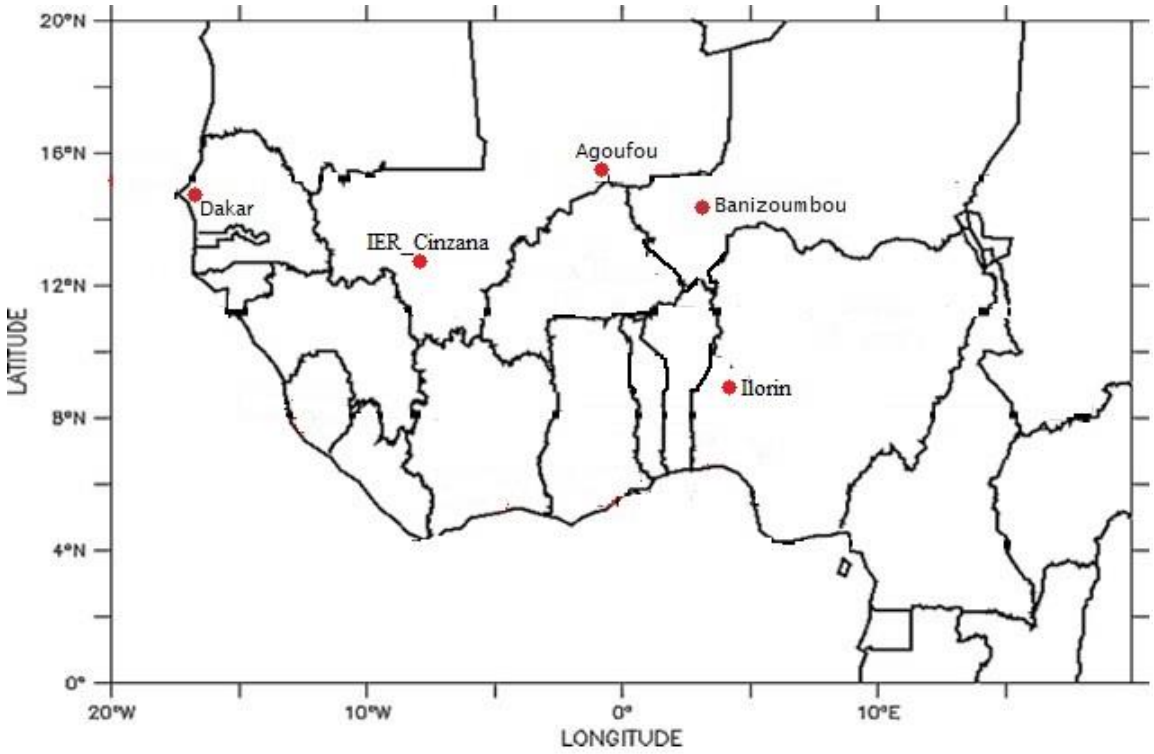

Figure 3.1: Map of West Africa showing the AERONET site used in this study

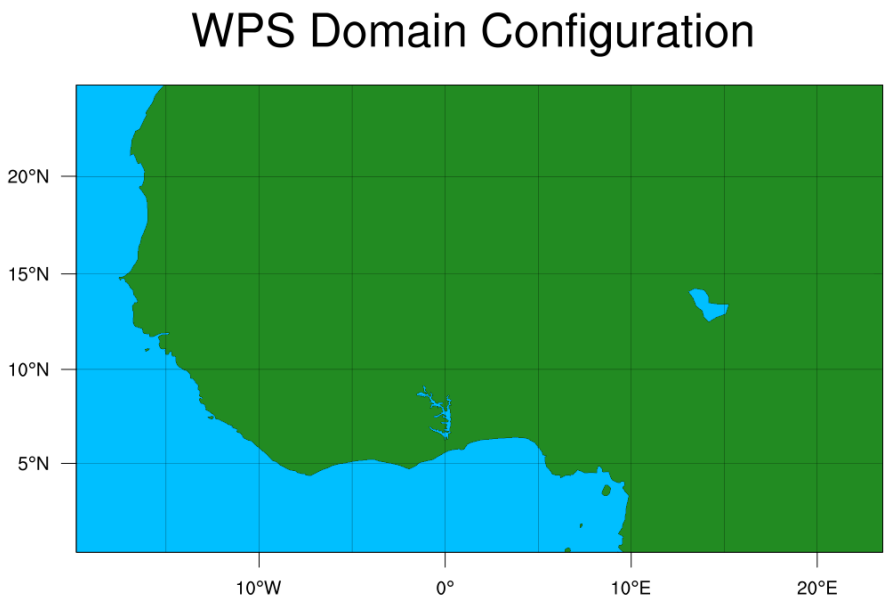

Figure 3.2: The West Africa domain configuration as generated by WRF Processing System (WPS) showing the coastal areas in blue and The land in color green

3.2 DATA

3.2.1 AERONET Data

The Aerosol Robotic Network (AERONET) is a network of ground-based Sun photometers that measure atmospheric aerosol properties. The standard measurement system is a solar-powered CIMEL Electronique 318A spectral radiometer shown in figure 3.4 is used to measure Sun and sky radiances at several fixed wavelengths within the VNIR spectrum (Emery *et al.,* 2017). The automatic tracking Sun and sky scanning radiometers make direct sun measurements with a 1.2^{o} full field of view at least every 15 min at 340nm, 380nm, 440nm, 500nm, 675nm, 870nm, 940nm, and 1020nm (nominal wavelengths). The direct sun measurements take 8 seconds to scan all 8 wavelengths, with a motor-driven filter wheel positioning each filter in front of the detector. A sequence of 3 measurements (termed a triplet) taken 30 seconds apart are made resulting in 3 measurements at each wavelength within one minute (Ogunjobi *et al.,* 2007). Three observations were made during morning and afternoon Langley calibration sequences and at standard 15mins intervals (Holbin *et al.,* 1998; 2001). The filters utilized in these instruments are interference filters with bandpass (full width at half maximum) of the 340 nm channel at 2 nm and the 380 nm filter at 4 nm, while the bandpass of all other channels is 10 nm.

Sky measurements were performed at 440 nm, 670 nm, 870 nm, and 1020 nm. A single spectral measurement sequence was made immediately after the Langley air-mass direct Sun measurement at 20^{o} from the sun. AERONET provides continuous cloud-screened observations of spectral AOD, perceptible water, and inversion aerosol products in diverse aerosol regimes. Inversion products are retrieved from almucantar scans (circle on the celestial sphere parallel to the horizon) of radiance as a function of scattering angle and include

products such as aerosol volume size distribution, aerosol complex refractive index, optical absorption (single scattering albedo), and the aerosol scattering phase function. All these products represent an average of the total aerosol column within the atmosphere.

Figure 3.3: CIMEL Sun photometer (William Emery, Adriano Camps, in Introduction to Satellite Remote Sensing, 2017)

In this study, the monthly average AOD data for 440 nm and 675 nm wavelengths from the five (5) AERONET sites were used to investigate the climatology of AOD for the selected five sites. These data were also used to calculate the values of Angstrom Exponent (AE_440-675 nm) for the stations used in this study. AE_440-675 nm data were then used to investigate the climatology of the Angstrom Exponent for each station. The AOD_440 was plotted against AE_440-675 nm to help in the classification of different types of aerosols present in each station.

3.2.2 ERA5 Daily Precipitation and Outgoing Longwave Radiation Data

The ERA5 daily precipitation data were downloaded from Climate Explorer for West Africa from 1998 to 2021. With the use of the Climate Data Operator (CDO), the data for the stations under study (Agoufou, Banizoumbu, Dakar, IER_Cinzana, and Ilorin station) were extracted from the regional daily data. These daily data were then converted into monthly, annual, and seasonal for each station, which was used for the rainfall distribution, variability, and trend analysis. Two seasons were considered in this study namely March to May (MAM) season and June to August (JJA) sub-season. ERA5 mean 6-hourly top net thermal radiation was downloaded from National Centers for Environmental Prediction (NCEP). Top net thermal radiation commonly known as outgoing longwave radiation (OLR) is equal to negative OLR. With the use of a Climate Data Operator (CDO), the OLR data was converted from the negative OLR to the positive OLR. CDO was also used to convert 6-hourly to daily, monthly, and seasonal mean OLR. The monthly OLR for March, April, May, June, July, and August along with monthly OLR data from WRF-Chem simulation output, was plotted to evaluate the model performance on how well it captured the effect of biomass burning aerosols on

cloudERA5 mean hourly top net thermal radiation was downloaded from Copernicus. Top net thermal radiation is commonly known as outgoing longwave radiation (OLR) and is equal to negative OLR. CDO was used to convert the negative OLR to a positive OLR. CDO was also used to convert 3-hourly to daily and monthly mean OLR. This data was used to evaluate the model performance on how well it captured the effect of biomass-burning aerosols on the cloud.

3.2.3 Biomass Burning Emissions Datasets

The Fire INventory from NCAR (FINN) program (Wiedinmyer *et al.*, 2011) was used to provide fire emissions data for WRF-Chem simulation. FINN uses daily, one-kilometer resolution, global estimates of the trace gas and particle emissions from open burning of biomass, which includes wildfire, agricultural fires, and prescribed burning. However, it does not include biofuel use and trash burning. Emission factors used in the calculations have been updated with recent data, particularly for the non-methane organic compounds (NMOC).

The resulting global annual NMOC emission estimates are as much as a factor of 5 greater than some prior estimates. Chemical speciation profiles, necessary to allocate the total NMOC emission estimates to lumped species for use by chemical transport models, were provided for three widely used chemical mechanisms: FINN also provides global estimates of key organic compounds, including formaldehyde and methanol.

Any uncertainties in the emissions estimates arise from several of the method steps. The use of fire hot spots, assumed burned area, land cover maps, biomass consumption estimates, and emission factors all introduce errors in the model estimates. The uncertainty in the FINN emission estimates is about a factor of two; but the global estimates agree reasonably well

with other global inventories of biomass burning emissions for CO, CO_2, and other species with less variable emission factors. FINN emission estimates have been developed specifically for modeling atmospheric chemistry and air quality in a consistent framework at scales from local to global. The product is unique because of the high temporal and spatial resolution, global coverage, and the number of species estimated. FINN can be used for both hindcast and forecast or near-real-time model applications and the results are being critically evaluated with models and observations whenever possible.

3.3 METHODS

3.3.1 Descriptive analysis

Descriptive analysis was done on the AOD, AE, and rainfall data. Time series plots were done for annual AOD and AE with some statistical analysis (mean, standard deviation, minimum and maximum) to investigate the climatology of the variables in all the AERONET selected sites. Scatter plots of AOD against AE were also plotted for annual and seasonal data for all sites in the study areas. In this study, the relationship between AOD and AE was explored to understand the various aerosol types. This kind of relationship has been widely used based on both satellites as well as ground-based aerosol data over a wider region (Bi *et al.*, 2011; Boiyo *et al.*, 2018; Rupakheti *et al.*, 2018). The classification of aerosol includes three main different aerosol types. These were maritime (sea-salt), biomass burning (BB), and desert dust (DD) as shown in Table 1. The remaining aerosols, which do not belong to the threshold presented in table 1. are characterized as mixed type or undetermined aerosols.

Table 3.2: The threshold values based on AOD and AE for aerosol-type classification

Aerosol type	**Aerosol optical depth (AOD)**	**Angstrom exponent(AE)**
Maritime	< 0.3	0.5-1.7
Desert dust	> 0.45	0.4-2.0
Biomass Burning	> 0.7	> 1.0

The annual, monthly, and seasonal rainfall data were used to plot time series graphs to investigate the annual, monthly, and seasonal distribution of rainfall amount over Agoufou, Banizoumbou, Dakar, Ilorin, and IER_Cinzana. All the graphs were plotted using the MicroCal Origin software.

3.3.2 Wet, Dry, and Normal Conditions

Meteorologically, dry and wet climatic conditions occur when rainfall is below and above the long-term mean normal (Huho *et al.*, 2017). However, knowing the fact that a 1 mm drop in rainfall amounts below the long-term mean does not necessarily lead to drought. According to Huho *et al.* (2017) normal rainfall period was included in this study and climate conditions were categorized as dry (drought), normal, and wet. When rainfall amount was below two-thirds of the standard deviation from the mean ($\bar{x} - 2/3(SD)$, the climatic condition is considered as dry (drought) when rainfall amount was in-between $\bar{x} - 2/3\ (SD)$ and $\bar{x} + 2/3\ (SD)$ is considered normal and wet when rainfall amount was above $\bar{x} + 2/3\ (SD)$ (Julius *et al.*, 2017).

3.3.3 The coefficient of variation (CV)

The coefficient of variation (*CV*) was used to establish annual and seasonal rainfall variations. *CV* is simply obtained by dividing the standard deviation by the long-term mean and it is expressed as a percentage.

$$CV = \frac{\sigma}{\bar{x}} \times 100 \qquad (3.1)$$

3.3.4 Mann Kendall test

Mann Kendall test is a statistical test widely used for the analysis of trends in climatologic and hydrologic time series (Yue *et al.,* 2004; Mavromatis *et al.,* 2011). Mann Kendall test is a non-parametric test and does not require the data to be normally distributed. The test also has low sensitivity to abrupt breaks due to inhomogeneous time series (Tabari *et al.,* 2011). Any data reported as non-detects are included by assigning them a common value that is smaller than the smallest measured value in the data set (Neha, 2012). According to this test, the null hypothesis H_o assumes that no trend if the data is independent and randomly ordered and this is tested against the alternative hypothesis H_1, which assumes that there is a trend (Onoz *et al.,* 2012).

The computational procedure for the Mann-Kendall test considers the time series of n data points and T_i and T_j as two subsets of data where $i = 1,2,3, \ldots n-1$ and $j = i+1, i+2, i+3, \ldots, n$. The data values are evaluated as an ordered time series. Each data value is compared with all subsequent data values. If a data value from a later period is higher than a data value from an earlier period, the statistic S is incremented by 1. On the other hand, if the data value from a later period is lower than a data value sampled earlier, S is decremented by 1. The net result of all such increments and decrements yields the final value of S (Drapela *et al.,* 2011). The Mann-Kendall S Statistic is computed as follows:

$$S = \sum_{i=1}^{n-1} \sum_{j=i+1}^{n} sign\,(T_j - T_i) \qquad (3.2)$$

$$sign\left(T_j - T_i\right) = \begin{cases} 1\ if\ T_j - T_i > 0 \\ 0\ if\ T_j - T_i = 0 \\ -1\ if\ T_j - T_i < 0 \end{cases} \quad (3.3)$$

Where T_j and T_i are the annual values in years j and i, $j > i$ respectively (Motiee *et al.,* 2009). The two-tailed test is used. At a certain probability level, H_0 is rejected in favor of H_1 if the absolute value of S equals or exceeds a specified value $S_{\alpha/2}$, where $S_{\alpha/2}$ is the smallest S which has the probability less than $\alpha/2$ to appear in case of no trend. A positive (negative) value of S indicates an upward (downward) trend. (Drapela *et al.,* 2011) For n ≥ 10, the statistic S is approximately, normally distributed with the mean and variance as follows:

$$E(S) = 0 \quad (3.4)$$

The variance (σ^2) for the S-statistic is defined by:

$$\sigma^2 = \frac{n(n-1)(2n+5) - \sum t_i(i)(i-1)(2i+5}{18} \quad (3.5)$$

Where t_i denotes the number of ties to extent i. The summation term in the numerator is used only if the data series contains tied values. Kendall's tau is another statistic obtained by running the Mann-Kendall test, which measures correlation and the strength of the relationship between the two variables. Kendall's tau, like Spearman's rank correlation, is carried out on the ranks of the data. That is, for each variable separately, the values are put in order and numbered, 1 for the lowest value, 2 for the next lowest, and so on. In common with other measures of correlation, Kendall's tau will take values between ± 1 and $+1$, with a

positive correlation indicating that the ranks of both variables increase together whilst a negative correlation indicates that as the rank of one variable increases, the other decreases (Neha 2012).

In time series analysis it is essential to consider autocorrelation or serial correlation, defined as the correlation of a variable with itself over successive time intervals, before testing for trends. Autocorrelation increases the chances of detecting significant trends even if they are absent and vice versa. To consider the effect of autocorrelation, Hamed and Rao (1998) suggest a modified Mann-Kendall test, which calculates the autocorrelation between the ranks of the data after removing the apparent trend. The adjusted variance is given by

$$Var(S) = \frac{1}{18}[N(N-1)(2N+5)]\frac{N}{NS^*} \quad (3.6)$$

$$\text{Where } \frac{N}{NS^*} = 1 + \frac{2}{N(N-1)(N-2)}\sum_{i=1}^{p}(N-i)(N-i-2)p_s(i) \quad (3.7)$$

N is the number of observations in the sample, $NS*$ is the effective number of observations to account for autocorrelation in the data, $p_s\ (i)$ is the autocorrelation between ranks of the observations for lag i, and p is the maximum time lag under consideration (Sinha *et al.,* 2007). Addinsoft's XLSTAT Software was used to calculate the statistical Mann-Kendall test. The 95% confidence level was adopted for testing the H_0 Where the p value was less than *alpha = 0.05*, the H_0 was rejected indicating that there was a trend in the time series of rainfall data. Where the *p*-value was greater than 0.05, the H_0 was accepted indicating that the trend was not detected.

3.4 WRF-CHEM MODEL SETUP FOR SIMULATION

The fully coupled meteorology-chemistry-aerosol model WRF-Chem Version 4.1.2 (Fast *et al.* 2006; Grell *et al.,* 2005) was used in this study to investigate the effect of biomass-burning aerosols on rainfall. The domain for the regional simulation is centered over West Africa with 159 × 149 grid cells and a spatial resolution of 40 X 40 km^2. Vertical levels between the surface and 50 hPa were 27. The initial and boundary conditions for the WRF-Chem model were provided by National Centers for Environmental Prediction (NCEP)/National Center for Atmospheric Research (NCAR) Global Final Analysis (FNL) data with 1° × 1° spatial resolution in every 6-h interval. NCAR fire inventory data (FINN; Wiedinmyer *et al.,* 2011) was used in the model for the online plume-rise module. Mineral dust and sea salt emissions are parameterized using the Goddard Chemistry Aerosol Radiation and, Transport (GOCART) aerosol module. Model of Emissions of Gases and Aerosols (MEGAN), provides global biogenic emissions of trace species with 1km resolution (Guenther *et al.,* 2006), which is used in the model simulations too. The Carbon-Bond gas-phase chemical mechanism (CBMZ; Zaveri and Peters, 1999) and Model for Simulating Aerosol Interactions and Chemistry (MOSAIC; Zaveri *et al.,* 2008) both were included using four sectional aerosol bins with dimethyl sulfide (DMS) and aqueous reactions. The simulation uses the Bougeault-Lacarrere boundary layer scheme (Bougeault and Lacarrere, 1989) and the Noah land surface model (Ek *et al.,* 2003). In this study, two simulations were set up; the first is with the radiative effects of biomass burning aerosols and the second is without BBA radiative effect and the period of studies focuses on the months of March, April, May, June, July, and August 2012. Table 3.2 illustrates the model setup briefly.

Table 3.3: The model configuration and physical parameterization options used in this study

Processes	**WRF-Chem Parameterizations**
Land Surface Model	Noah
Microphysics	Morrison
Planetary boundary layer	YSU scheme
Gas-chemistry module	CBMZ
Aerosol module	MOSAIC 4 bin model
Cumulus	Grell 3d ensemble
Shortwave and longwave Radiation	Rapid Radiative Transfer Model (RRTMG)
Domain resolution	40 X 40 km^2
Vertical layers	24
Time step	6 hourly
Simulation time	48 hours per wall time
Anthropogenic emission inventory	EDGAR-HTAP
Fire emission inventory	FINN
Dust emissions	Gocart model
Sea emissions	Gocart model
IC/BC (meteorology)	FNL global analyses
Biogenic emission inventory	MEGAN
IC/BC (chemistry)	MOZART global model runs

CHAPTER FOUR

4.0 RESULTS AND DISCUSSION

4.1 ANALYSIS OF AEROSOLS

This section presents discusses the results of the time series analysis of Aerosol Optical Depth and Angstrom Exponent over the selected AERONET sites in West Africa. It also presents and discusses the result of the scatted plots of AOD against AE.

4.1.1 Climatology of Aerosol Optical Depth (AOD)

The time series analysis shown in figure 4.1 – 4.5 represents the monthly average of AOD for Agoufou, Banizombou, Dakar, Ilorin, and IER_Cinzana. The summarized result of the analysis were shown in table 4.1. The AOD exhibits variations throughout the study period at Agoufou showed in figure 4.1. The maximum value of AOD was 1.07 during the month of May and the minimum was 0.17 during the month of December. The mean value of AOD for the study period was 0.52. The annual AOD standard deviation value was 0.20, which means the AOD values were not dispersed or there was inconsistency in the AOD distribution in Agoufou. As AOD values vary throughout the study in Banizoumbou, the highest value was observed in the month of June with a value of 1.21. The month of January recorded the lowest value of AOD at 0.19 with a mean of 0.54 and an SD of 0.23. In Dakar, the highest AOD value was in March, which recorded an amount of 0.86 with a corresponding mean value of 0.46. The record indicated the standard deviation of 0.14 with the lowest AOD value of 0.15 in December. The highest and lowest AOD values observed over Ilorin from figure 4.4 and table 4.1 were 1.48 and 0.24, which correspond to the months of January and August, respectively. Ilorin recorded a mean AOD value of 0.65 and an SD value of 0.32 for the study

period. In IER_Cinzana, the mean and SD AOD values for the study period were 0.46 and 0.22 respectively. These values corresponded with the highest AOD value of 1.34 in April and the lowest AOD value of 0.21 in November and July.

The over roll means AOD values range from 0.46-0.65. AOD values peak at 0.86-1.48 and minimum AOD values range from 0.15-024. The over roll highest AOD value corresponded to the highest value of mean and SD. The SD is a measure of dispersion. A small value indicates that the data were tightly grouped about the mean and a high value indicates that the data is spread widely on either side of the mean.

Table 4.1: Monthly mean, Standard Deviation (SD), the minimum and maximum value of AOD estimated for the Sites

Site	Mean	SD	Minimum	Maximum
Agoufou	0.52	0.20	0.17	1.07
Banizoumbou	0.54	0.23	0.19	1.21
Dakar	0.46	0.14	0.15	0.86
Ilorin	0.65	0.32	0.24	1.48
IRE_Cinzana	0.46	0.22	0.21	1.34

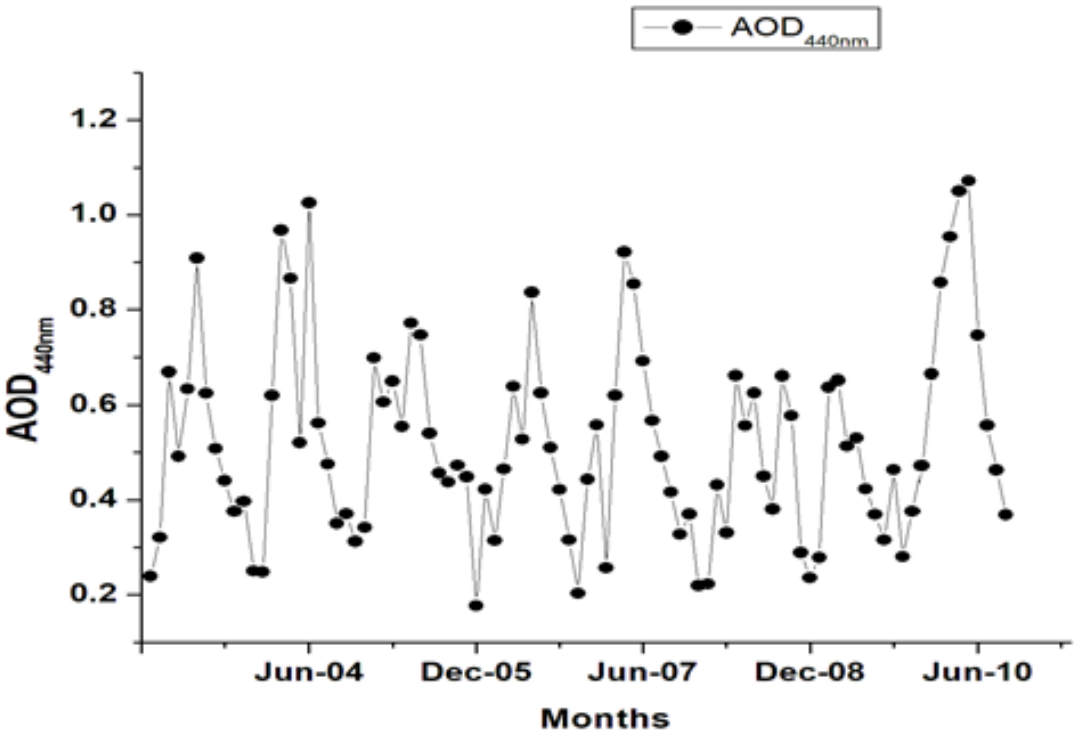

Figure 4.1: Temporal distribution of AOD over Agoufou (2003-2010)

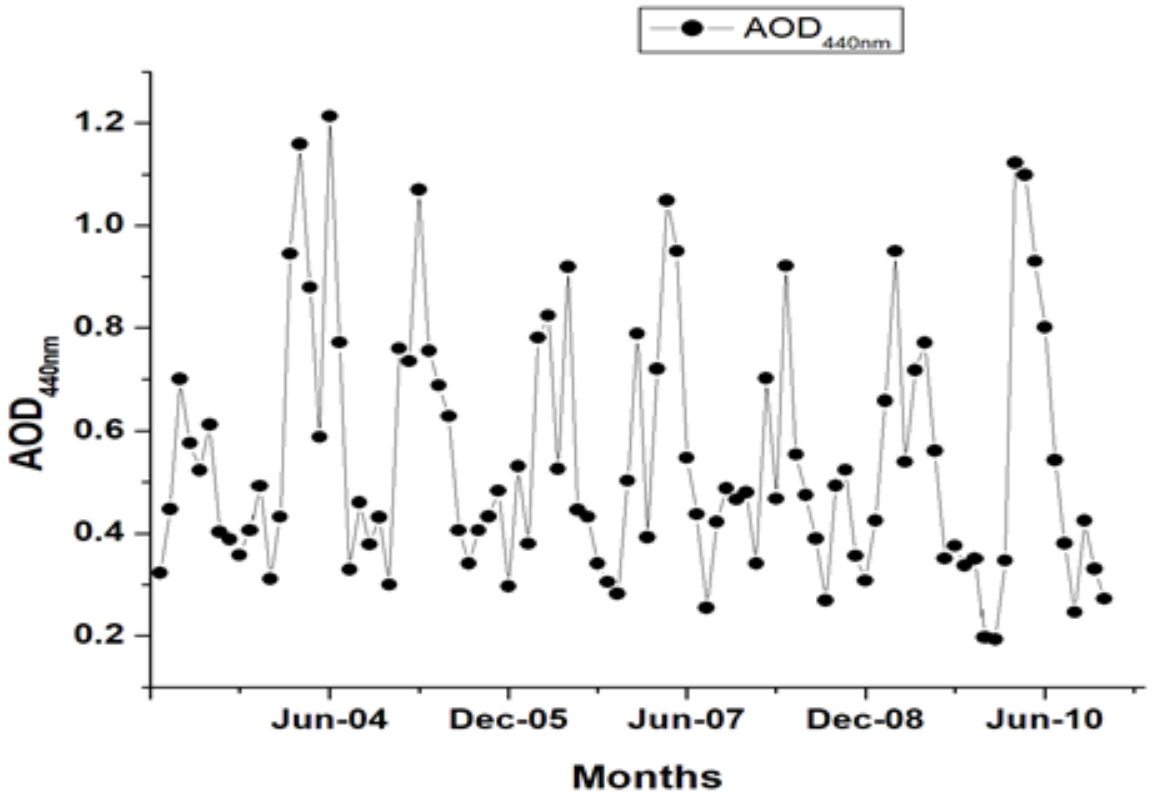

Figure 4.2: Temporal distribution of AOD over Banizoumbou (2003-2010)

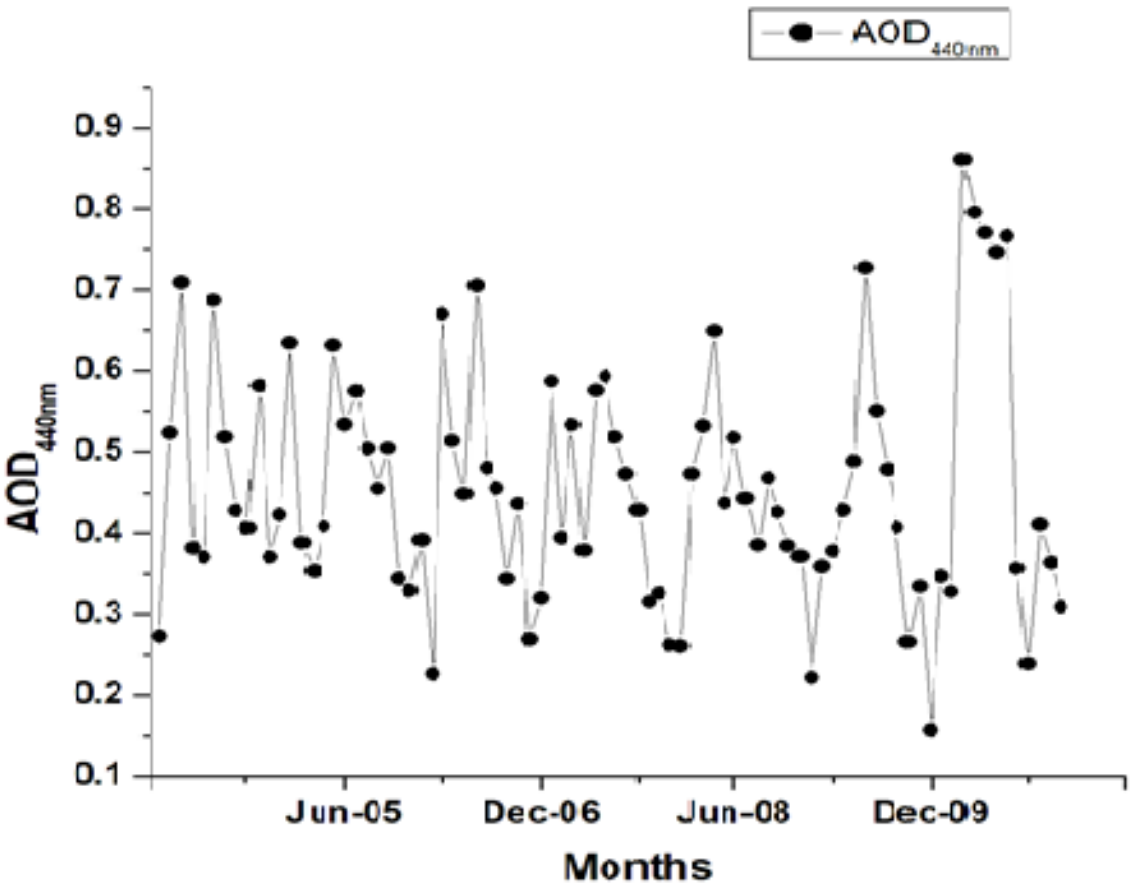

Figure 4.3: Temporal distribution of AOD over Dakar (2004-2010)

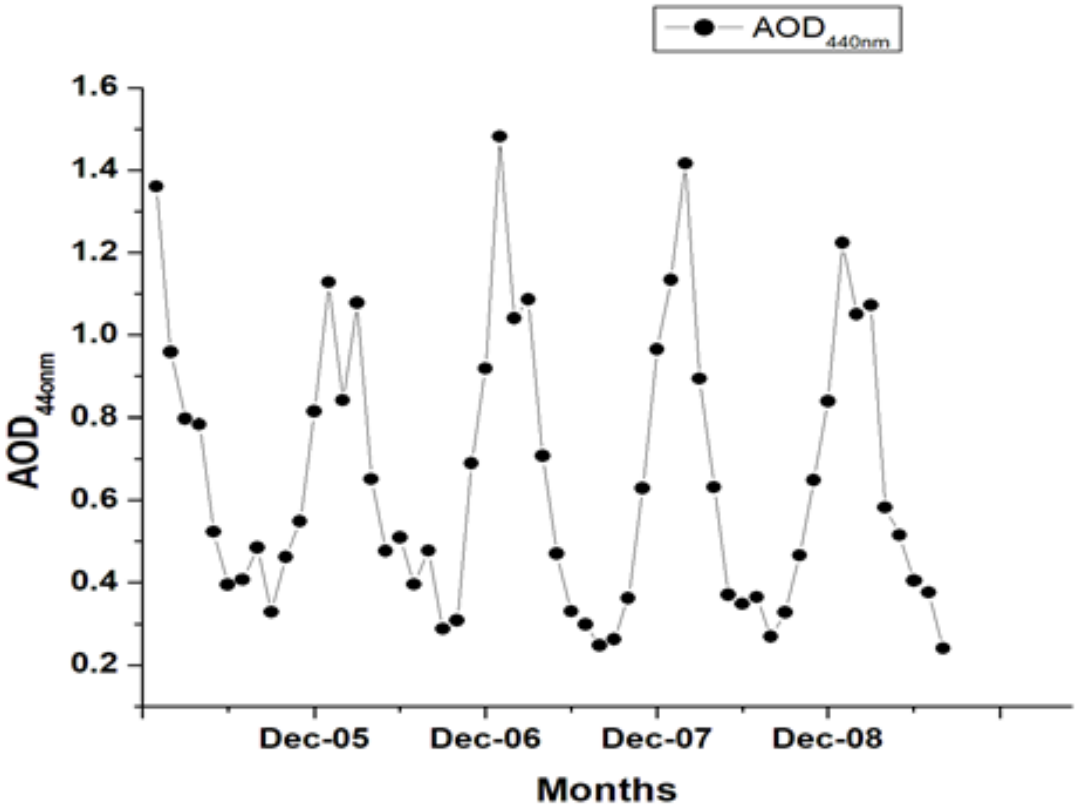

Figure 4.4: Temporal distribution of AOD over Ilorin (2004-2009)

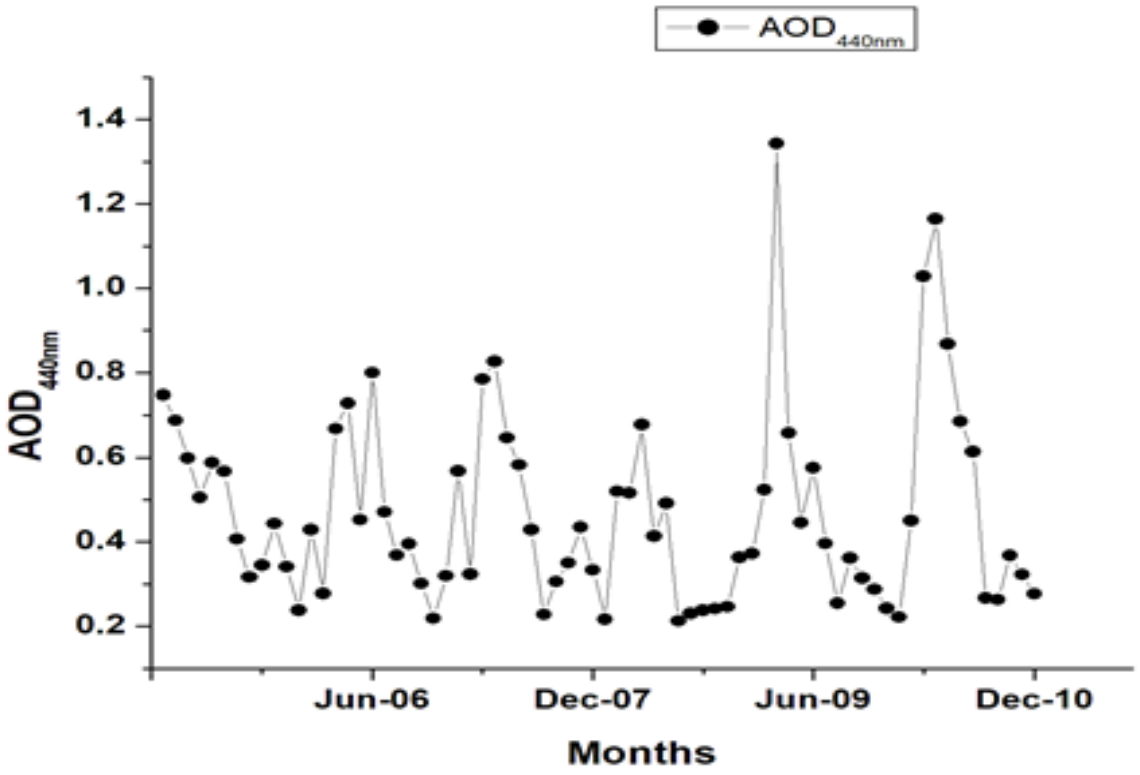

Figure 4.5: Temporal distribution of AOD over IER_Cinzana (2005-2010)

4.1.2 Climatology of Angstrom Exponent (AE)

Angstrom Exponent is a commonly used parameter that represented the wavelength dependence of AOD and it is a significant indicator of aerosol size and its variation. Angstrom Exponent (AE) is an empirical representation that can give information on particle size, with values varying between approximately 0 for coarse dust particles to 2 for submicron particles (Horowitz *et al.,* 2017; Leon *et al.,* 2009; Hamonou *et al.,* 1999). The lower values of AE denote the large diameter of the aerosol particles e.g. desert dust, while higher values of the AE mark the presence of fine particles in the ambient environment (i.e. both types of aerosols, resulting from biomass burning, continental aerosols, and other anthropogenic activities).

The descriptive statistics of monthly AE are tabulated in Table 4.2. Figures 4.6- 4.10 shows the time series of monthly mean AE values over five AERONET sites in the study area.

Table 4.2: Monthly mean, Standard Deviation (SD), the minimum and maximum value of AE estimated for the Sites

Site	Mean	SD	Minimum	Maximum
Agoufou	0.18	0.15	-0.08	0.80
Banizoumbou	0.27	0.16	**-0.02**	0.78
Dakar	0.30	0.2	0.04	0.92
Ilorin	**0.61**	**0.35**	-0.49	**1.27**
IRE_Cinzana	0.30	0.17	0.00	0.84

Angstrom Exponent (AE_440-675nm) values shown in figure 4.6 for the Agoufou site exhibit the highest AE value of 0.80 during the month of January. The lowest AE value (-0.08) was recorded in July with a mean value of 0.18 and a standard deviation (SD) of 0.15. The AE values vary throughout the study period in Banizombou with a maximum and minimum value of 0.78 and -0.02 during the month of January and June respectively. Banizoumbou has a mean AE of 0.27 with SD of 0.16. From table 4.2 and figure 4.8, the highest AE value was recorded in December with an amount of 0.92 for Dakar. The lowest AE value recorded was 0.04 during the month of June with mean and SD of 0.3 and 0.2 respectively. Ilorin's highest AE value 1.27 was recorded during the month of August and the lowest value 0.61 was recorded during the month of April. This is similar to findings previously made by Horowitz *et al.*, 2017. The mean and SD AE values for the study period recorded for Ilorin were 0.61 and 0.35 respectively. In IER_Cinzana, the mean and SD AE values for the study period were 0.30 and 0.17 respectively. These values corresponded with the highest AE value of 0.84 during the month of March and the lowest AE value of 0.00 during the month of January.

Generally, the over roll means AE values range from 0.18-0.61. AE values peak at 0.78-1.27 and minimum AOD values range -0.02-0.04. The over roll highest AE value (1.27) corresponded to the highest value of mean (0.61) and SD (0.35). The maximum AE values for Agoufou. Banizoumbou, Dakar, and IER_Cinzana fell under the month of December/January except for Ilorin whose maximum fell under the month of August. This is so because all the other sites were found in the Sahel region except Ilorin is found in the south of the other site.

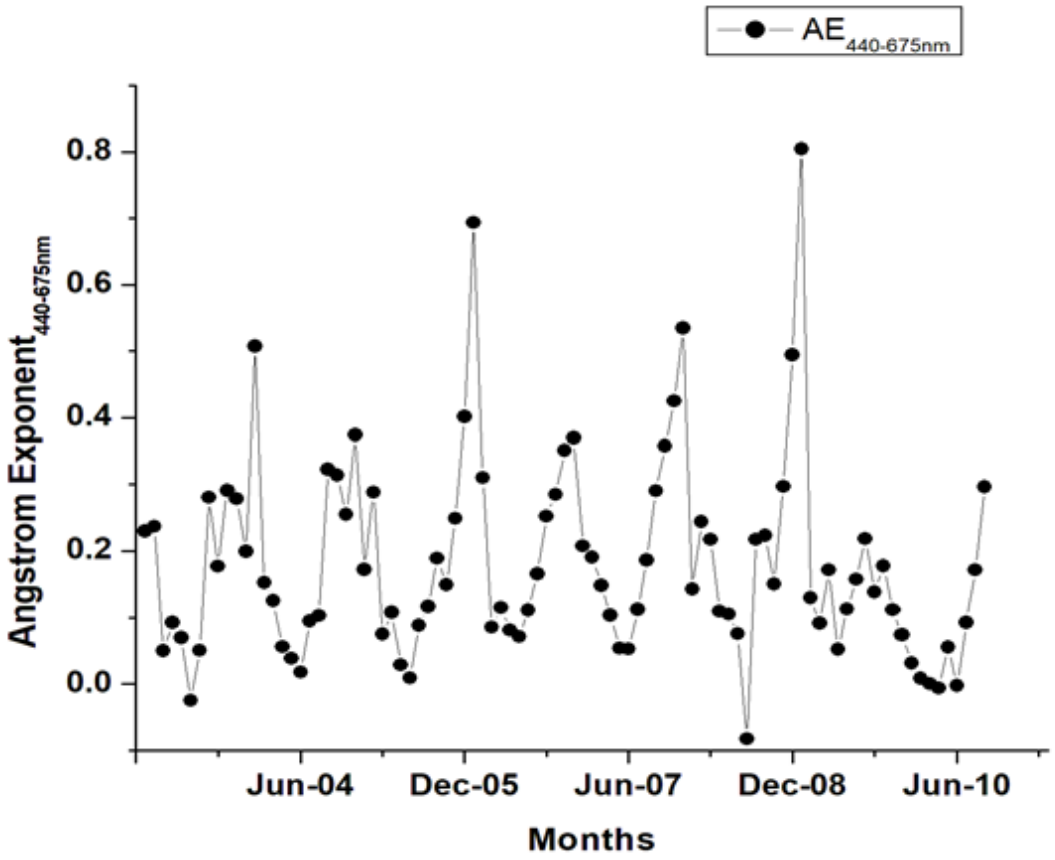

Figure 4.6: Temporal distribution of AE over Agoufou (2003-2010)

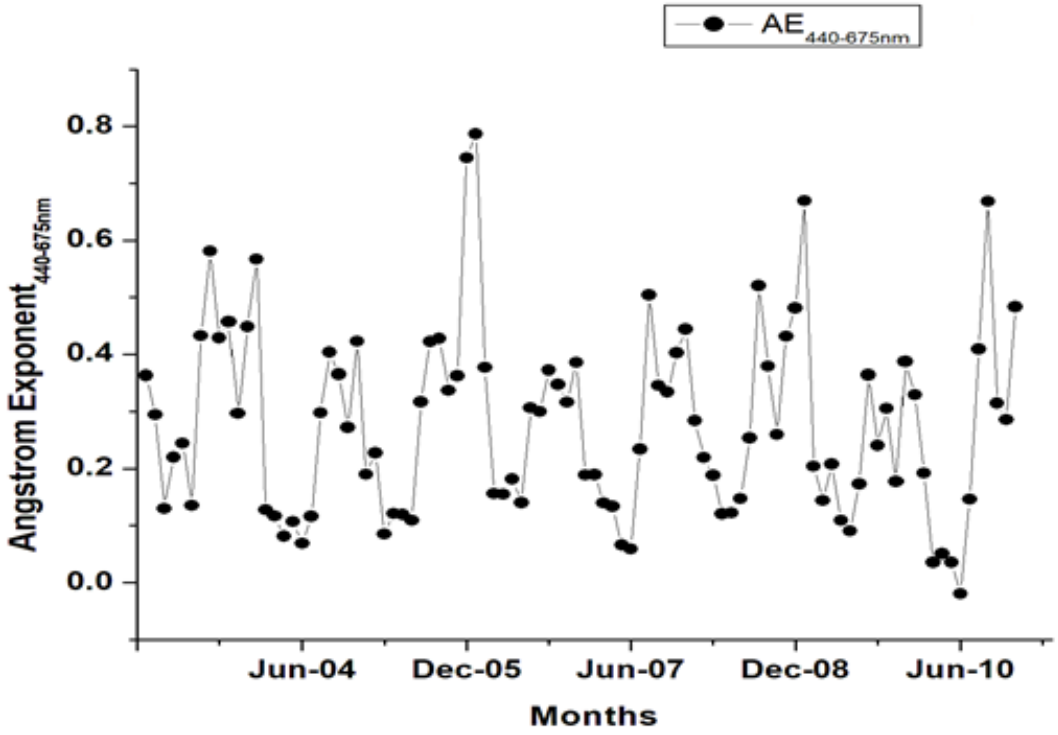

Figure 4.7: Temporal distribution of AE over Banizoumbou (2003-2010)

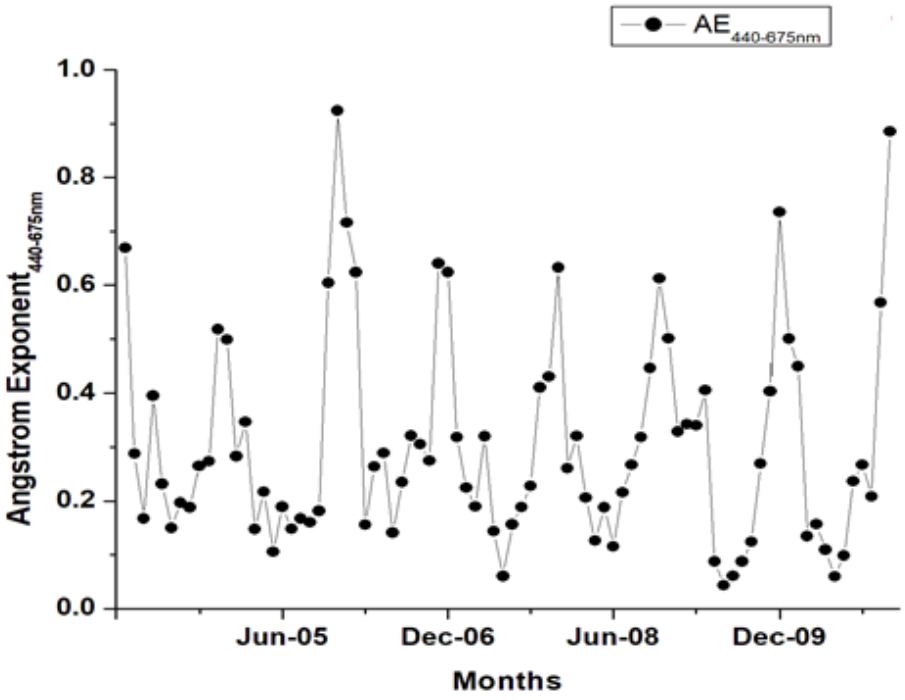

Figure 4.8: Temporal distribution of AE over Dakar (2004-2010)

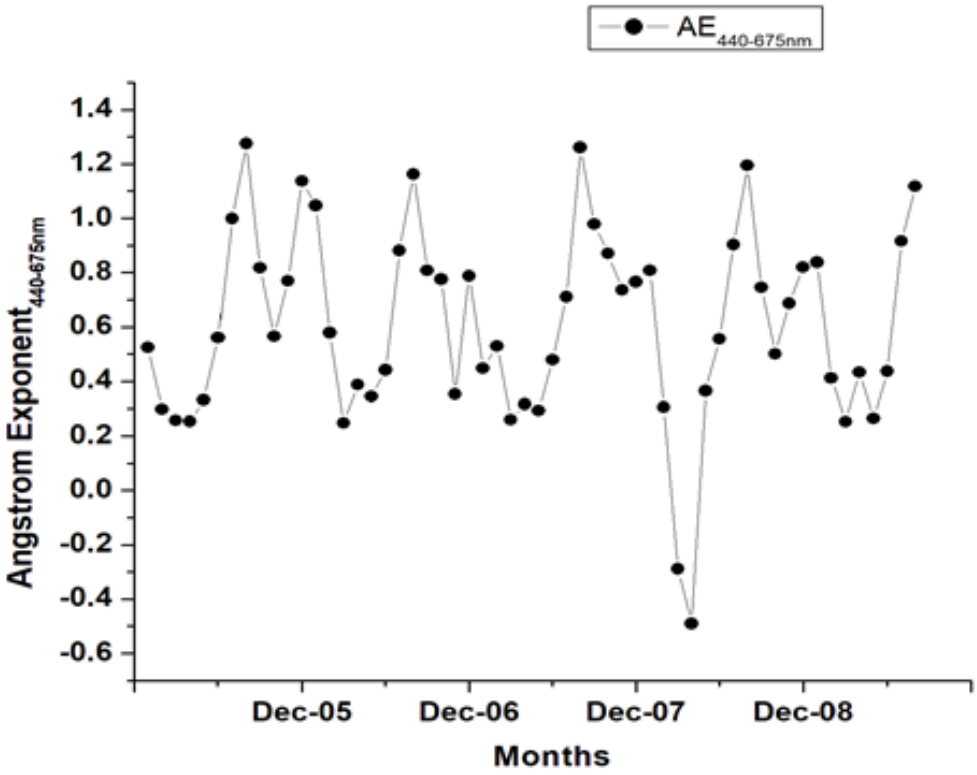

Figure 4.9: Temporal distribution of AE over Ilorin (2005-2009)

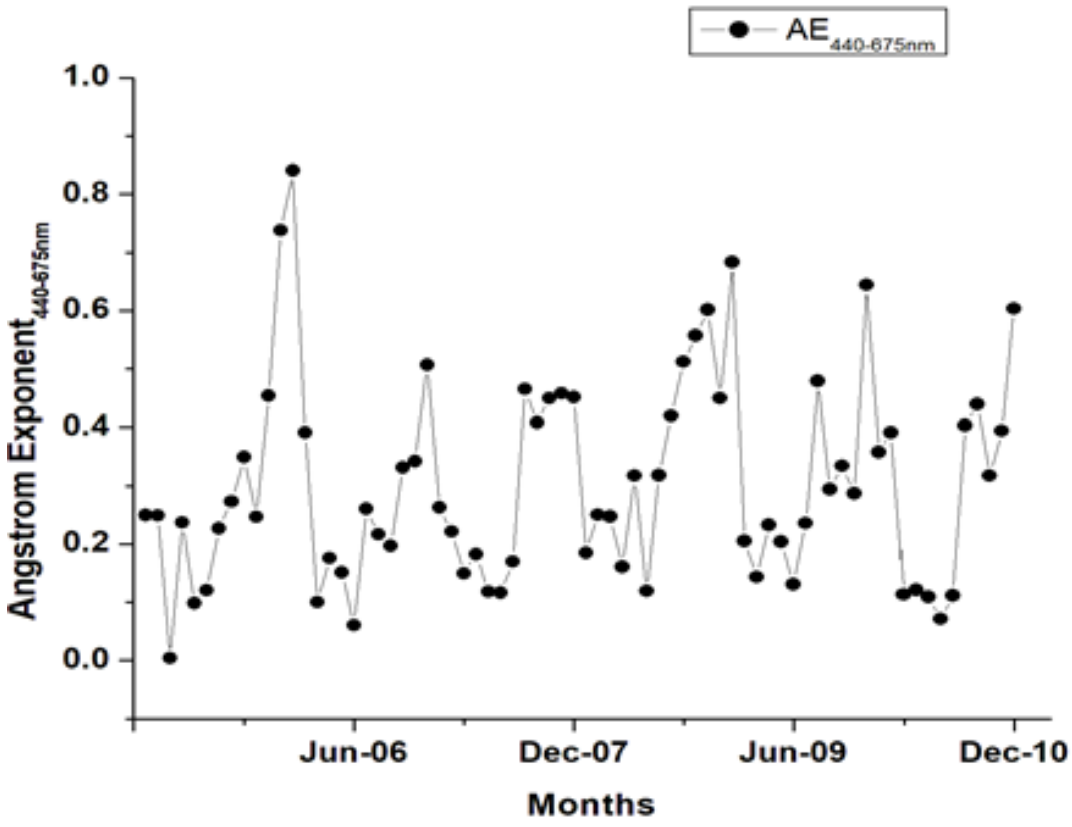

Figure 4.10: Temporal distribution of AE over IER_Cinzana (2005-2010)

4.1.3 Annual Classification and Distribution of Aerosols

The average daily AOD_440nm and AE_440-675nm data for the year 2006 from the various AERONET site used in this study were used to classify the different types of aerosols in each site. The seasonal AOD and AE were also extracted from the daily data and were used to classify the type of aerosols for MAM, JJA, SON, and DJF seasons for all the study areas.

Figure 4.11 - 4.15 showed the scatter plot of AE_440-675nm versus AOD_440nm daily means for each site. In general, as AOD values increase, AE values decrease to low values, and this would suggest that the variation in AOD was dominated by the variation in coarse dust aerosol. This type of aerosol was found in Agoufou, Banizoumbou, Dakar, Ilorin, and IER_Cinzana. A similar relationship was found previously for Banizoumbou (Holben *et al.,* 2001; Ogunjobi *et al.,* 2008; Rajot *et al.,* 2008). Aerosol types with higher values of AE (fine particles) coupled with a relatively higher AOD value indicating the presence of biomass-burning aerosols (Holben *et al.,* 2001 and Ogunjobi *et al.,* 2007) were also observed in all the sites. The figures also show that the desert dust is present in various sizes of particles, widespread and well mixed higher up, though the mixed aerosols are having particles of fine to coarse mode but are confined to low AOD values. It is clearly shown that the prevailing aerosol type was dust coming from the Saharan/Sahelian zone and transported over the area in Agoufou, Banizoumbou, Dakar, Ilorin, and IER_Cinzana.

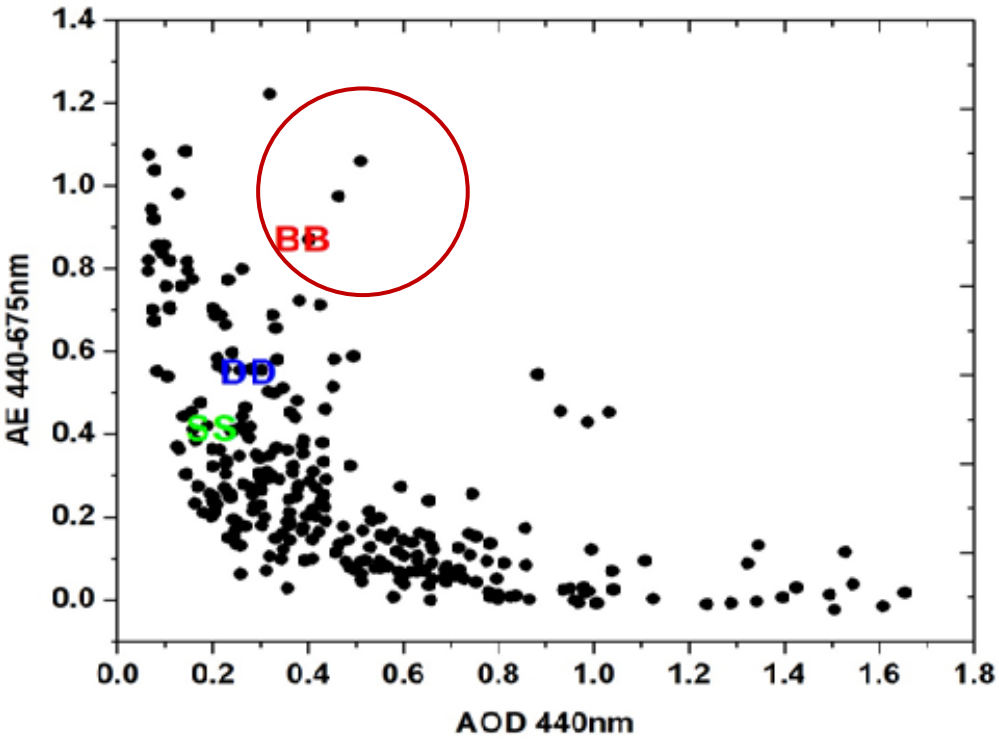

Figure 4.11: Classification and distribution of aerosols over Agoufou

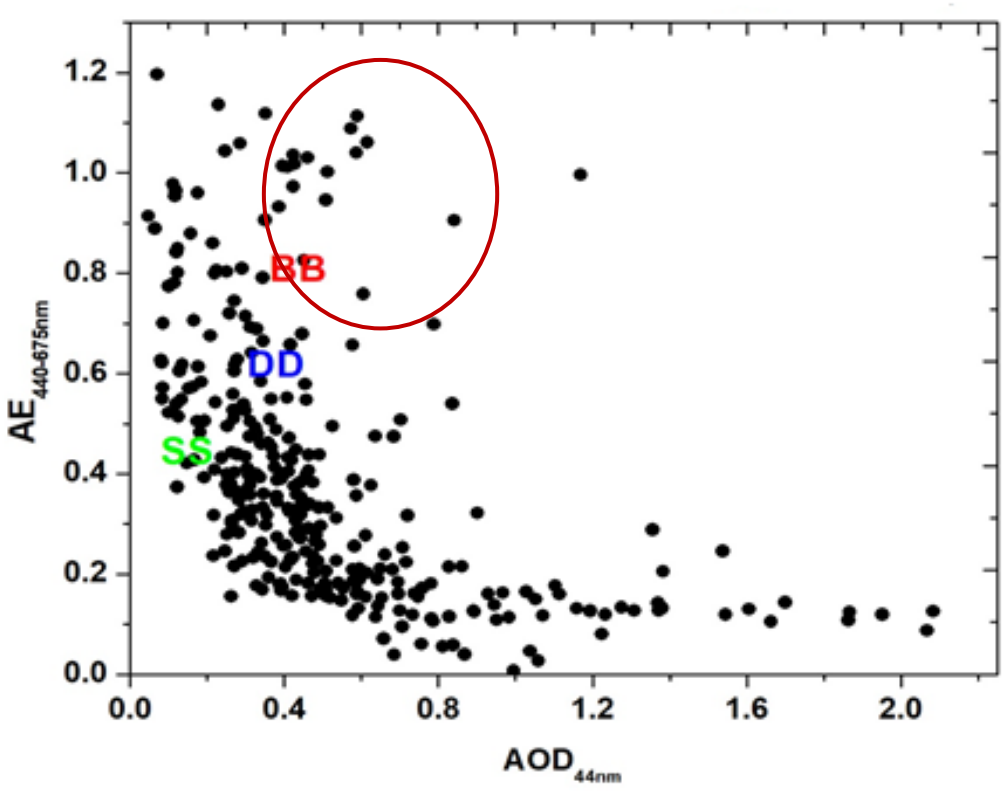

Figure 4.12: Classification and distribution of aerosols type over Banizoumbou

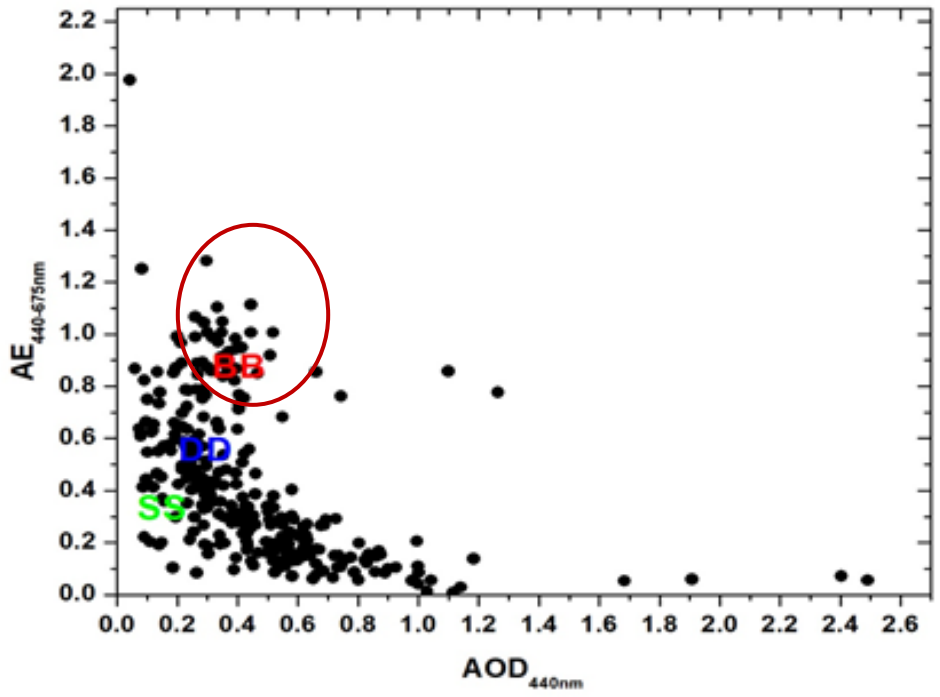

Figure 4.13: Classification and distribution of aerosols type over Dakar

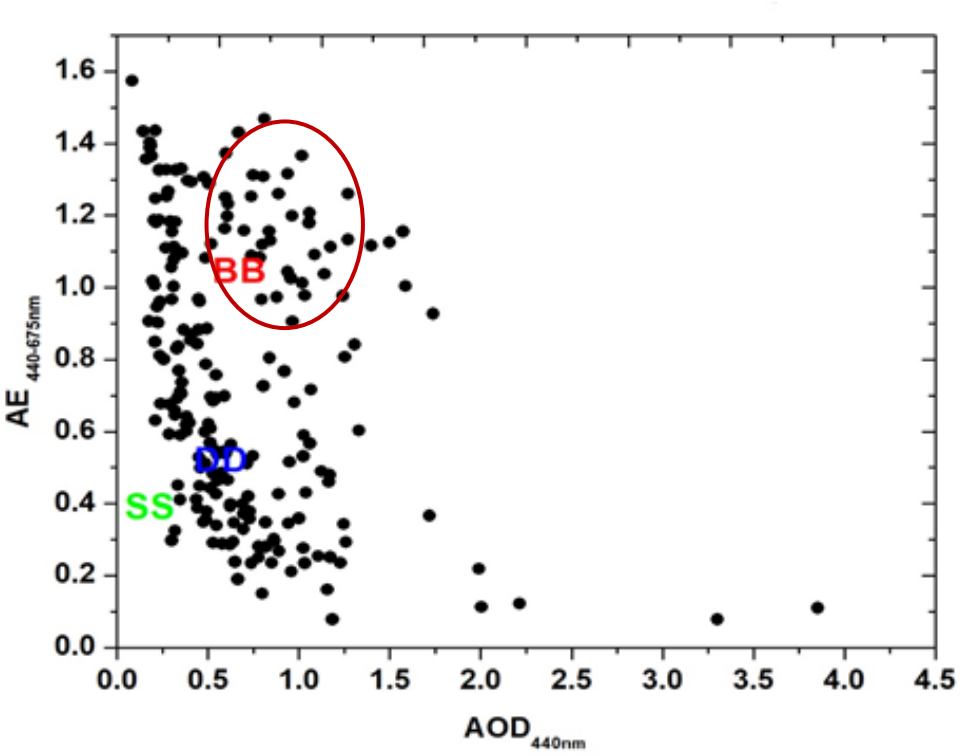

Figure 4.14: Classification and distribution of aerosols type over Ilorin

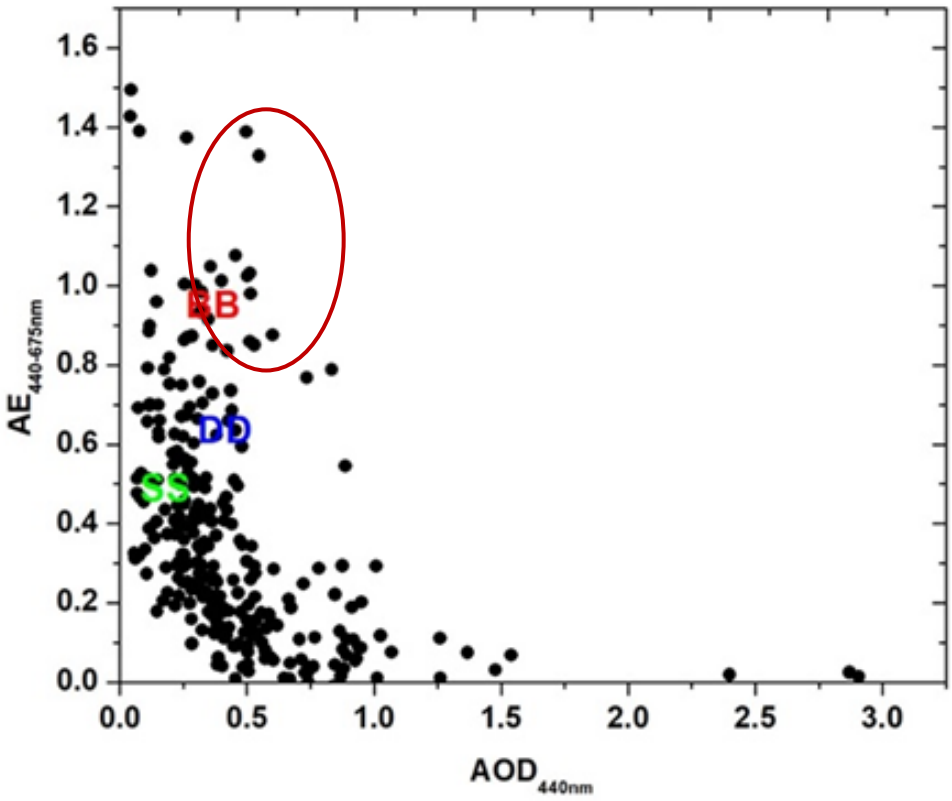

Figure 4.15: Classification and distribution of aerosols type over IER_Cinzana

4.1.4 Seasonal Classification and Distribution of Aerosols

Figure 4.16 show the seasonal distribution of aerosol types in Agoufou. Aerosol particles with high AOD values and low AE values were observed during the MAM, JJA, SON, and DJF seasons. This indicates the presence of desert dust throughout the year. The maximum value of AE in January corresponds to the presence of biomass-burning aerosols during the DJF seasons. JJA and SON seasons were relatively clear due to the scavenging of the atmosphere by precipitation. The presence of desert dust was observed throughout the year in Banizoumbou. These were aerosol particles with high AOD values corresponding with low AE values observed for all the seasons as shown in figure 4.17. The large values of AOD associated with large values of AE in DJF correspond to the presence of biomass burning as reported by Holben *et al.*, 2001. The savanna vegetation is characteristic of the Sudanian zone and fire activities are important in the zone from December to February. DJF was the only season during which biomass-burning aerosols were observed in Banizoumbou. The seasonal distribution of different aerosol types was shown in figure 4.17**.** Most of the aerosols observed during the MAM season have a low value of AOD with a high value of AE. These can be an indication of the presence of maritime aerosols (SS) and mixed aerosols (aerosols from transportation, industries, and anthropogenic emissions). These types of aerosols have been observed in all the seasons except for JJA, which has, but few of such aerosols type.

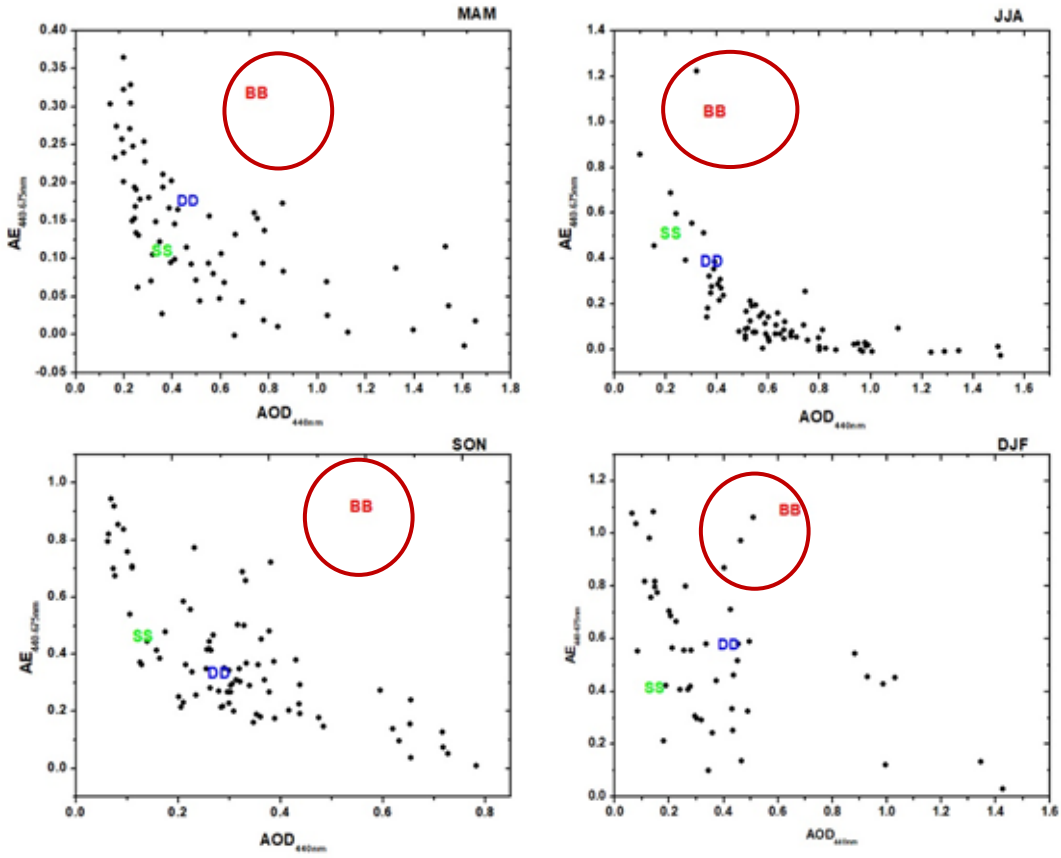

Figure 4.16: Seasonal Classification and distribution of aerosols over Agoufou

The presence of desert dust (DD) has been observed under MAM, JJA, SON, and DJF and was dominant during the JJA and SON seasons. The biomass-burning aerosols were observed during the JJA and DJF seasons. So many different types of aerosols were observed over Dakar. This finding is similar to the (Leon *et al.* 2009) study that established Dakar is subject to the transport of both dust and biomass-burning aerosols, depending on the season, as well as poorly constrained anthropogenic emissions from the city and other nearby urban centers. Aerosol particles with higher AOD values corresponding to low AE values were observed throughout the study year in Ilorin. The presence of desert dust was observed throughout the year. Biomass-burning aerosols were also observed during the JJA and DJF seasons. Other types of aerosols such as sea salt (maritime aerosols) and mixed aerosols were observed too.

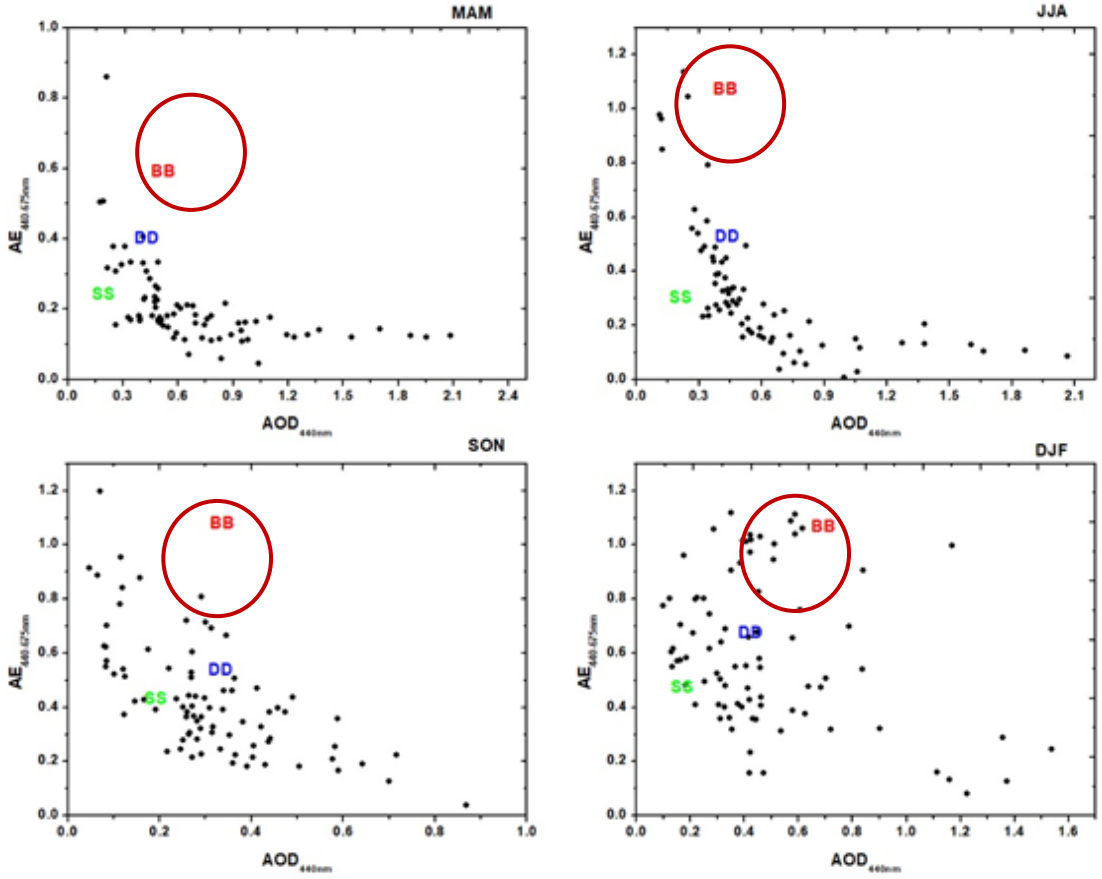

Figure 4.17: Seasonal Classification and distribution of aerosols over Banizoumbou

The maximum AE under Ilorin was not found during the DJF season but DJF season was dominated by biomass-burning aerosols, this is so because Ilorin is closer to the primary area of biomass burning during this time (Liousse *et al.*, 2010; Pinker *et al.*, 2010). This suggests that biomass-burning aerosols could make up a larger fraction of total AOD at Ilorin during this study period. In IER_Cinzana, the presence of desert dust was observed during the JJA, SON, and DJF seasons. There was no sign of biomass burning aerosols during the study period. The area was dominated by sea salt aerosols and mixed aerosols throughout the study period, as shown in figure 4.20.

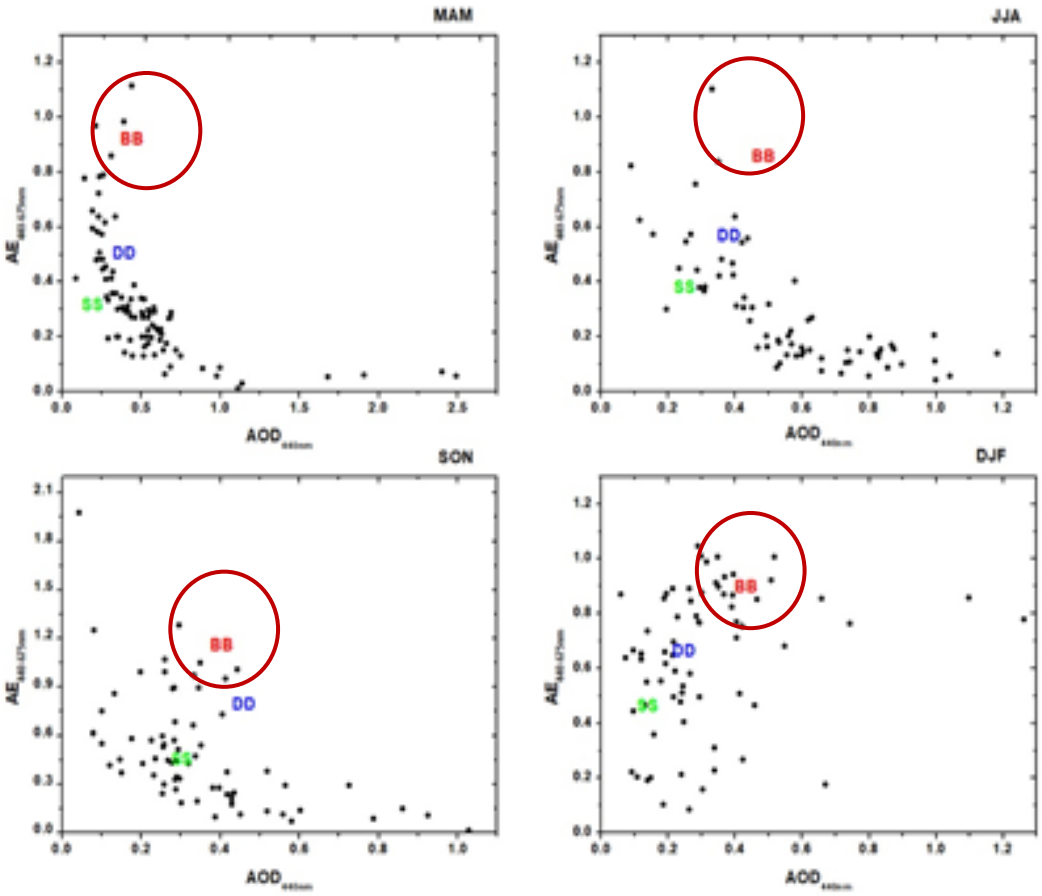

Figure 4.18: Seasonal Classification and distribution of aerosols over Dakar

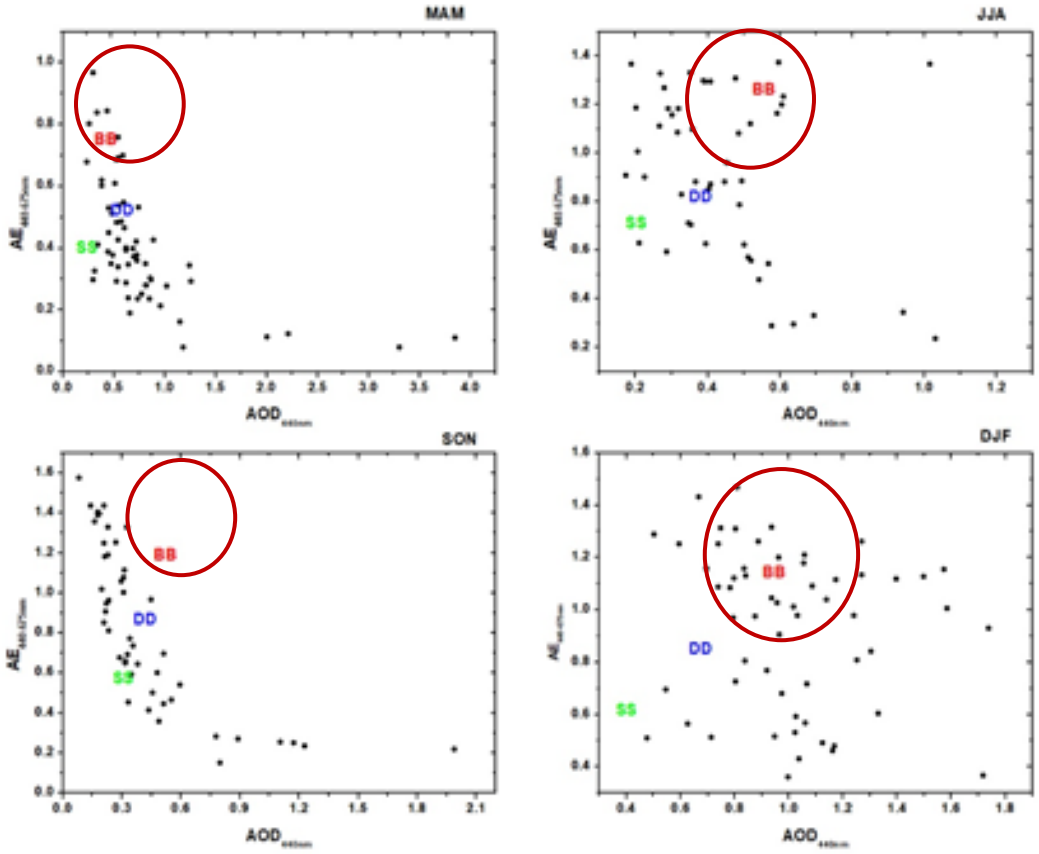

Figure 4.19: Seasonal Classification and distribution of aerosols over Ilorin

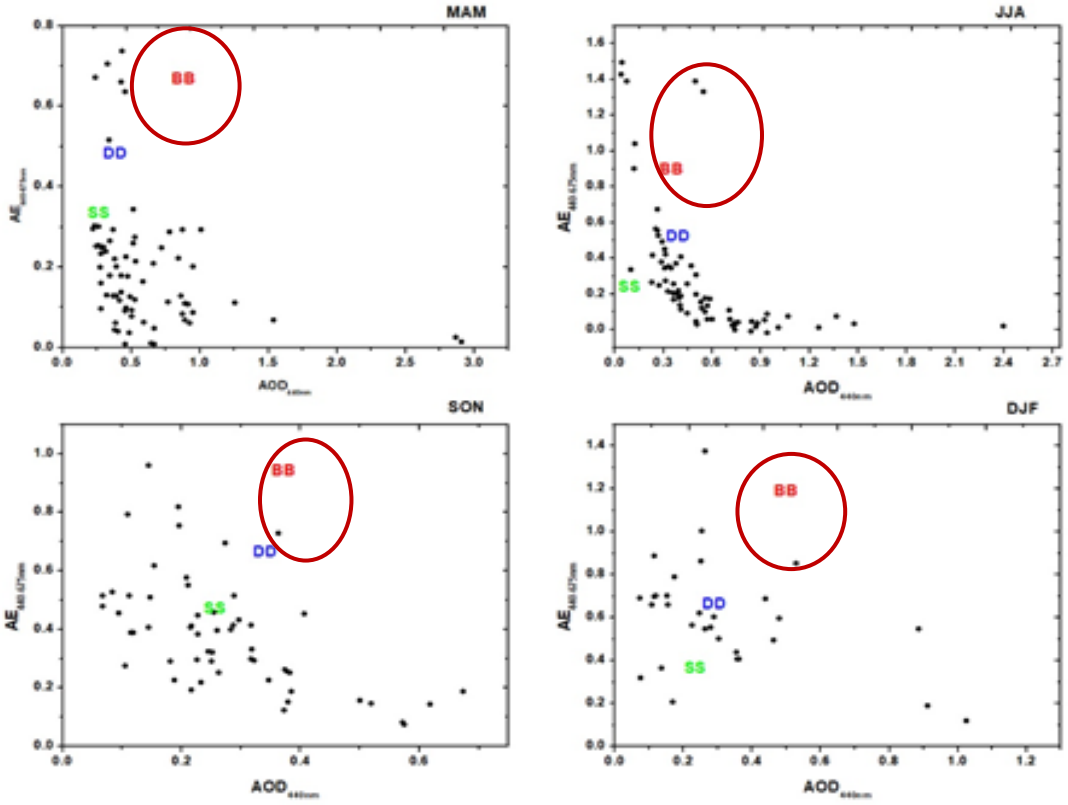

Figure 4.20: Seasonal Classification and distribution of aerosols over IER_Cinzana

4.2 RESULTS FROM THE RAINFALL ANALYSIS

This section intends to look at the rainfall characteristics such as distribution, variability over time, and trend.

4.2.1 Annual and Monthly Rainfall Distribution

Figure 4.21 shows the annual and monthly rainfall distribution at Agoufou (15.35, 1.48) using ERA5 data from 1998-2021. The figure has shown that the highest amount of rainfall was received in 1999 and the lowest was in 2021 with an amount of 375 mm and 100 mm respectively in Agoufou. The mean annual rainfall was 240 mm and out of 24 years under study, only 11 years have their rainfall amount above the mean annual rainfall and the rest fell below the mean line. Agoufou has only one rainy season which starts in May and lasts for 6 months and ends in October. The highest amount of rain was received in August with a value of 80 mm. For Banizoumbou which is shown in figure 4.22, the years 1999 and 2020 received the highest rainfall amounting to 600 mm with an annual mean of 450 mm. The least amount of rainfall recorded is 275mm which occurred in 2011. Most of the annual rainfall amount recorded fell below the mean annual rainfall line.

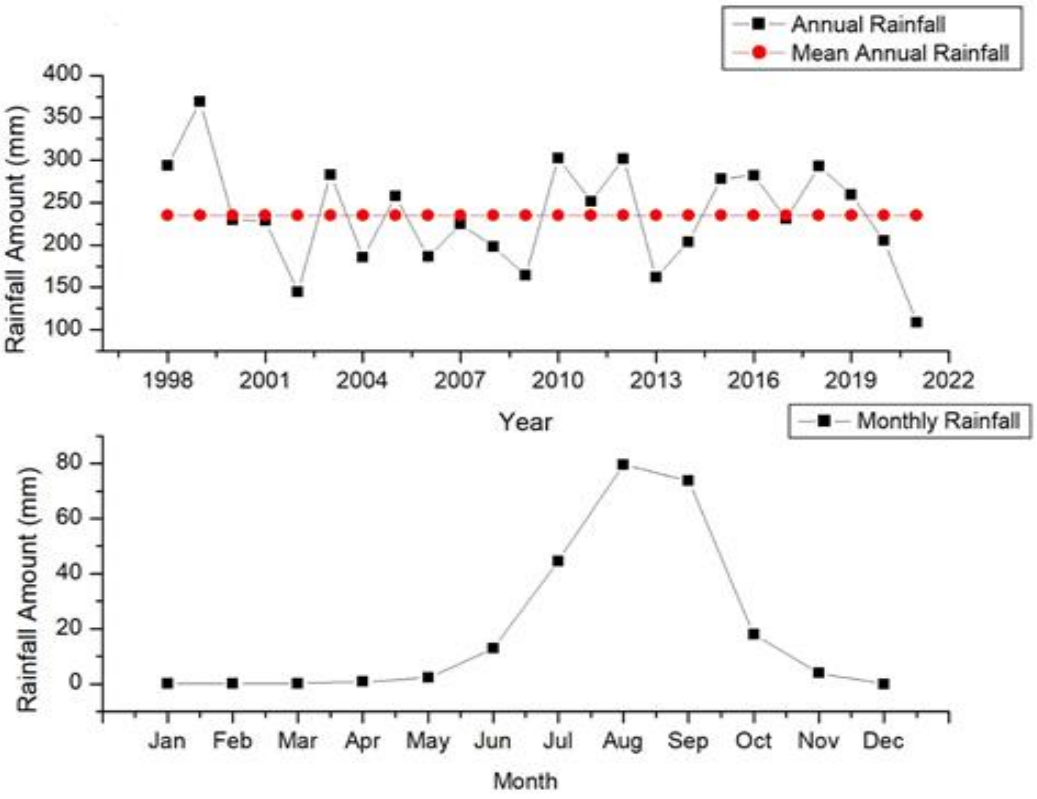

Figure 4.21**:** Annual and monthly rainfall distribution at Agoufou (ERA5 data from 1998-2021)

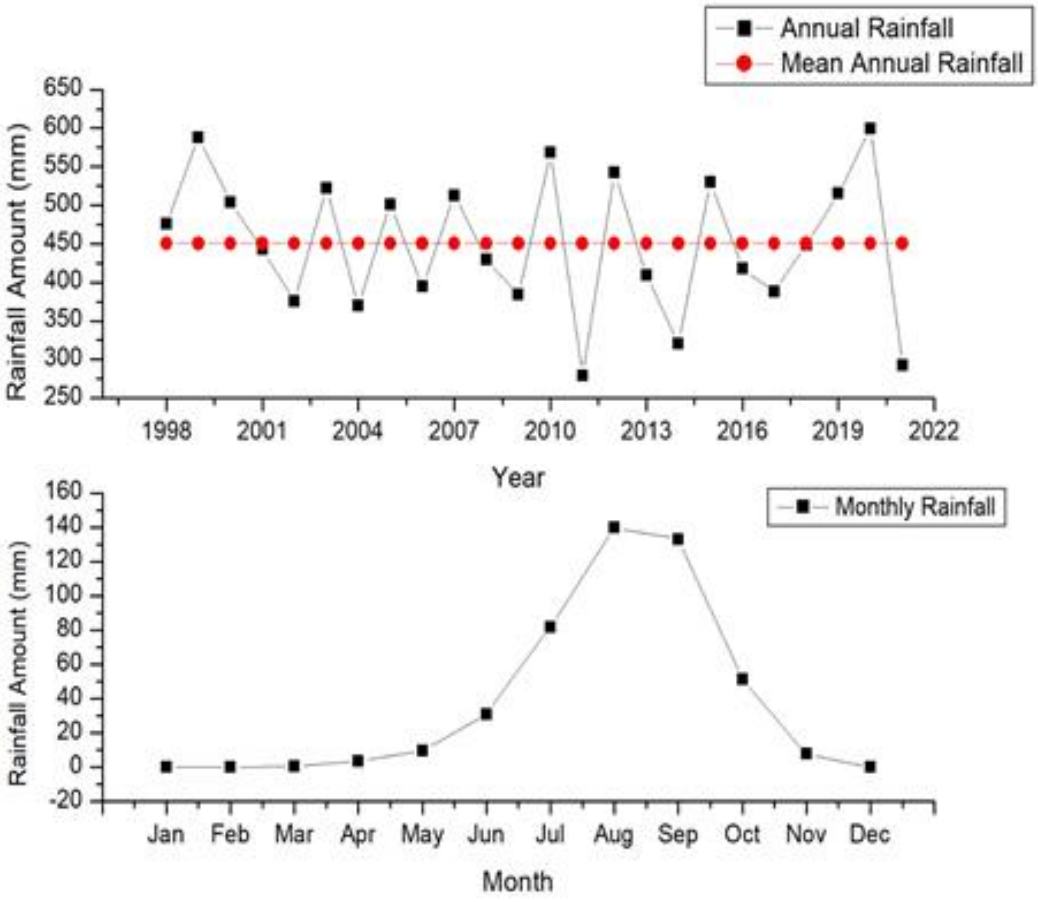

Figure 4.22**:** Annual and monthly rainfall distribution at Banizoumbu (ERA5 data from 1998-2021)

The monthly rainfall distribution has shown that Banizoumbou has only one rainy season, which starts in May extending to October (same as for Agoufou). The season has its peak in August with an amount of 150 mm. Annual rainfall distribution in Dakar (14.39 -16.96) is shown in figure 4.23, the highest amount of rainfall is 570 mm received in 2013 and the lowest is marginally above 200 mm in 2004. The mean annual rainfall is 480 mm the majority of the years under study receive more than the annual mean amount of rainfall. The monthly distribution shows that Dakar has one rainy season which starts in June, peck in September, and ends in October. The highest monthly rainfall amount is 155 mm. Figure 4.24 shows the annual and monthly distribution of rainfall in Ilorin. The highest amount of rainfall was received in 2016 with an amount of 1430 mm. The lowest amount of rainfall was observed in 2021 with an amount of 765 mm. The mean annual rainfall amount is 1500 mm with 11 of the years under study receiving an amount below the mean rainfall amount. A 9-month long single rainy season had been observed which starts from March up to November.

The monthly rainfall peck in September with an amount of 180 mm. For annual rainfall distribution in IER_Cinzana shown in figure 4.25, the mean amount is 800mm with 8 years out of the study years having annual rainfall amount above the mean value. The highest rainfall amount received is 1120 mm in 2009 and the lowest amount was 600 mm in 2006. The monthly distribution shows a single rainfall season starting from May to October. The highest rainfall amount was received in August and September with an amount of 225 mm to 235 mm.

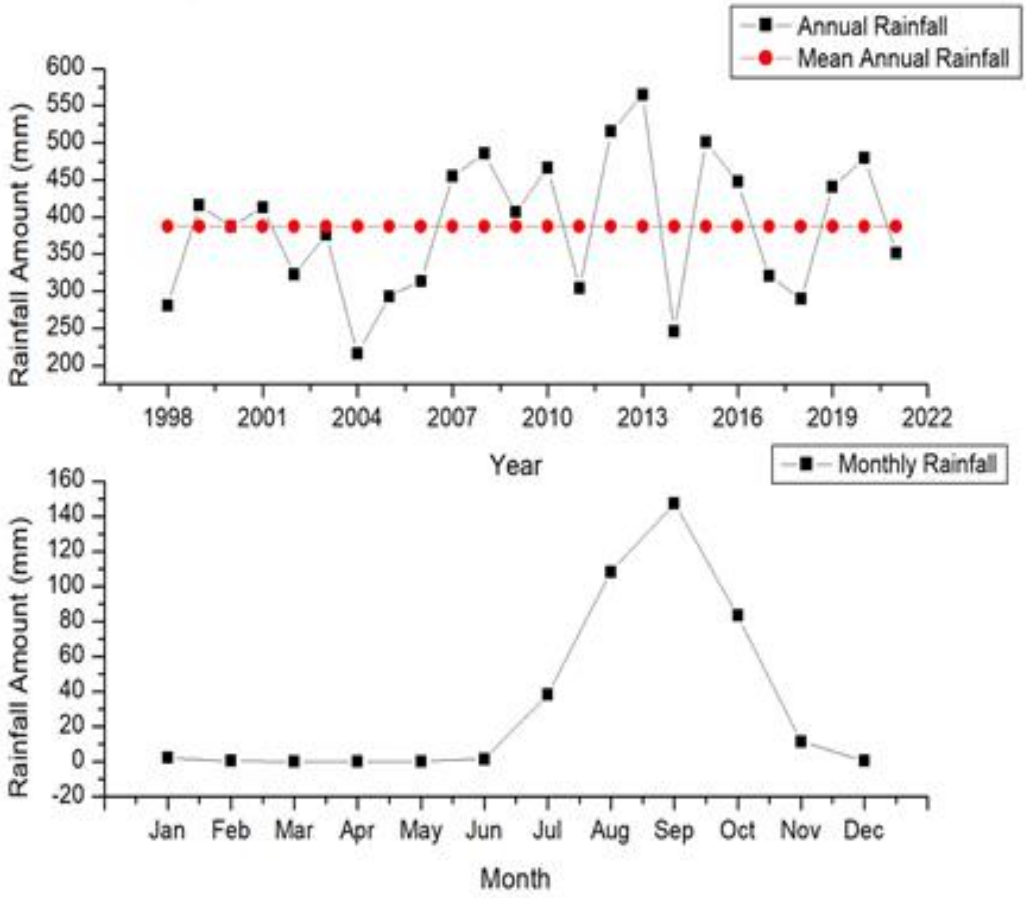

Figure 4.23: Annual and monthly rainfall distribution at Dakar
(ERA5 data from 1998-2021)

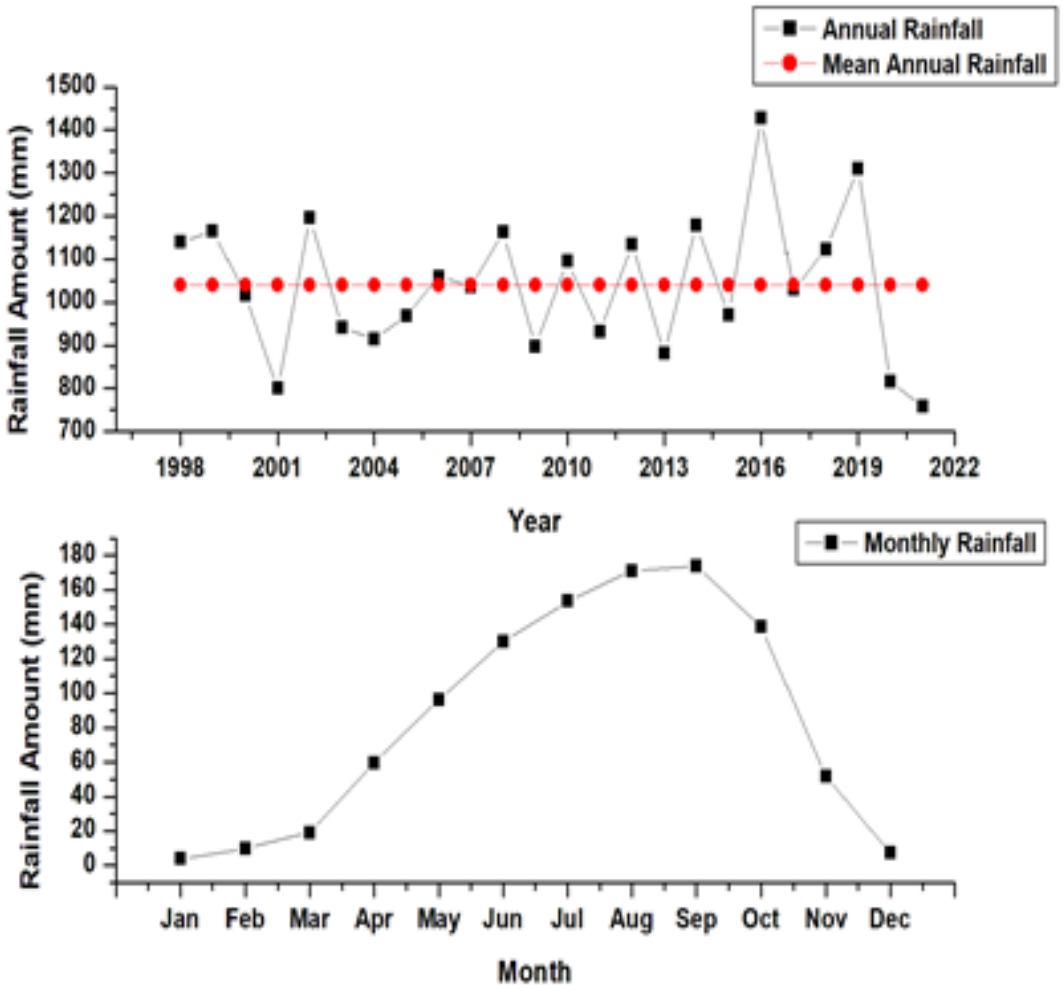

Figure 4.24: Annual and monthly rainfall distribution at Ilorin
(ERA5 data from 1998-2021)

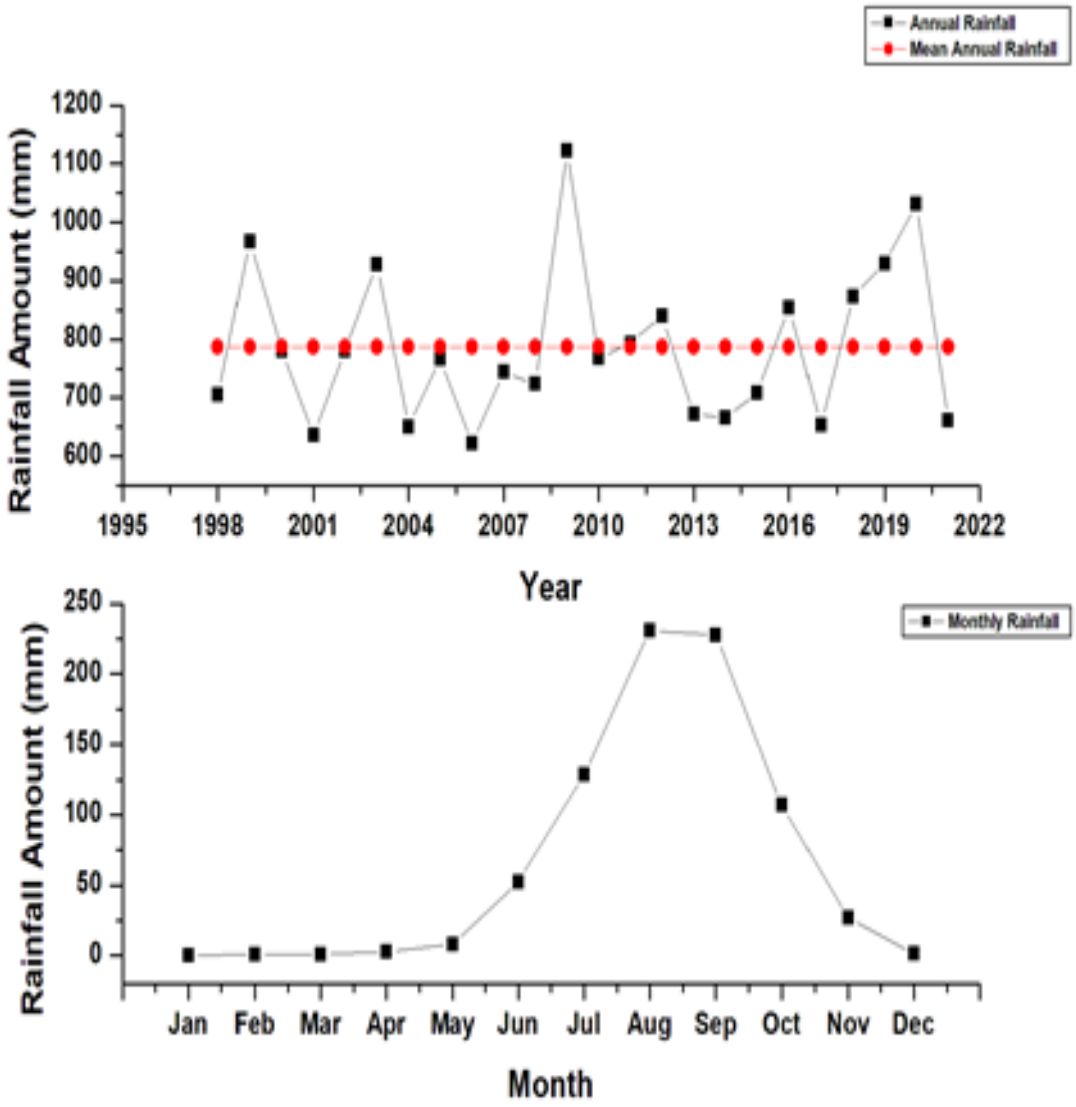

Figure 4.25**:** Annual and monthly rainfall distribution at IER_Cinzana (ERA5 data from 1998-2021)

The seasonal rainfall distribution was also looked into in all five stations and the two seasons consider are March, April, May (MAM) and June, July, and August (JJA). These periods are the pre-monsoon and monsoon periods in West Africa. Figure 4.26 shows the distribution of rainfall during MAM and JJA in Agoufou. JJA has received the highest amount of rainfall with a mean amount of 150mm and MAM has a mean amount of 4 mm. More rainfall is also seen in the JJA season in Banizoumbou with a mean seasonal rainfall amount of 250 mm. Like in Agoufou and Banizoumbou, Dakar and IER_Cinzana also receive more rainfall amount in the JJA season. MAM season being the pre-monsoon period in the shale region of West Africa has lesser rainfall amount. Seasonal rainfall distribution in Ilorin (figure 4.29) has shown that both MAM and JJA seasons receive rain but JJA receives more with a seasonal mean of 450 mm.

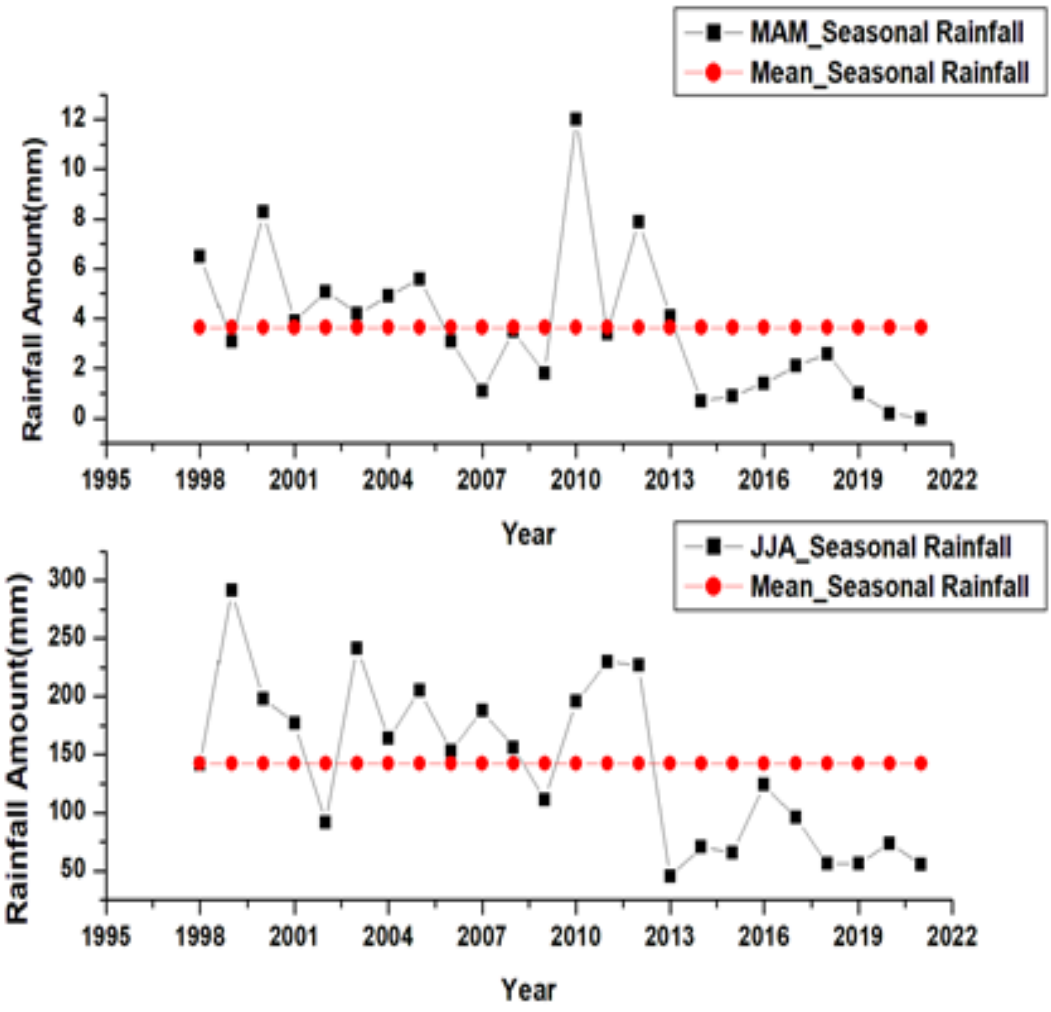

Figure 4.26**:** Seasonal rainfall distribution at Agoufou (ERA5 data from 1998-2021)

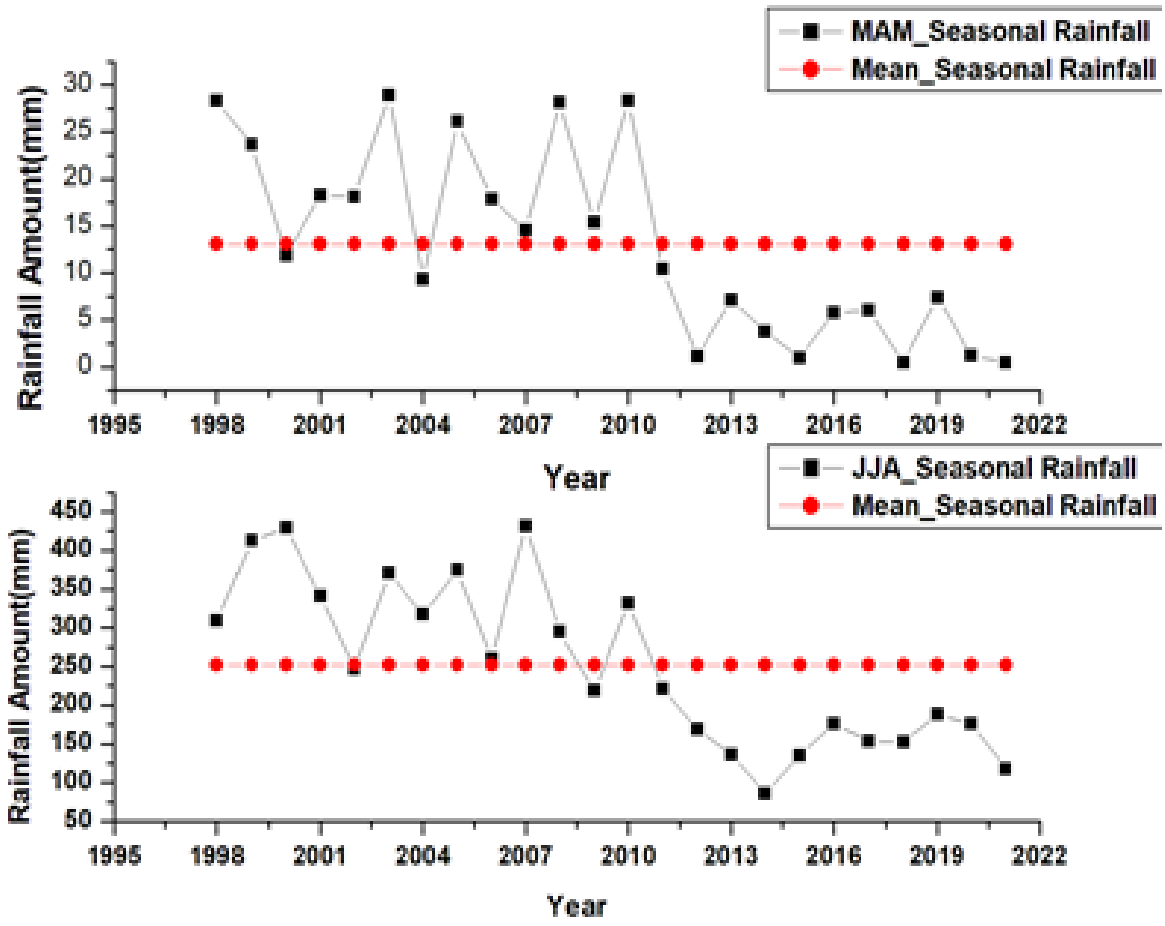

Figure 4.27**:** Seasonal rainfall distribution at Banizoumbu (ERA5 data from 1998-2021)

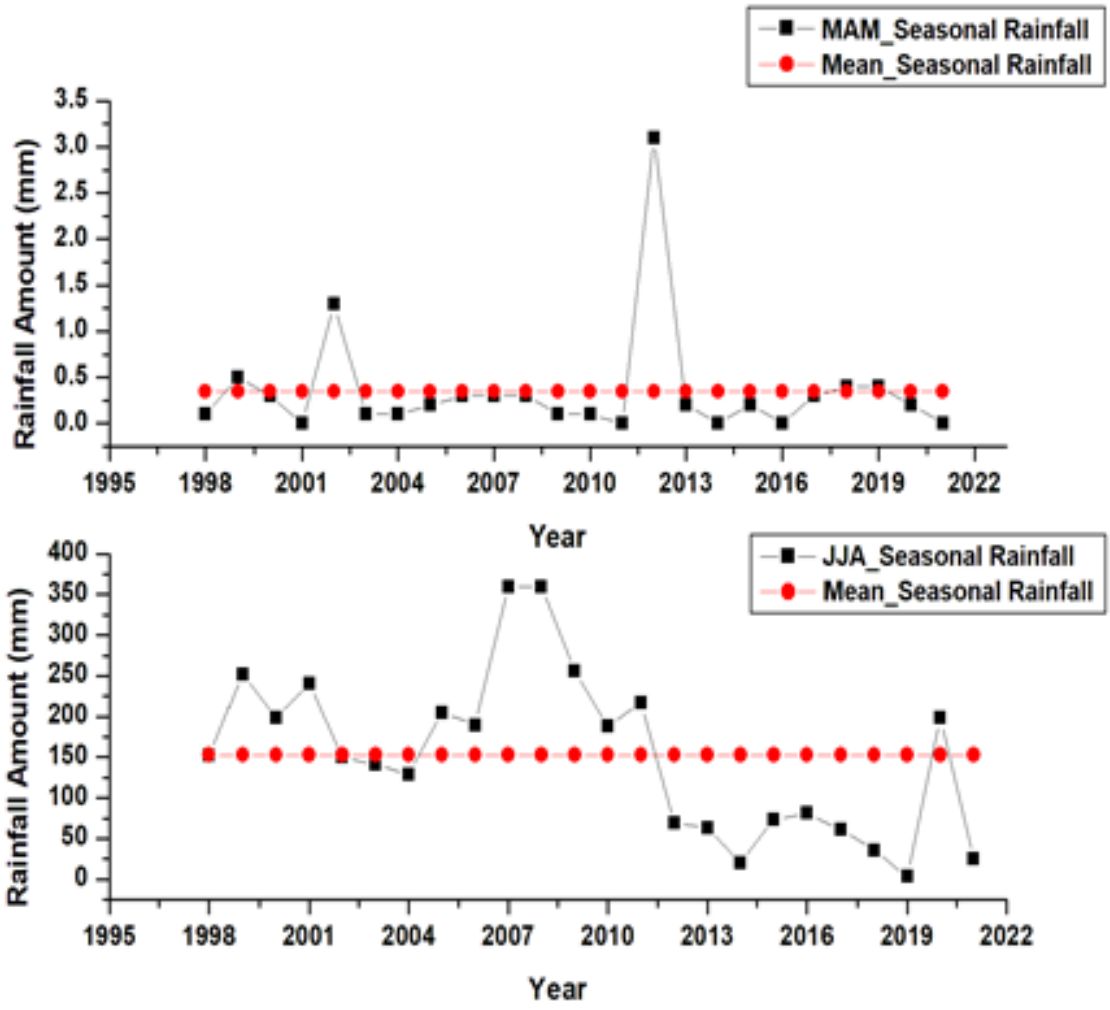

Figure 4.28**:** Seasonal rainfall distribution at Dakar (ERA5 data from 1998-2021)

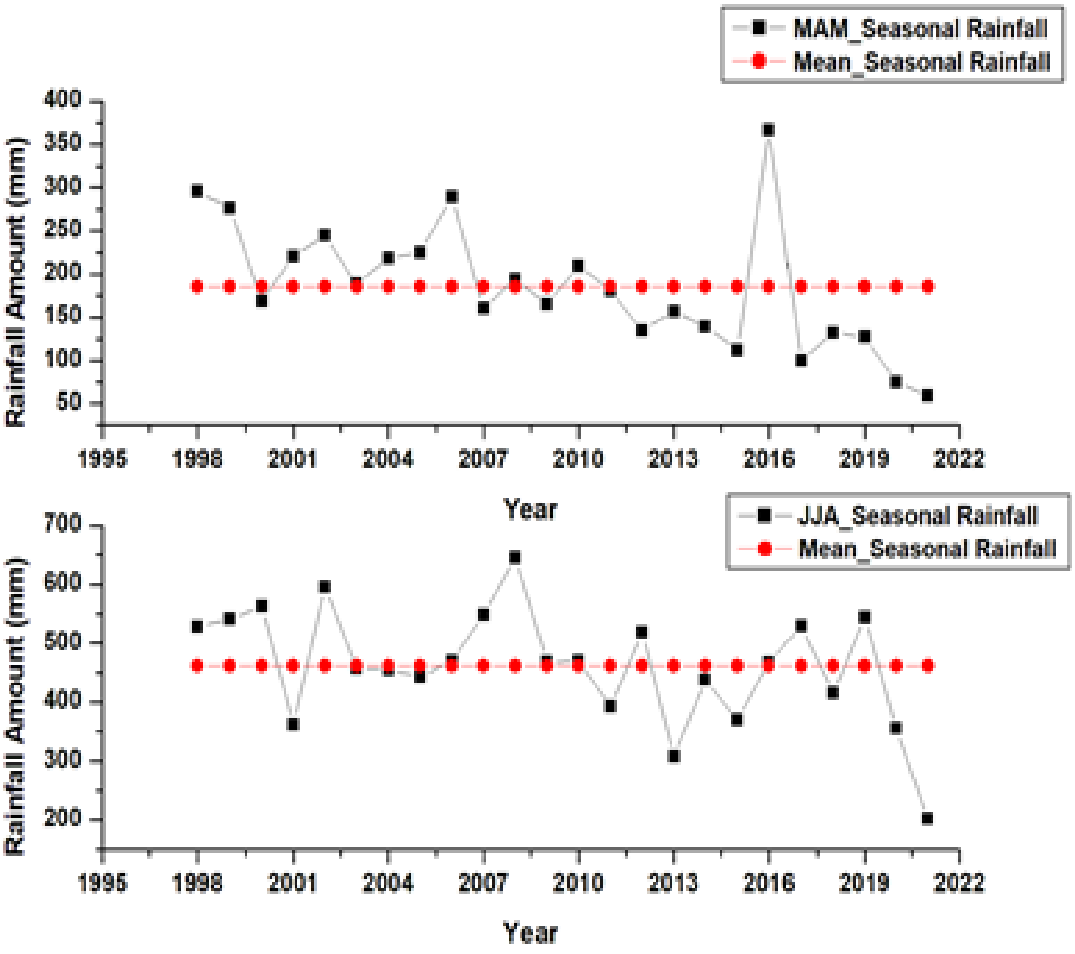

Figure 4.29**:** Seasonal rainfall distribution at Ilorin (ERA5 data from 1998-2021)

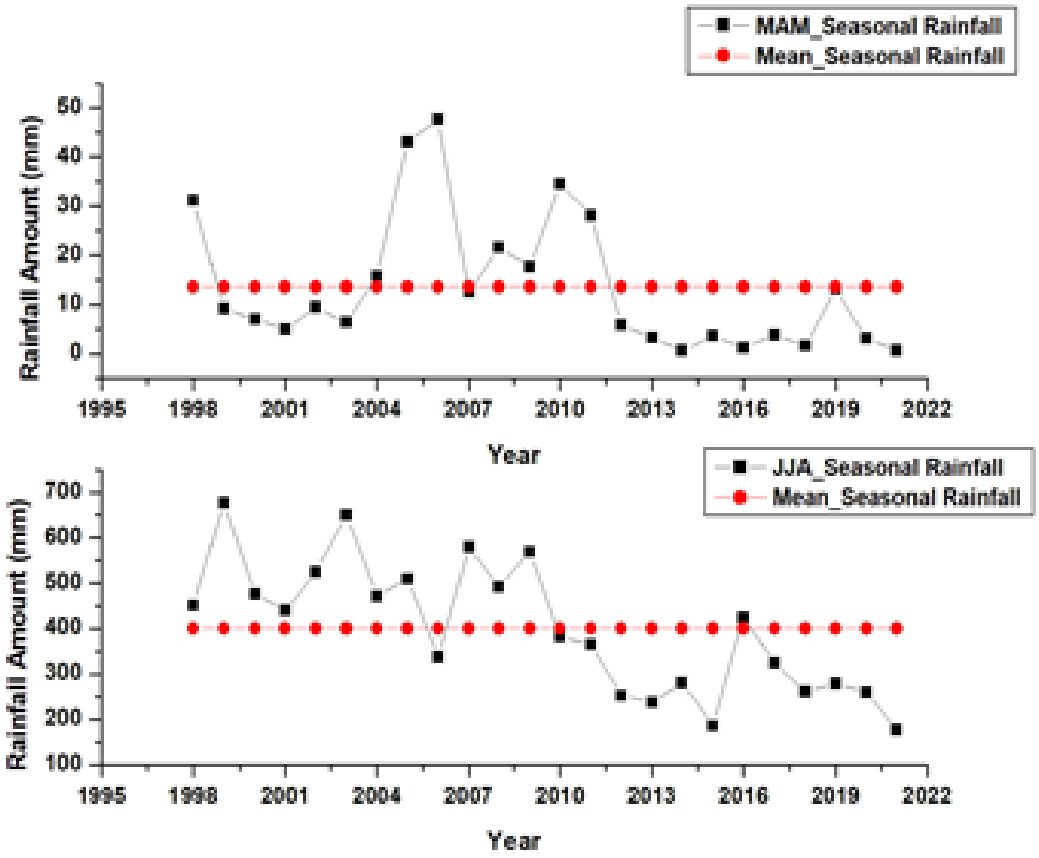

Figure 4.30**:** Seasonal rainfall distribution at IER_Cinzana (ERA5 data from 1998-2021)

4.2.2 Rainfall Variability

The amount of rainfall received in a given area varies from year to year and from season to season. The variations increase with a decrease in rainfall amount. High variability characterizes the arid and semi-arid regions where rainfall is low and erratic. The coefficient of variation (*CV)* was used to establish variations in annual and seasonal rainfall. Table 4.3 below showed the annual and seasonal *CV* for MAM and JJA seasons for each of the study sites.

Table 4.3: Mean Standard Deviation and Coefficient of Variation of Annual and Seasonal rainfall

Sites	Mean	Standard Deviation	Coefficient of variation CV
	Annual Rainfall		
Agoufou	235.24	60.52	26%
Banizoumbou	450.53	90.21	20%
Dakar	387.33	93.15	24%
IER_Cinzana	786.75	133.56	17%
Ilorin	1039.96	162.38	16%
	MAM Season		
Agoufou	3.64	2.89	80%
Banizoumbou	13.07	10.07	77%
Dakar	0.35	0.64	77%
IER_Cinzana	13.63	13.81	101%
Ilorin	185.17	74.07	40%
	JJA Season		
Agoufou	142.21	70.57	50%
Banizoumbou	252.31	106.10	42%
Dakar	152.99	100.58	66%
IER_Cinzana	400.72	143.67	35%
Ilorin	462.18	98.51	21%

From table 4.3, Agoufou had a coefficient of variation of 26%. This means that annual rainfall over Agoufou varies by +/-26% from the mean of 235.24mm for the period under study. The *CV* for Banizoumbou was 20%, meaning annual rainfall over Banizoumbou varied by +/-20% from the mean of 450.53mm. Annual rainfall amount over Dakar varied +/-24% from the mean of 387.33mm whiles annual rainfall amount IER_Cinzana and Ilorin varied by +/-17% and +/-16% from the mean of 786.75mm and 1039.96mm respectively. The variation in rainfall amount was higher during the MAM and JJA seasons. The *CV* for Agoufou was 80% and 50%for MAM and JJA seasons respectively, and 77% and 42% for MAM and JJA seasons respectively for Banizoumbou. Dakar's seasonal rainfall amount varied from the mean of 0.35mm and 152.99mm by +/-182% and +/-66% respectively. The *CV* for IER_Cinzana was higher during the MAM season at 101% than JJA at 35%. The *CV* for Ilorin during the MAM season was 40% and 21% for the JJA season.

4.2.3 Dry, Normal, and Wet Years

Dry and wet climatic conditions meteorologically occur if the rainfall amount is below and above the long-term mean (normal condition) (Huho, 2017). From this definition, the 24 years (1998 to 2021) under study dry and wet conditions are 46% and 42% of the period in Agoufou, 46% and 46% in Banizoumbou, 50% and 46% in Dakar, 46% and 46% in Ilorin and 33% and 54% for IER_Cinzana. However, knowing the fact that 1mm rainfall amount below the mean does not mean a lead drought (dry) period. Therefore, in this study, a period of normal rainfall is included and defined as in Huho 2017. When rainfall was below two-thirds of the standard deviation from the mean ($\bar{x}$ - 2/3(SD)) dry (droughts) climatic conditions were considered to have occurred. When rainfall amount falls in between ($\bar{x}$ - 2/3(SD)) and ($\bar{x}$ + 2/3(SD)), normal

climatic conditions were considered, and when rainfall amount was above ($\bar{x}$ + 2/3(SD)) wet climatic condition were considered. Annual rainfall analysis in figures 11-15 have shown that normal climatic conditions were more spread-out in 4 out of the 5 stations throughout the study period, Agoufou, Banizoumbou, Ilorin, and IER_Cinzana had 42%, 38%, 50%, and 50% respectively. Dakar had a 33% normal climatic condition for the study, which is a bit low compared to 38% dry condition. Wet climatic condition is the least frequently occurring condition in Banizoumbou, Dakar, and IER_Cinzana with 29%, 29%, and 21% respectively of the study period. The occurrence of wet and dry conditions was both 25% in Ilorin during the study period. Agoufou's wet and dry climatic conditions were 33% and 25% respectively. The normal and wet climatic conditions, which are favorable for crops growth, accounted for 75%, 67%, 62%, 75%, and 71% of the study period in Agoufou, Banizoumbou, Dakar, Ilorin, and IER_Cinzana respectively. While the dry (drought) conditions only accounted for 25%, 33%, 38%, 25%, and 29% of the study period in Agoufou, Banizoumbou, Dakar, Ilorin, and IER_Cinzana respectively.

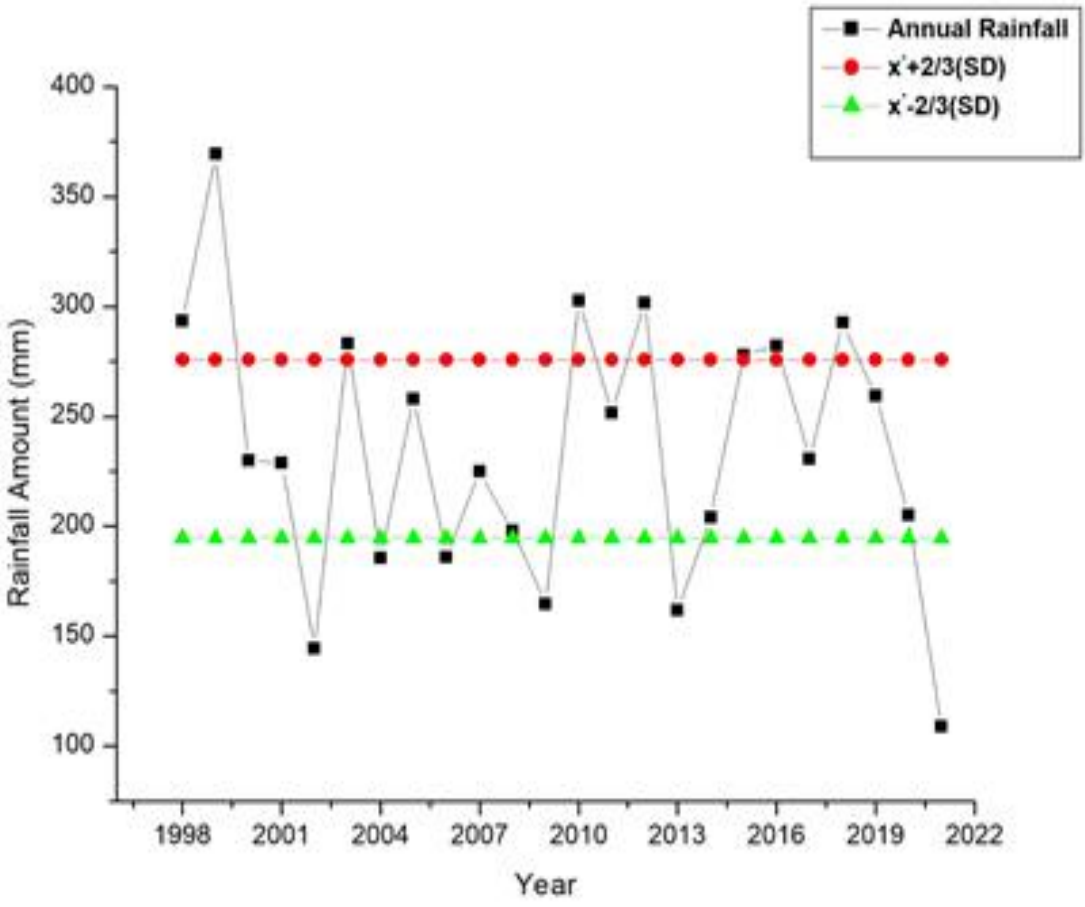

Figure 4.31: Drought, normal and wet years in Agoufou from 1998-2021

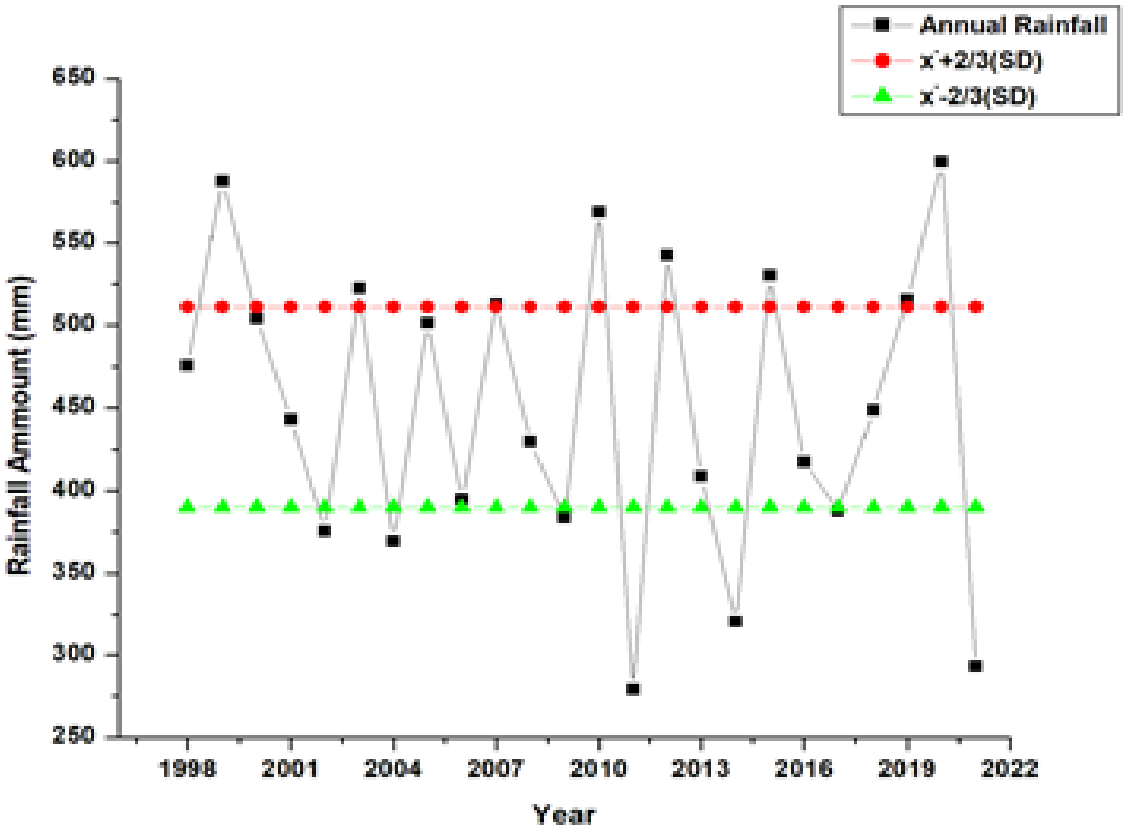

Figure 4.32: Drought, normal and wet years in Banizoumbou from 1998-2021

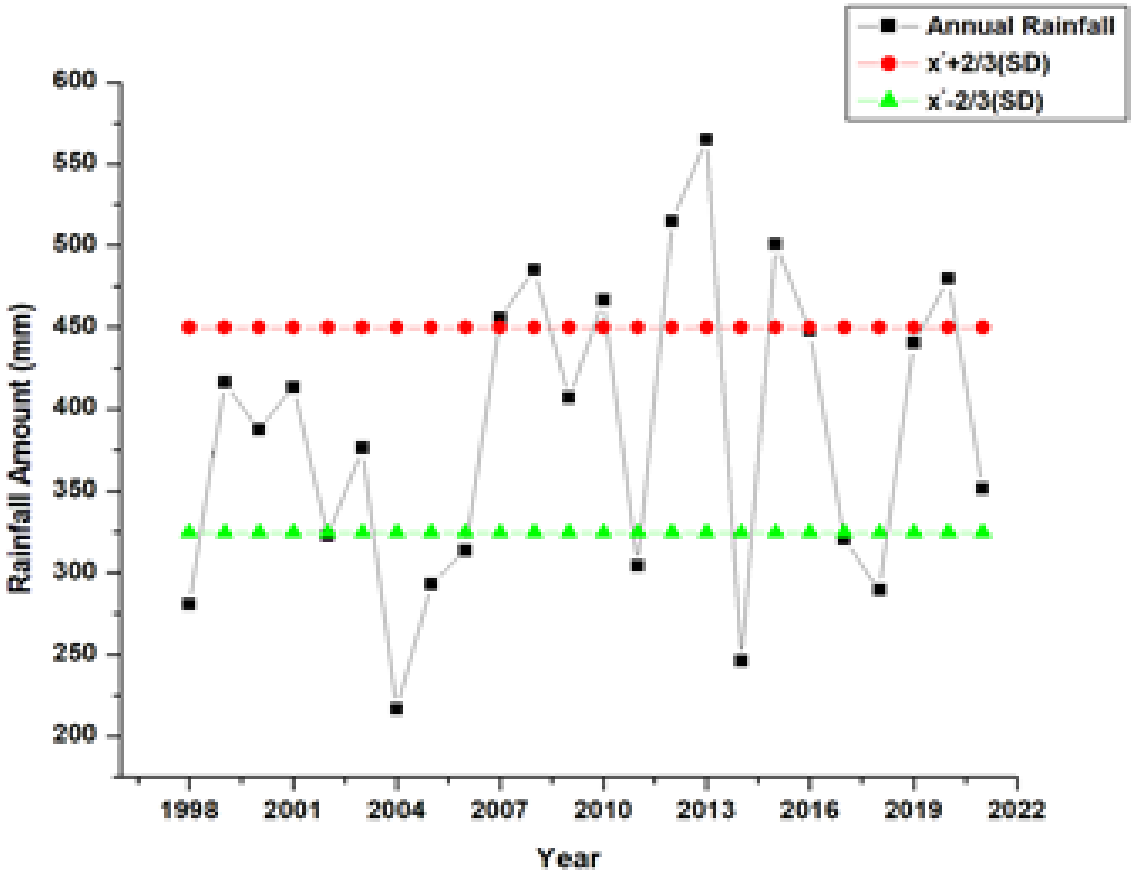

Figure 4.33: Drought, normal and wet years in Dakar from 1998-2021

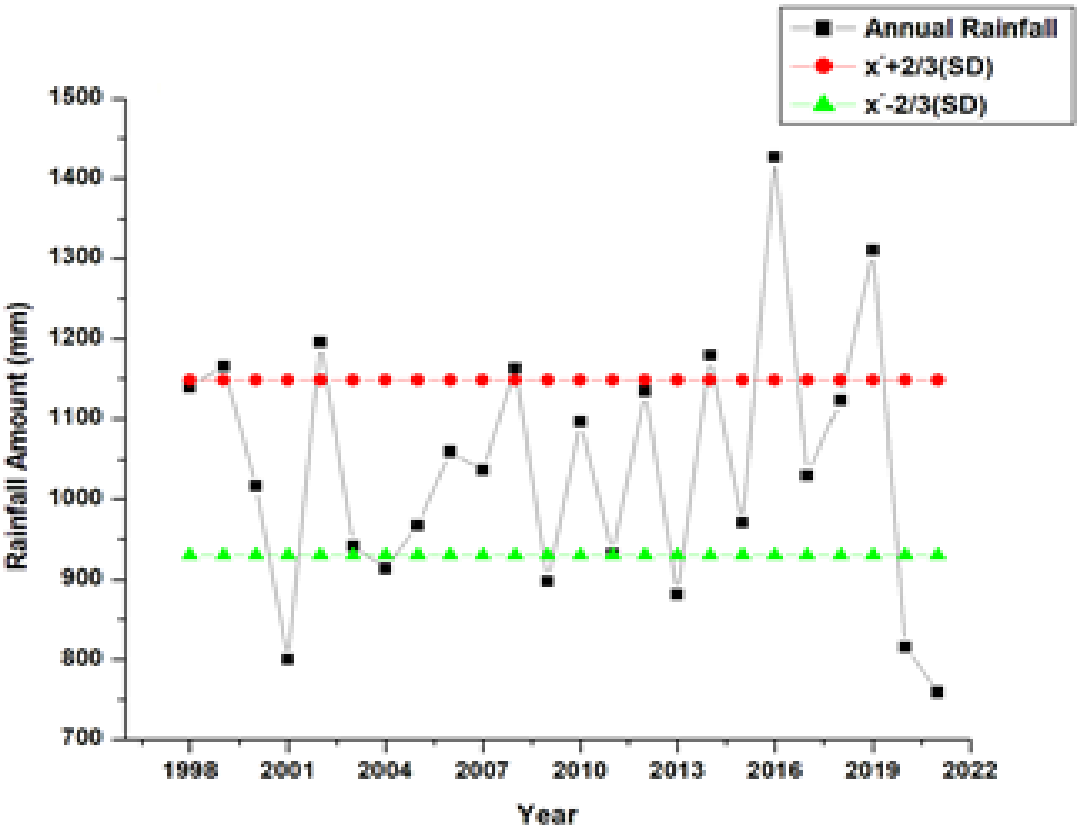

Figure 4.34: Drought, normal and wet years in Ilorin from 1998-2021

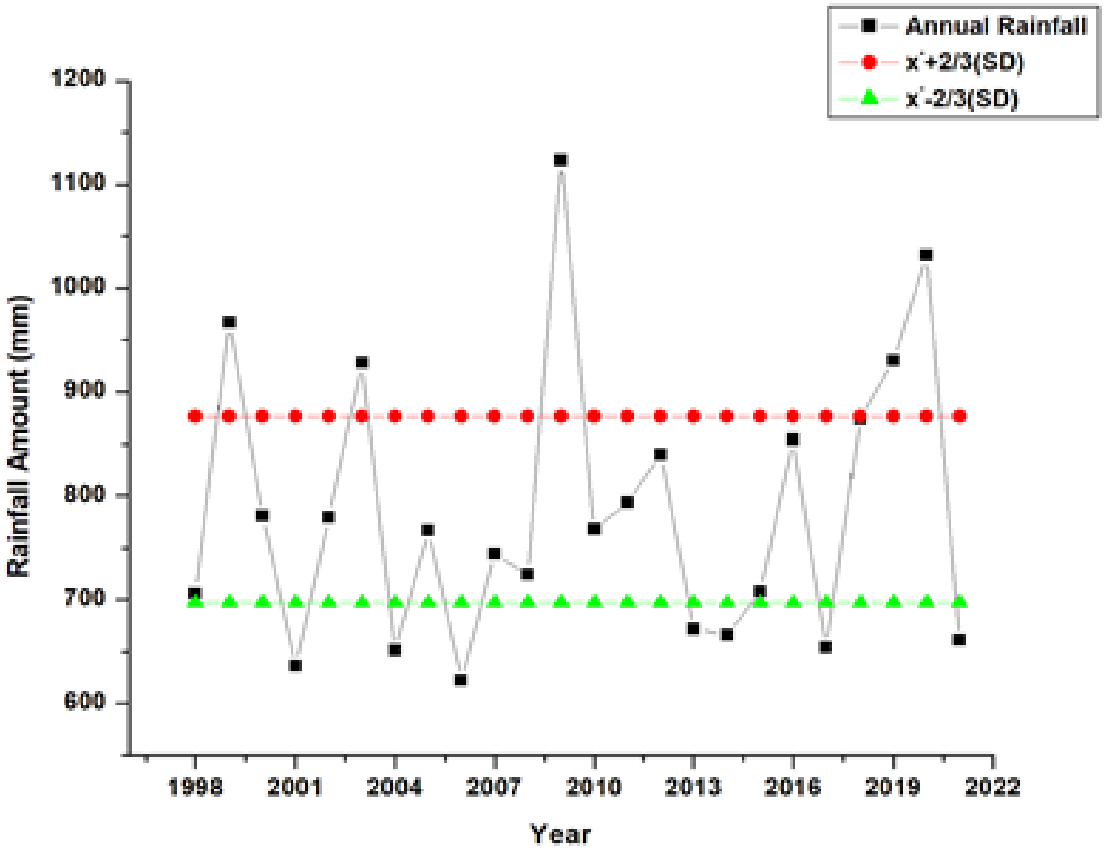

Figure 4.35: Drought, normal and wet years in IER_Cinzana from 1998-2021

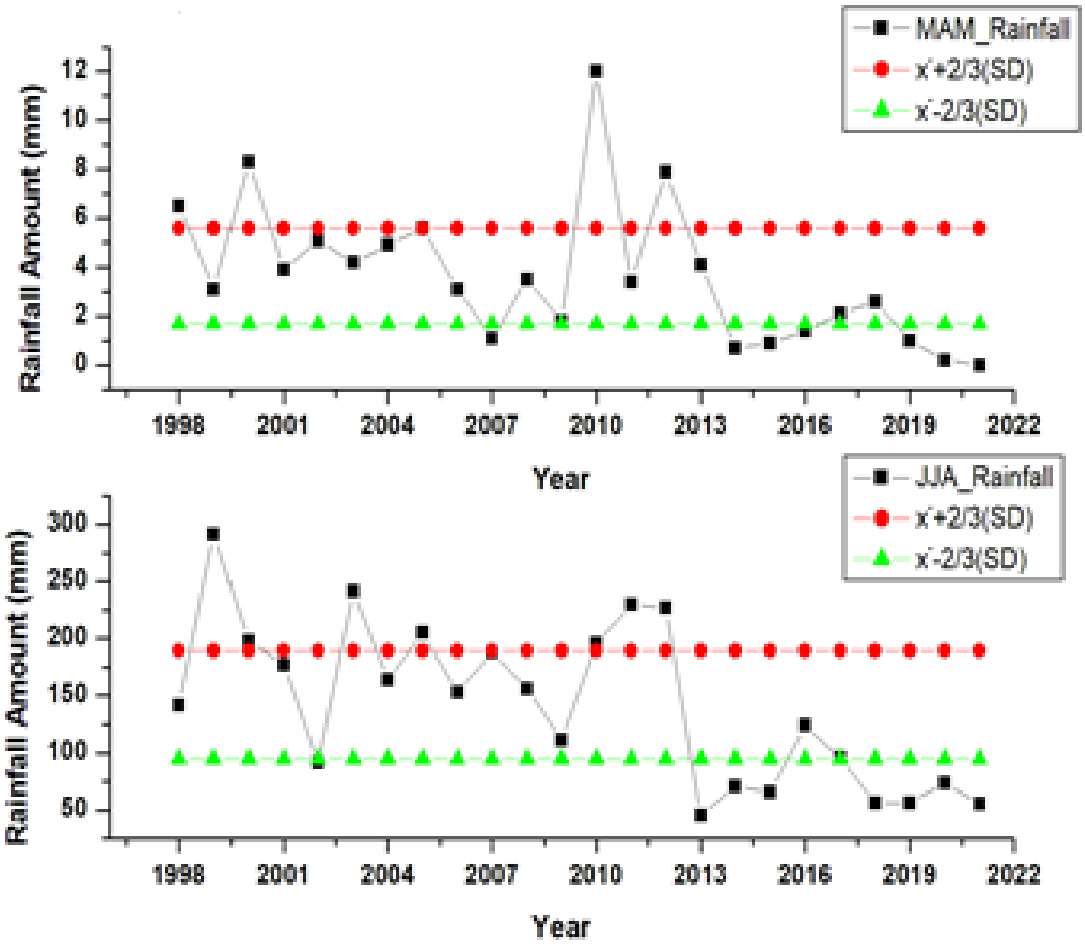

Figure 4.36: Drought, normal and wet seasons in Agoufou from 1998-2021

Seasonal rainfall in Agoufou was mainly normal climatic conditions as shown in figure 4.36. MAM and JJA seasons were 50% and 38% of the study period, experience normal climatic conditions. The frequency of wet climatic conditions for both the MAM and JJA season were 16% and 29% of the study period and Agoufou experienced 29% and 33% dry climatic conditions during the study period for the MAM and JJA season respectively. In both wet and normal conditions, Agoufou experiences 66% of the study period for the MAM season and 67% of the study period for the JJA season.

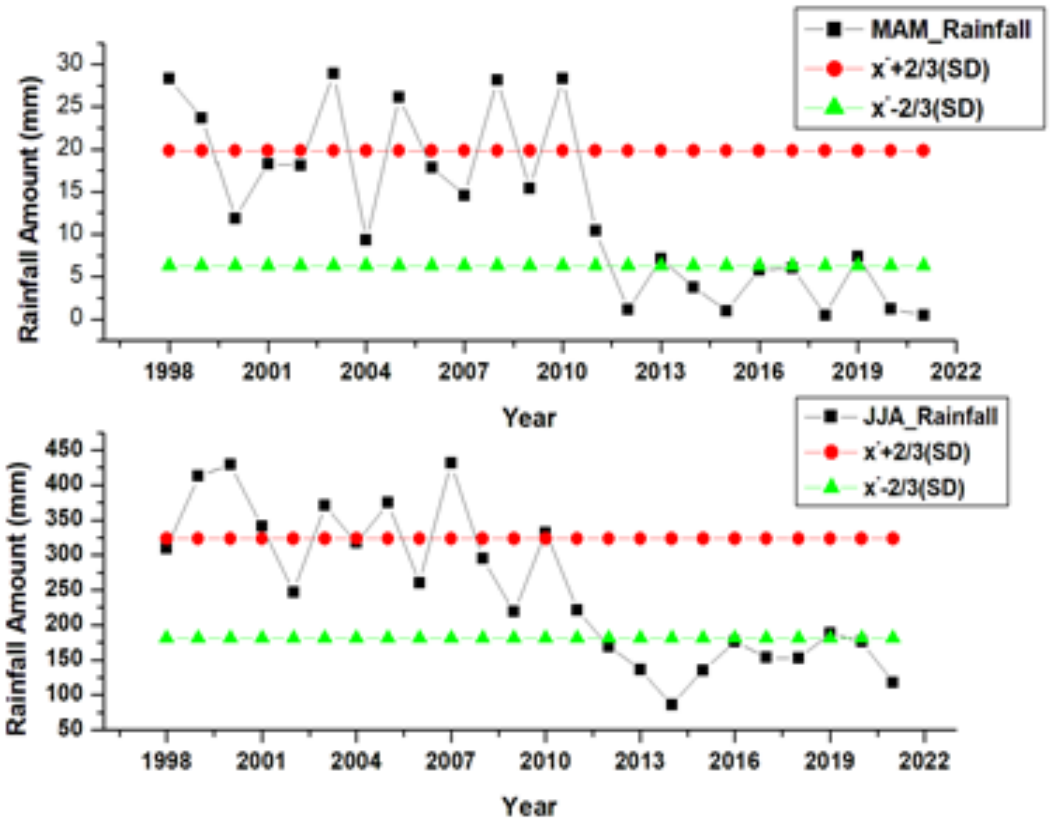

Figure 4.37: Drought, normal and wet seasons in Banizoumbou from 1998-2021

Seasonal rainfall in Banizoumbou in figure 4.37**,** shows that 42% of the study period for the MAM season experience normal climatic conditions and 33% of the study period for the JJA season. The dry climatic condition experienced in the MAM season and JJA season were 33% and 38% of the study period respectively most of which was during the year 2012 to 2021. The frequency of wet climatic conditions for both MAM and JJA seasons was 25% and 29% of the study period in Banizoumbou. Wet and normal climatic conditions combine in Banizoumbou during MAM and JJA were 67% and 62% of the study period respectively.

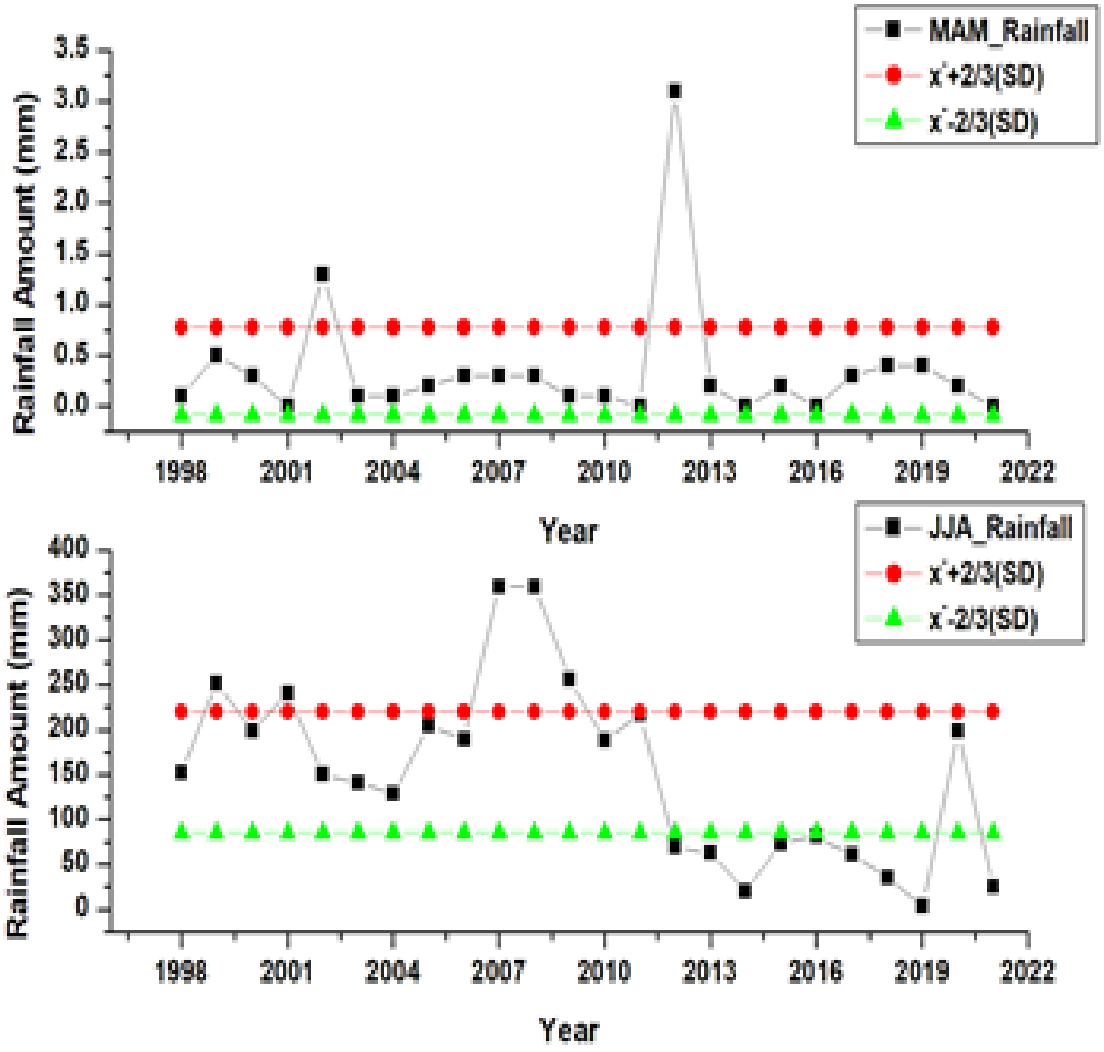

Figure 4.38: Drought, normal and wet seasons in Dakar from 1998-2021

From figure 4.38, Dakar has not experienced dry climatic condition during the study period in the MAM season but 38% of the study period were dry in the JJA season. 95% and 42% of the study period were normal climatic conditions experienced in the MAM season and JJA season respectively in Dakar, and only 8% of the study period experience wet climatic conditions in the MAM season and 21% of the study period in JJA season. Wet and normal climatic conditions together, Dakar experience 100% and 63% of the study period during the MAM and JJA season. MAM season in Ilorin had largely experienced normal climatic conditions with 54% of the study period, 25% of the study period experiencing dry climatic conditions, and 21% of the study period wet climatic conditions as shown in figure 4.39**.** Normal climatic conditions were 42% of the study period in Ilorin for the JJA season, and dry and wet climate conditions were 21% and 37% of the study period respectively. For both wet and normal climatic conditions, Ilorin experiences 75% and 79% of the study period respectively.

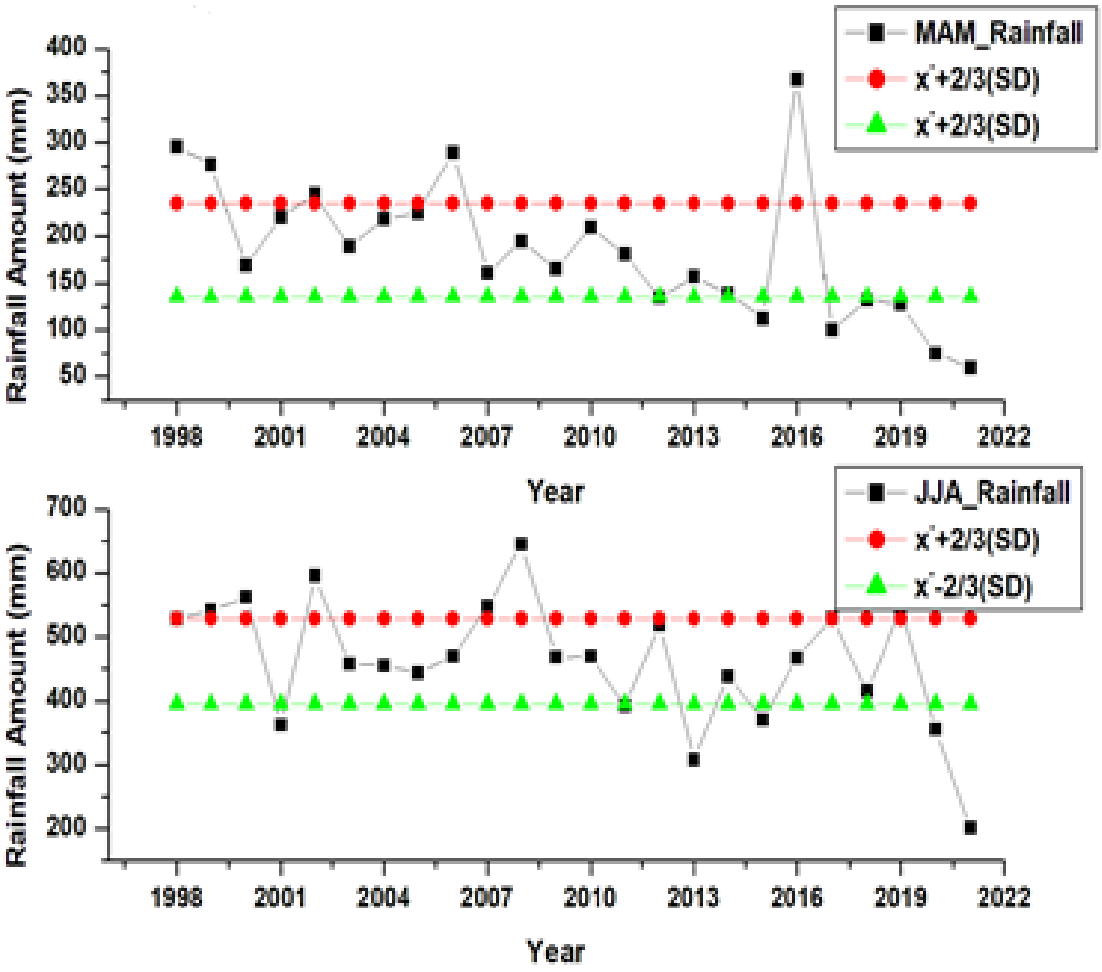

Figure 4.39: Drought, normal and wet seasons in Ilorin from 1998-2021

In IER_Cinzana as shown in figure 4.40, the MAM and JJA seasons experienced normal climatic conditions of rainfall with 46% and 42% respectively for the period under study. Dry climatic conditions for both seasons were 33% and 25% respectively. Wet climatic condition ranges between 21% and 33% of the study period during the MAM and JJA season respectively. Wet and normal climatic conditions together, IER_Cinzana experienced 67% and 75% of the study period during the MAM and JJA season.

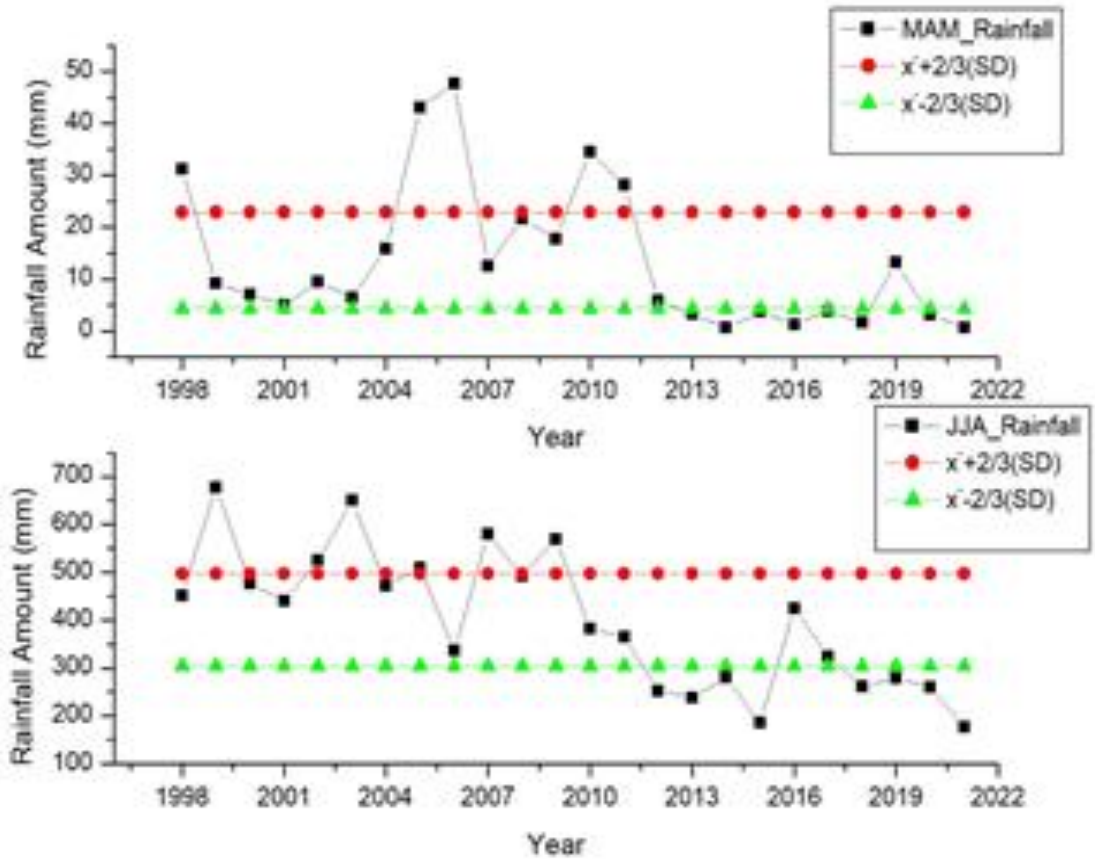

Figure 4.40: Drought, normal and wet seasons in IER_Cinzana from 1998-2021

4.2.4 Time Series Analysis

To detect whether there were trends in the time series for both annual and seasonal rainfall, the Mann-Kendal trend test was used. The null hypothesis *H0*, which states that the rainfall data in the time series had no trend, was tested at a 95% confidence level against the alternative hypothesis *H1*, which states that there was a trend in the series. Where the *p-value* was less than alpha = 0.05, the *H0* was rejected indicating that there was a trend in the time series of rainfall data. Where the *p-value* was greater than 0.05, the *H0* was accepted indicating that the trend was not detected.

Table 1 shows that the *p-values* were less than the alpha (0.05) for all the stations under the study are greater than the alpha (0.05). Therefore, the H_0 was accepted, meaning no trend was detected in the annual rainfall data time series. In MAM seasonal rainfall data, the p-value for all the stations under study was less than alpha (0.05) except Dakar which has a *p-value* greater than alpha (0.05). Therefore, the *H0* was rejected for Agoufou, Banizoumbou, IER_Cinzaza, and Ilorin station but not rejected for Dakar. This implies that there was no trend detected in the time series of MAM seasonal rainfall data for Dakar station but there was a trend detected in the time series of MAM seasonal rainfall for Agoufou, Banizoumbou, IER_Cinzaza, and Ilorin station.

The *p-value* was greater than the alpha (0.05) for the Ilorin station in the JJA season and less than the n alpha (0.05) for Agoufou, Banizoumbou, IER_Cinzaza, and Dakar stations. This implies that no trend was detected in the time series of JJA seasonal rainfall data for Ilorin and there was a trend detected in the time series of JJA seasonal rainfall for Agoufou, Banizoumbou, IER_Cinzaza, and Dakar station.

Table 4.4: Mann Kendall time series trend analysis for annual and seasonal rainfall

Sites	Mann Kendall Statistic (S)	Kendall's Tau	Var(S)	p-value (two-tailed)	Alpha (α)	Test Interpretation
Annual Rainfall						
Agoufou	-22	-0.08	1625.33	0.61	0.05	Accept H_0
Banizoumbu	-18	-0.065	1625.33	0.68	0.05	Accept H_0
Dakar	-42	0.152	1625.33	0.31	0.05	Accept H_0
IER_Cinzana	24	0.087	1625.33	0.57	0.05	Accept H_0
Ilorin	-8	-0.029	1625.33	0.86	0.05	Accept H_0
MAM_Seasonal Rainfall						
Agoufou	-133	-0.483	1624.33	0.001	0.05	Reject H_0
Banizoumbu	-160	-0.582	1623.33	0.001	0.05	Reject H_0
Dakar	-13	-0.051	1565.66	0.762	0.05	Accept H_0
IER_Cinzana	-98	-0.355	1625.33	0.016	0.05	Reject H_0
Ilorin	-170	-0.616	1625.33	<0.0001	0.05	Reject H_0
JJA_Seasonal Rainfall						
Agoufou	-128	-0.464	1625.33	0.002	0.05	Reject H_0
Banizoumbu	-158	-0.572	1625.33	<0.0001	0.05	Reject H_0
Dakar	-119	-0.432	1624.00	0.003	0.05	Reject H_0
IER_Cinzana	-156	-0.565	1625.33	0.000	0.05	Reject H_0
Ilorin	-78	-0.283	1625.33	0.056	0.05	Accept H_0

4.3 ANALYSIS OF WRF-CHEM MODEL OUTPUT

This section discussed the model output by comparing the model output data with observation data to evaluate how well Biomass Burning Aerosol (BBA) radiative effects affect rainfall over West Africa.

4.3.1 Comparisons of Convective Rainfall from ERA5 with Simulated Convective Rainfall

RainC in WRF-Chem output is the accumulated total cumulus precipitation, which is also referred to as convective precipitation. Below shows the comparison of monthly and seasonal precipitation from ERA5 as observed (OBS) and the two WRF-Chem simulated outputs; convective precipitation without radiative effect (WORad) and convective precipitation with radiative effect (WRad).

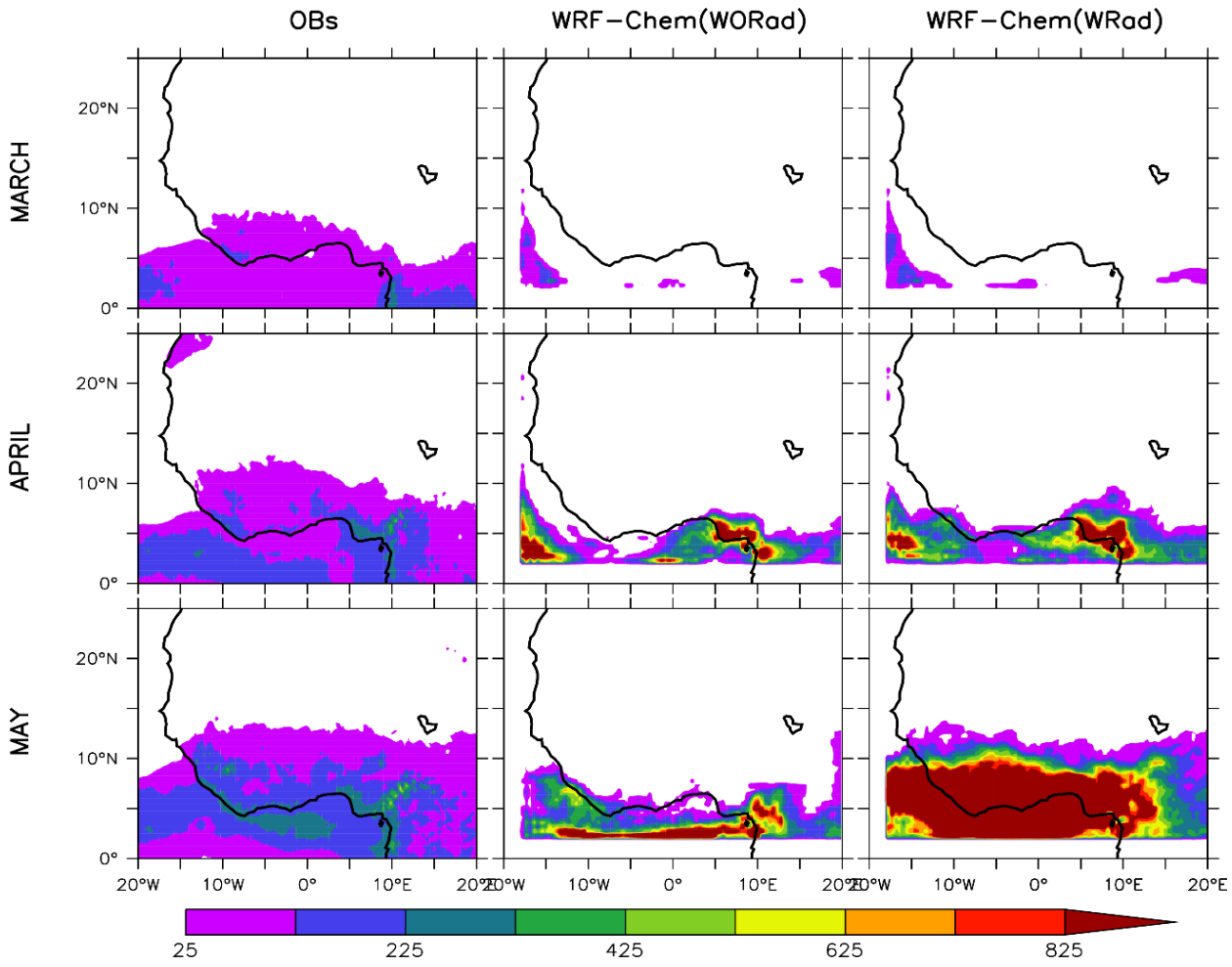

Figure 4.41: Convective rainfall distribution from ERA5, WRF-Chem (WORad and WRad) for the months of March, April, and May 2012

In figure 4.41, some convective activities were recorded under OBs for the month of March over the coast and the continent. They are recorded over the coastal cities of Liberia, Togo towards Nigeria. There was no convective activity observed over the continent of West Africa for both simulated outputs. The month of April has shown slit convective activities over the Atlantic Ocean on the 5^{o}N axis and the coastal cities of Nigeria and Cameroon for simulation WORad. Simulation WRad captured activities over similar locations but it has moved further inland of Nigeria and Cameroon along the axis of the Central African Republic. The OBs also showed activities over both the coast and inland along the 10^{o}N and below. Higher convective activities were captured under simulation WORad for the month of May. The activities were observed over the coast below the 5^{o}N and 0^{o} axes. It has moved a bit inland of Cameroon. Under simulated WRad, heavy convective activities were shown. The activities were captured over both the coast and the continent. They were seen over the Gulf of Guinea, on the axes of Sierra Leone and the Central African Republic, which have moved further inland of the countries along those axes to the 10^{o}N axis. The convective activities under WRad were heavier and more spared out over the coast and inland than under WORad.

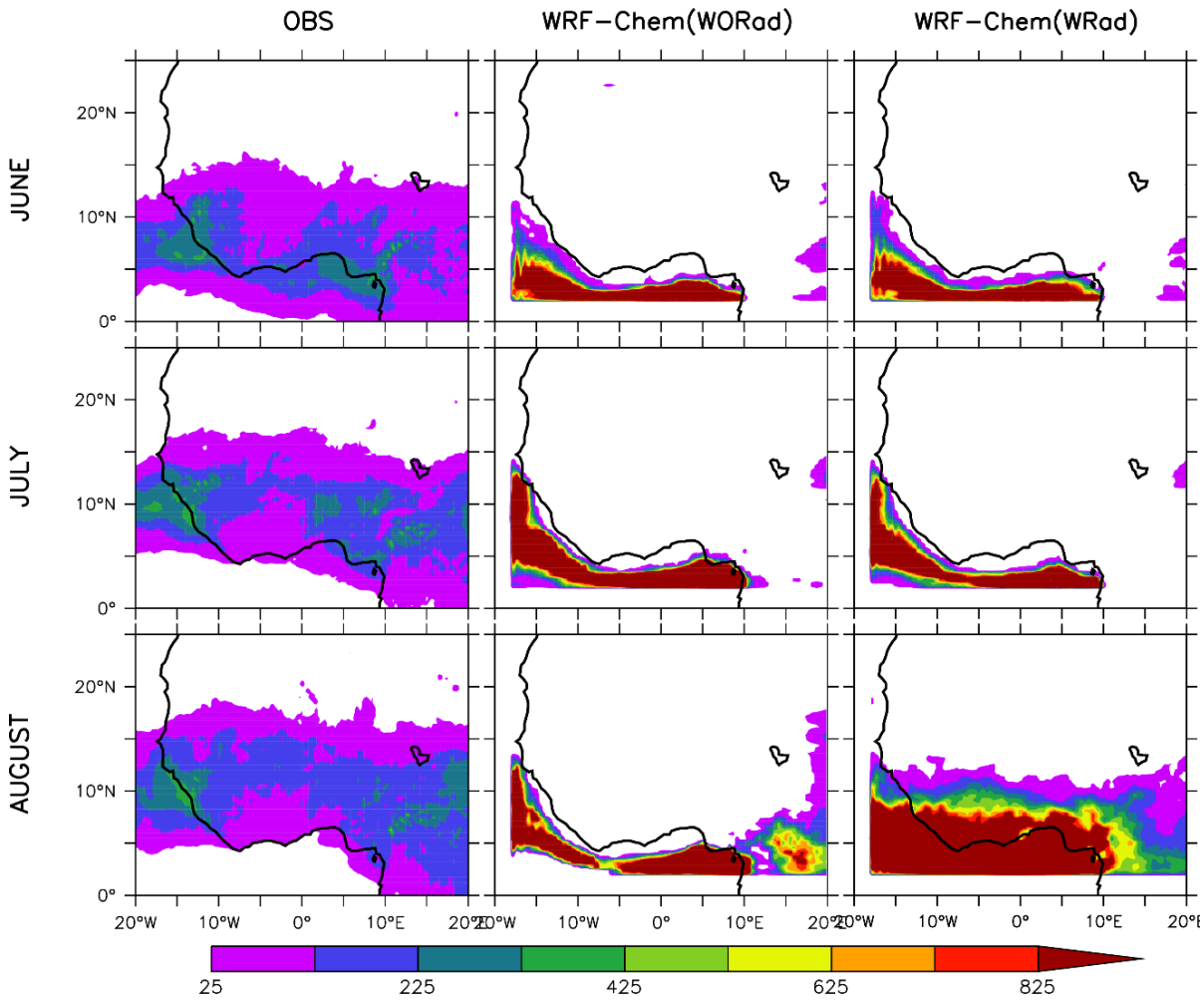

Figure 4.42: Convective rainfall distribution from ERA5, WRF-Chem (WORad and WRad) for the months of June, July, and August 2012

Figure 4.42 captured convective activities in all the months under study (June, July, and August). The convective rainfall recorded under OBs was all over the continent of the study area between the axes of 5^{o}N and 20^{o}N for all the months. The activities were over the Atlantic Ocean for all the months and under both simulations expect the month of August under simulated output WRad. There were activities observed over the continent along the coastline and over the cities along the 10^{o}N axis. There were silt differences in convective activities shown for the months of June and July under WORad and WRad. The WRad convective was heavier than the convective under WORad. The activities for July under both WORad and WRad were captured over the coastline from Senegal, Liberia to Nigeria. No activities were observed over the inland. The month of August has shown under WORad activities of convective too but was observed only over the coast of the study area. They were captured over the coast between the axes of around 3^{o}N and 15^{o}N. Convective activities were also seen inland of Cameroon.

4.3.2 Comparison of Seasonal Convective Rainfall from ERA5 with Simulated Convective Rainfall

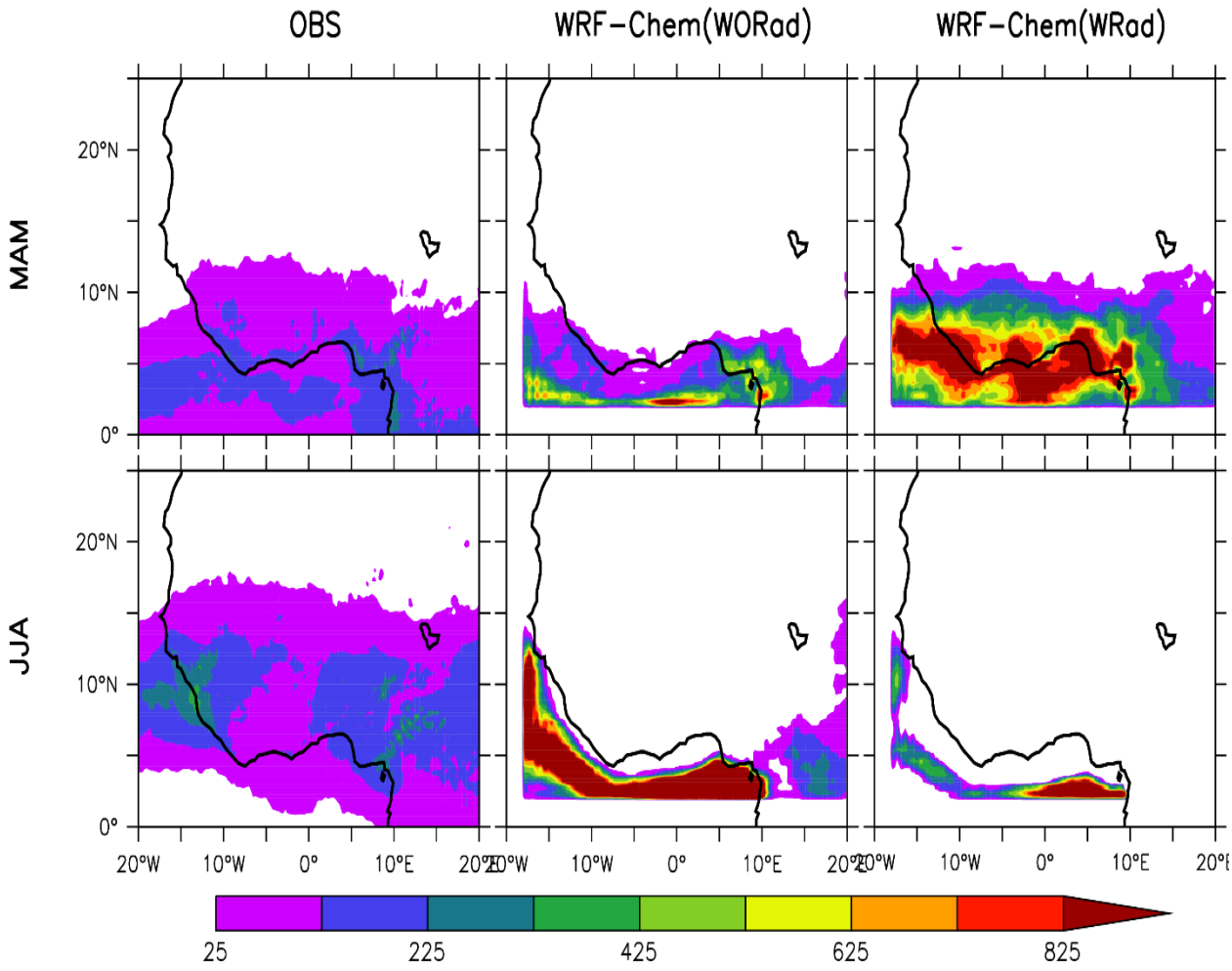

Figure 4.43: Convective rainfall distribution from ERA5, WRF-Chem(WORad and WRad) for MAM and JJA seasons 2012

Seasonal convective activities over West Africa are shown in figure 4.43 for the MAM and JJA. For the MAM season, strong convective activities were captured under WRad over the Gulf of Guinea on the Sierra Leone axis to the east over the Atlantic. The activities move further inland over the countries and cities under 15^{o}N and the activities die out as they move inland. The convective observed under WORad were not heavy and were observed over the Atlantic Ocean below the 10^{o}N axis to the coast of Cameroon and part of Nigeria. Part of the inland of Cameroon also experiences the activities. Comparing the simulation outputs with the observed, the number of convective activities was underestimated for WORad and overestimated for WRad for the MAM season. Convective activities for the JJA season were heavier under WORad over the coast of Nigeria on the axis of the Central African Republic. The activities under WRad were observed over the Atlantic. No activities were captured over the continent

4.3.3 Evaluating Biomass-Burning Aerosol Radiative Effects on Convective Rainfall

To evaluate the effect of aerosol radiative effect on convective activities over the study area, the difference between simulated output WORad and simulated output WRad was calculated (hereafter called differences) for each month and season.

The differences under March have not recorded any convective activities both over the coast and over the land. Convective activities were captured under April over the coastline of Ghana, Togo, and Nigeria and it moves a little bit inland over Nigeria. Differences for May have captured convective activities over both the coast and the continent. The activities were observed between the 0^{o}N and 15^{o}N axes and becomes less strong as it moves inland. The BBA radiative effect has been shown to increase the amount of convective rainfall for the months of April and May, while March has not shown any effect.

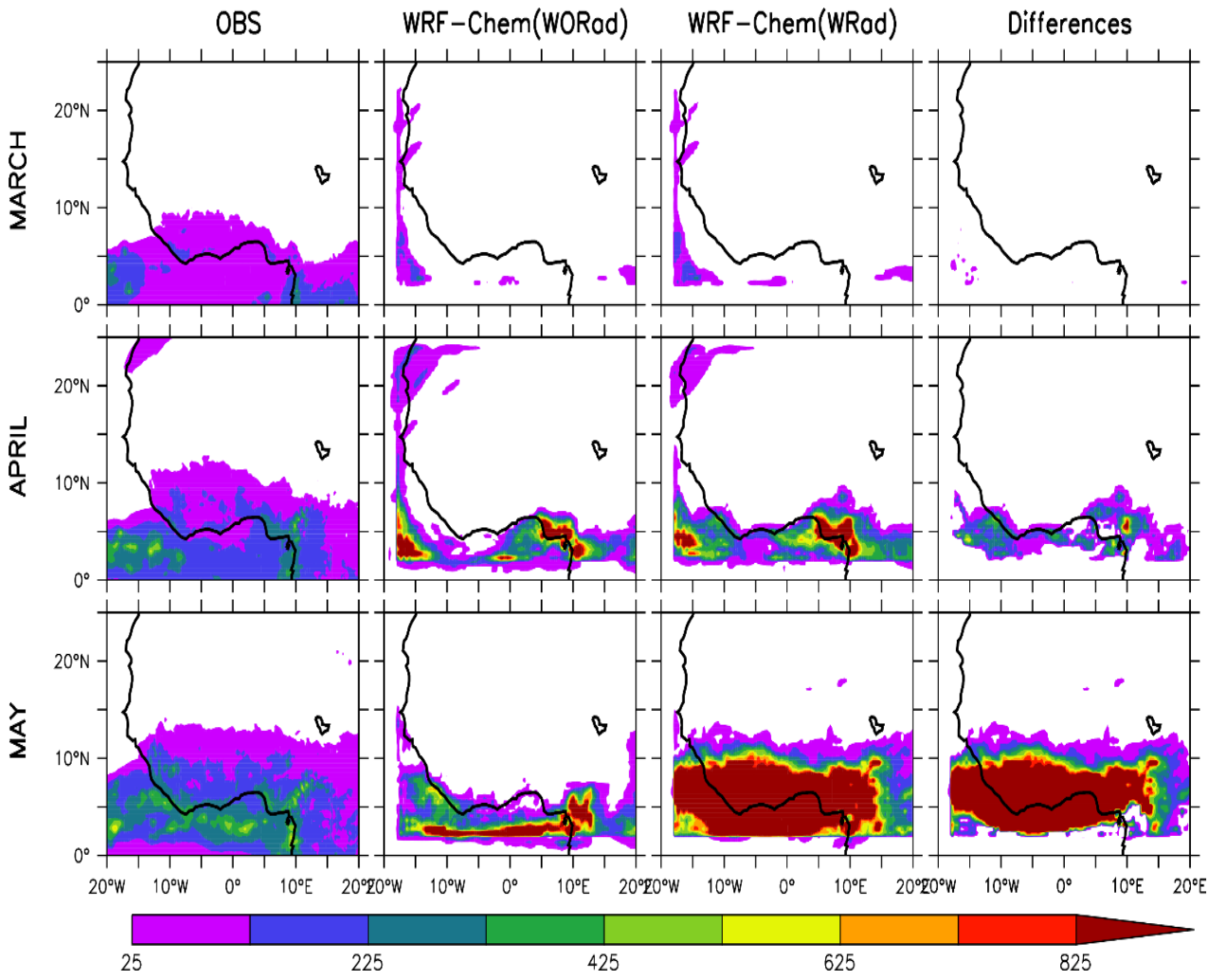

Figure 4.44: Convective rainfall distribution from ERA5, WRF-Chem (WORad and WRad) and Differences for the months of March, April, and May 2012

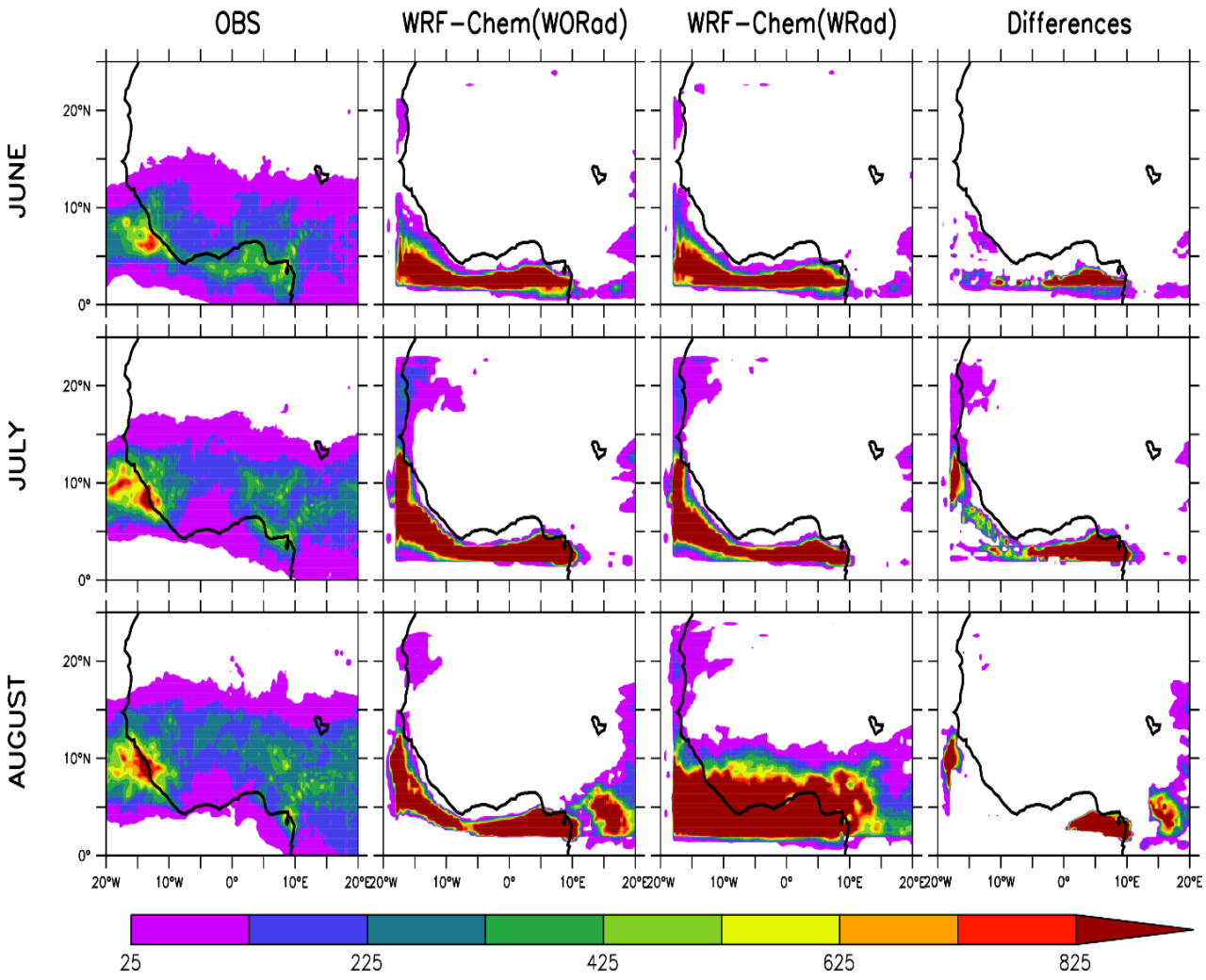

Figure 4.45: Convective rainfall distribution from ERA5, WRF-Chem (WORad and WRad) and Differences for the months of June, July, and August 2012

The differences between simulated WORad and WRad for the months of June, July, and August were shown in figure 4.45. Convective activities were observed in all the months. The activities for the month of June were observed over the coast on the axis of the Central African Republic. No convective activities were observed over the continent. The month of July observed convective activities over the coastline of Dakar down to the axis of the Central African Republic. No convective activities were recorded over the inland. The month of August has shown little or no activity under the difference.

The seasonal differences for MAM season has shown negative values. This simply means that the simulation output with BBA radiative effects have over estimated the convective rainfall amount by increasing during the MAM season. On the other hand, the JJA season have shown an under estimation of convective rainfall amount under the BBA radiative effect.

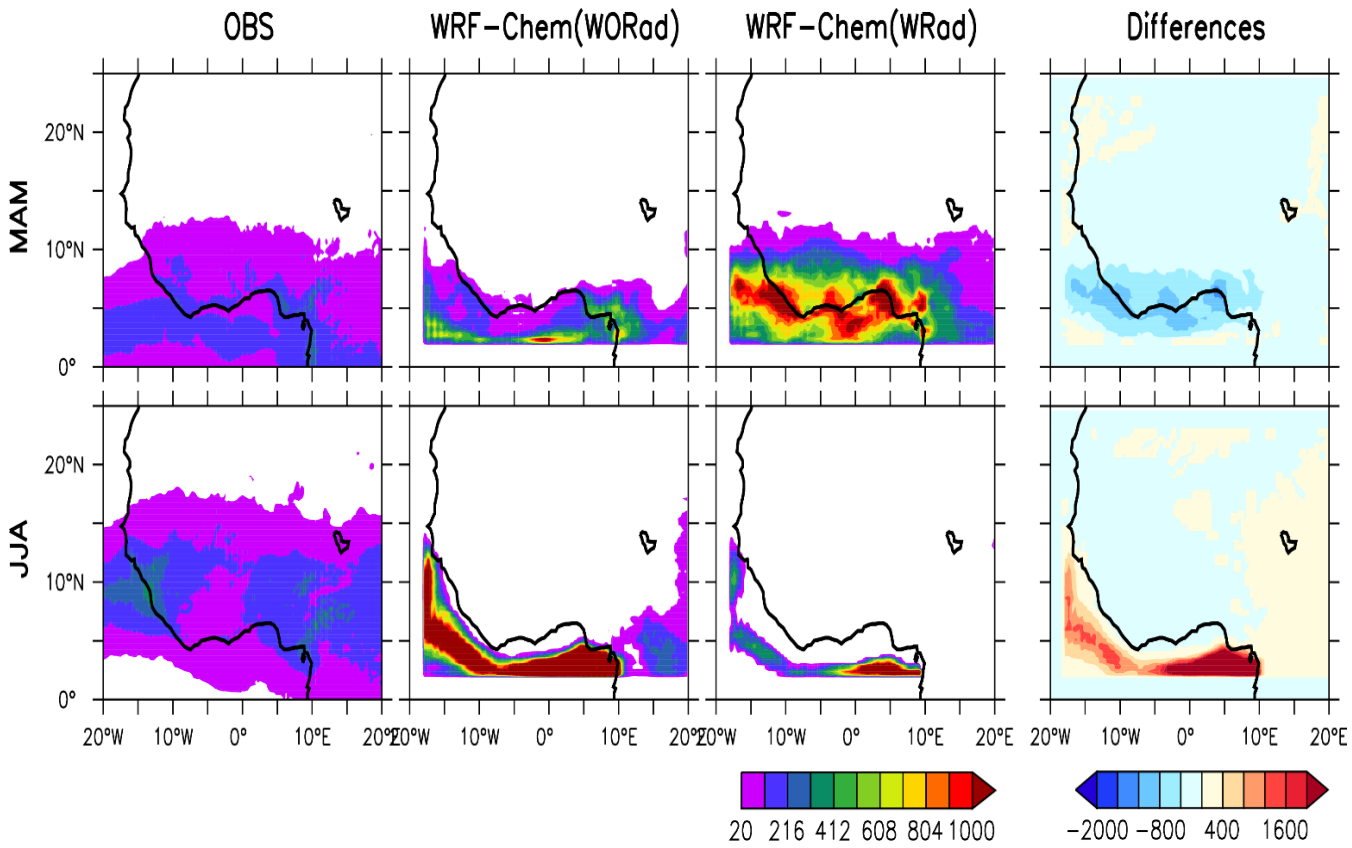

Figure 4.46: Seasonal convective rainfall distribution from ERA5, WRF-Chem (WORad and WRad) and Differences for MAM and JJA seasons, 2012

4.3.4 Comparisons of Total Rainfall from ERA5 with Simulated Total Rainfall

In comparison between the ERA5 (OBS) total rainfall and WRF-Chem output (WORad and WRad) for the months of March, April, and May, it can be observed that the simulated output of April was overestimated over the Atlantic but underestimated over the continent compared to the observe. These activities were recorded over the Atlantic Ocean, stretching the full length of the coast of West Africa through to that of the Central African Republic**.** The activities were also captured around the axes of Mauritania and Dakar, which were not present in the observed. The month of March under observation showed the presence of convective precipitation around the Gulf of Guinea on the Sierra Leone axis and to the coastal axis of the Central African Republic to the Atlantic. The activities further moved inland towards the 10^{o}N axis. The simulated output for the month of May under WORad observed rainfall over the coast, which was heavier than the one, recorded under OBS, but no activity was observed inland. Rainfall under WRad was overestimated in comparison to the OBS for both activities over the Atlantic and the continent. The result showed the simulated output captured heavy rainfall offshore on the Gulf of Guinea and the activities die off as they move further inland towards the 15^{o}N axis. This observation as recorded under the biomass radiative feedback mechanism differs from the output of the non-feedback mechanism. Hence, it can be deduced that biomass burning played a major role in the estimation of the rainfall system.

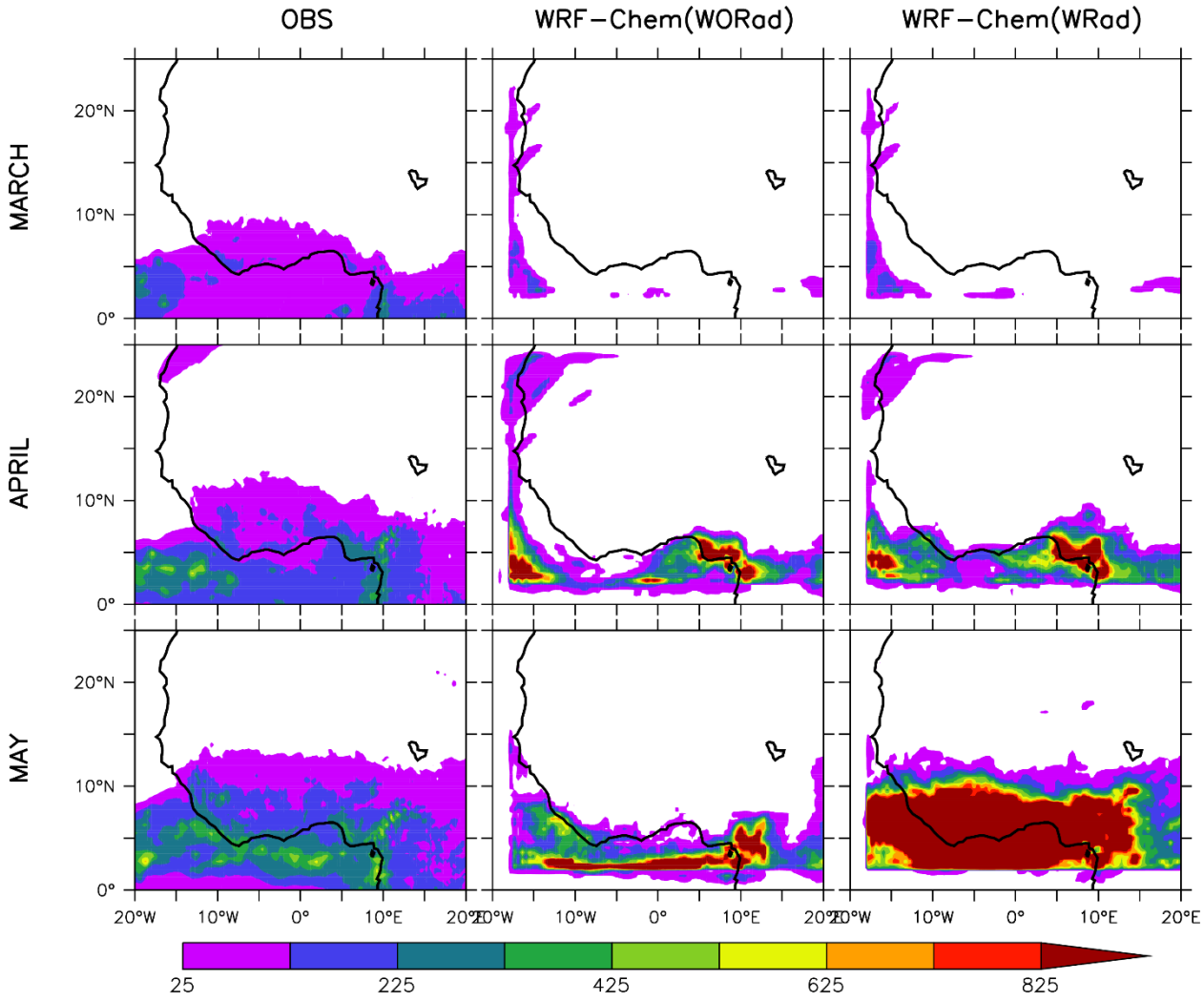

Figure 4.47: Total rainfall distribution from ERA5, WRF-Chem (WORad and WRad) for the month of March, April, and May 2012

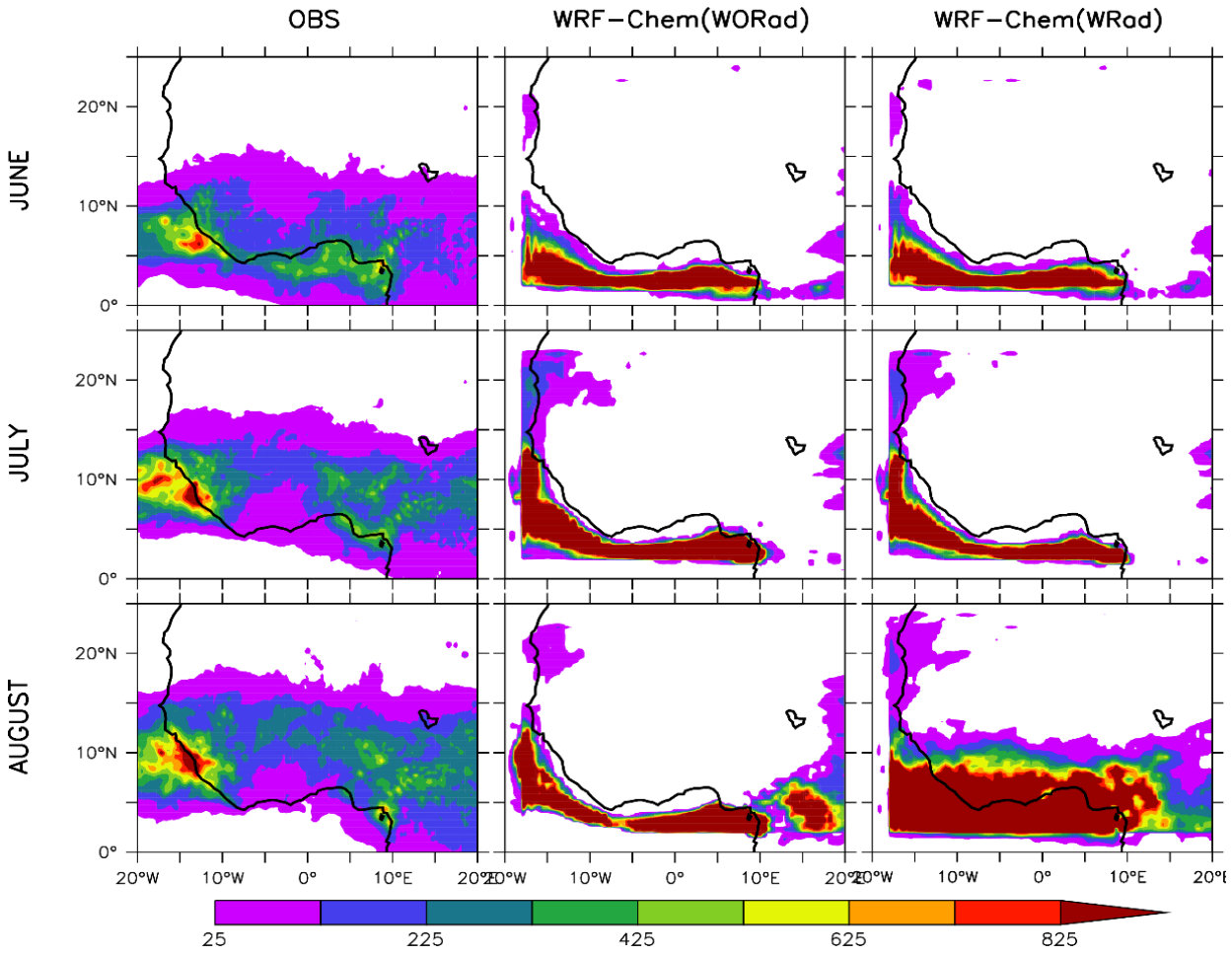

Figure 4.48: Convective rainfall distribution from ERA5, WRF-Chem (WORad and WRad) for the months of June, July, and August 2012

Figure 4.48 illustrates the comparison of the observed data and the two WRF-Chem outputs for the months of June, July, and August. It shows an overestimation of rainfall for all the simulated outputs over the Atlantic. The month of June under observation has recorded rainfall activities of about 25 – 425mm, both on the coast and inland. The simulated outputs also showed rainfall activities over the coast but the rainfall amount was heavier (over 800mm).

The month of July and August under OBS experienced heavy rainfall activities over the continent between 5^{o}N and 15^{o}N and over the coast of The Gambia and Senegal. The simulated outputs for July showed rainfall activities over the Atlantic and along the coastline of West Africa. The activity has also been captured in the cities of Dakar and Mauritania. The results for the month of August under WRad have shown much effect of radiation. The BBA radiative has overestimated the rainfall amount compared to OBS and WORad. It has captured heavy rainfall over the coast axes of Sierra Leone through to the axis of the Central African Republic. These activities were moving inland of Cameroon, Nigeria, Togo, Ghana, and Liberia. These activities were shown inland Mauritania of about 25-75mm.

4.3.5 Comparisons of Seasonal Rainfall from ERA5 with Simulated Seasonal Rainfall

Figure 4.49 presents spatial maps of rainfall from ERA5 and the simulated outputs for March, April, and May (MAM) seasons and June, July, and August (JJA) seasons. It has been observed that the simulated outputs have overestimated the rainfall amount for both MAM and JJA. The observed under MAM has recorded the amount of rain over the coast and the continent. The activities are mainly recorded between the equator and the 15^{o}N axis. The amount of rainfall becomes lesser as it moves further inland. The simulated output without radiative effect has observed rainfall activities over the Atlantic and along the coastal cities of Guinea, Sierra

Leone, Benin, and Nigeria. The activity was overestimated over the coast and underestimated over the continent compared to the OBS as there was no rainfall observed over the continent. On the other hand, simulated output with radiative effect overestimated over not only the coast but also further inland in the coastal countries from Guinea, Liberia to Nigeria and Cameroon.

The season of JJA has recorded a significant amount of precipitation activities under observation. The activities were captured over both the inland and the coast. The activities were observed over the Gulf of Guinea along the Sierra Leone axis to the coastal axis of the Central African Republic to the Atlantic. The inland activities were observed over Guinea, Sierra Leone, Benin, Nigeria, and some part of the Southern part of Africa. The simulated outputs overestimated the amount of rainfall from about 25-250mm under OBS to over 800mm. The simulated output without radiative effects, light precipitation activities was observed over the coast of West Africa. No precipitation activities were captured over the continent.

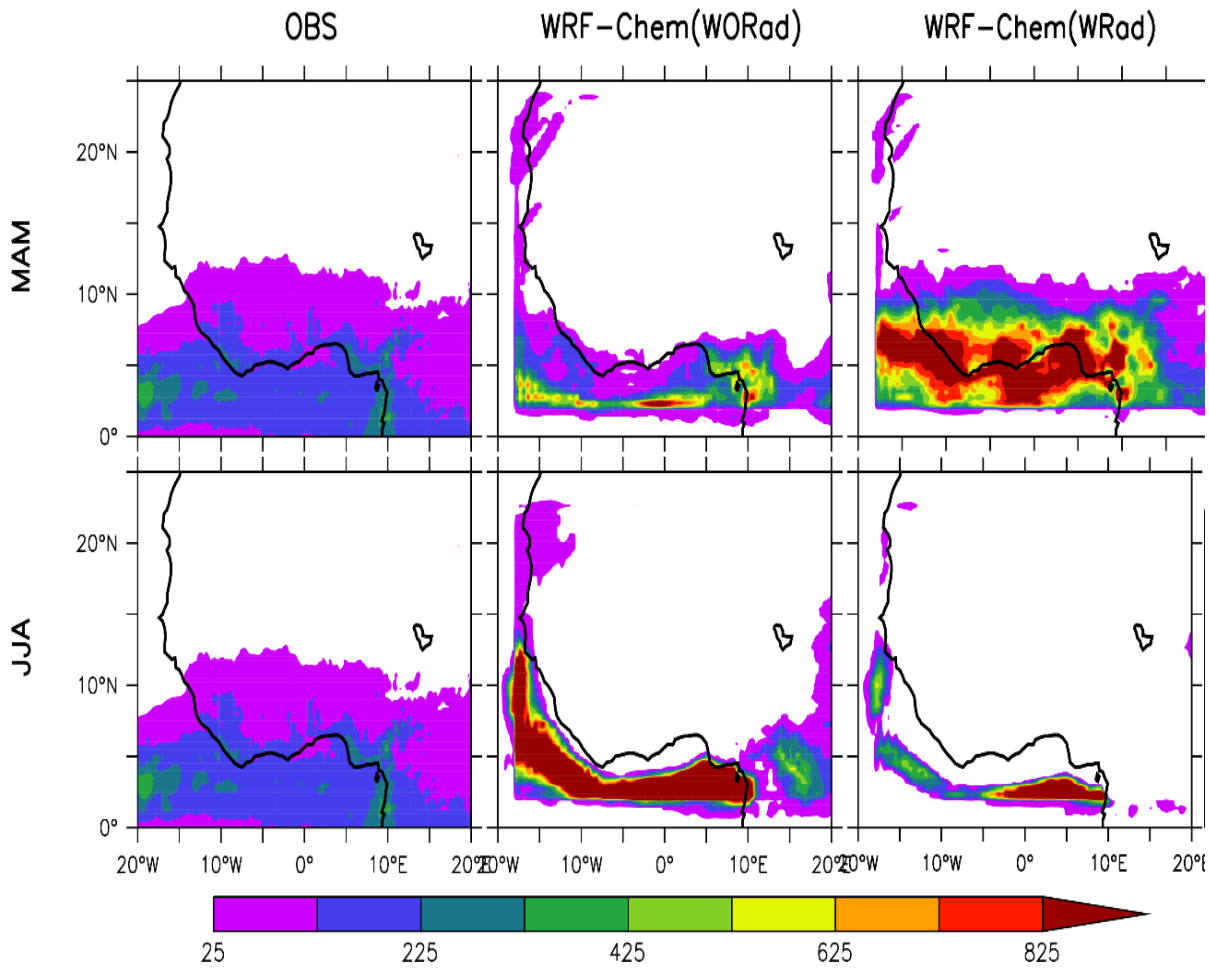

Figure 4.49: Seasonal rainfall distribution from ERA5, WRF-Chem (WORad and WRad) for MAM season and JJA season 2012

4.3.6 Evaluating Biomass-burning Aerosols Radiative Effects on Total Rainfall

The WRF-Chem without radiation minus WRF-Chem with radiation (WORad-WRad) were calculated and the results hence (hereafter) referred to as differences were compared with the observed, WRF-Chem without radiation and WRF-Chem with radiation in figure 4.50.

In the month of March, there was no activity observed under the differences. This shows that the effect of BBA radiation on the March rainfall was so insignificant. Some activities were shown under differences for the month of April; these were observed over the coast of Togo and Ghana and the inland areas of Nigeria and the Central African Republic. There was a huge difference shown in the rainfall amount after the BBA radiation reaction in the month of May. With the effect of BBA radiation, the model has overestimated the amount of rainfall ranging from 425mm to over 1000mm.

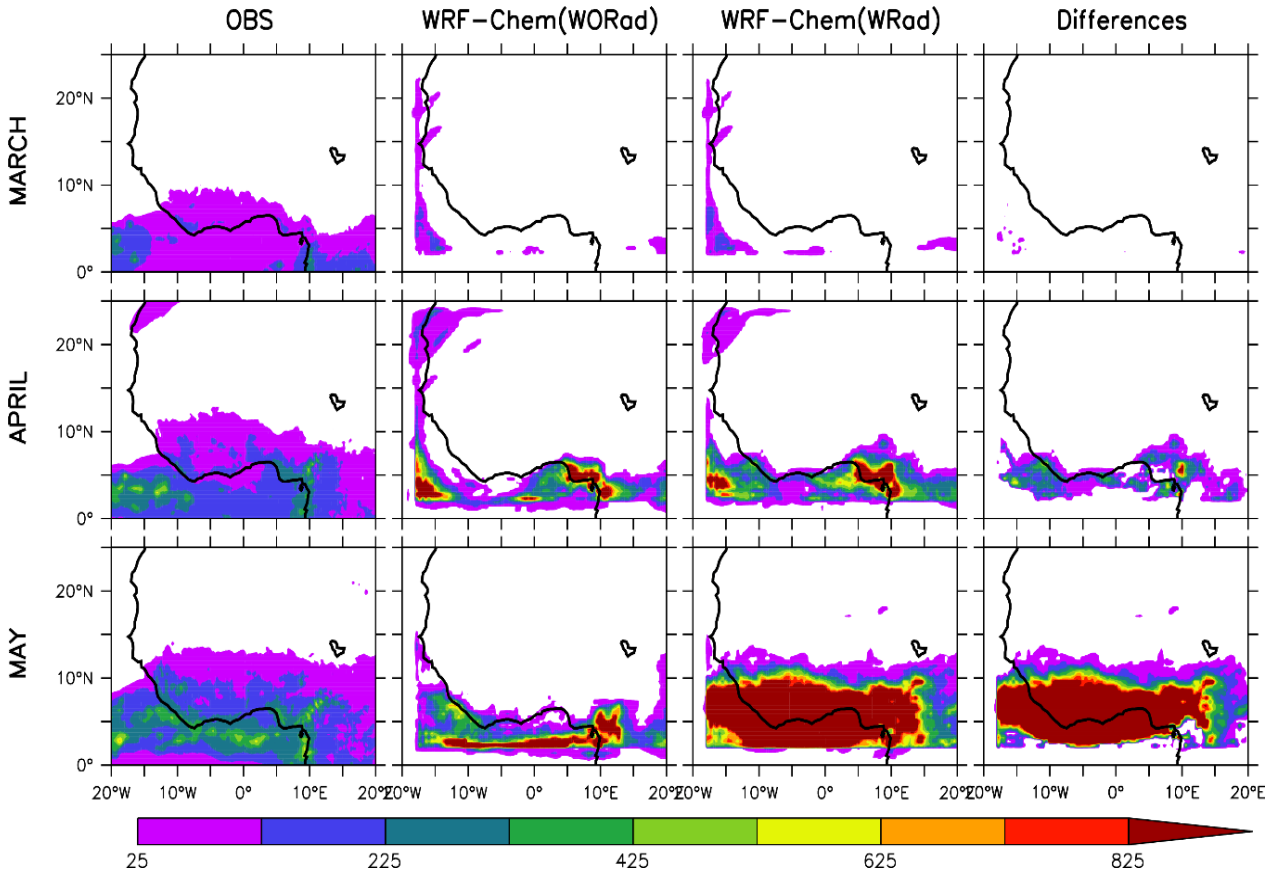

Figure 4.50: Total rainfall distribution from ERA5, WRF-Chem (WORad and WRad) and Differences for the months of March, April, and May 2012

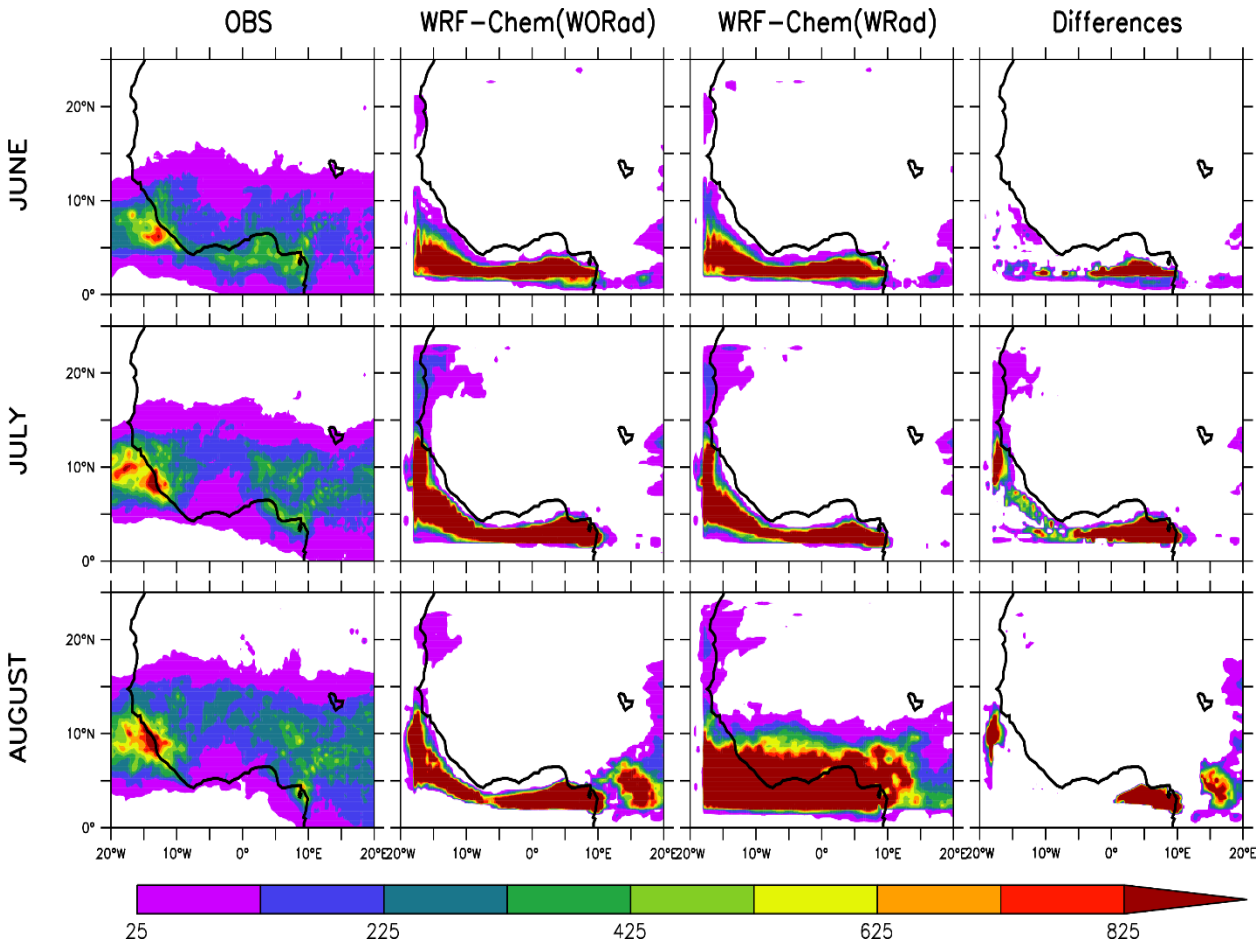

Figure 4.51: Total rainfall distribution from ERA5, WRF-Chem (WORad and OWad) and Difference for the months of June, July, and August 2012

It can be observed in figure 4.51, that the differences in simulated outputs have shown some rainfall activities for the months of June, July, and August. These have shown that the introduction of BBA radiation to the model has some influence over the model output. The differences have shown activities over the Atlantic between the axes of Sierra Leone and the Central African Republic. No activity was captured over the continent for all the months.

Figure 4.52 show the distribution of seasonal rainfall amount, the observed from ERA5 (OBS), the two model outputs (WORad and WRad) and WORad minus WRad (differences) for MAM and JJA seasons. The result under MAM differences shows an overestimation/increase of rainfall amount from the simulation output with BBA radiative effects, while the JJA season shows an under estimation/decrease of rainfall amount compared to the output without BBA radiative effects.

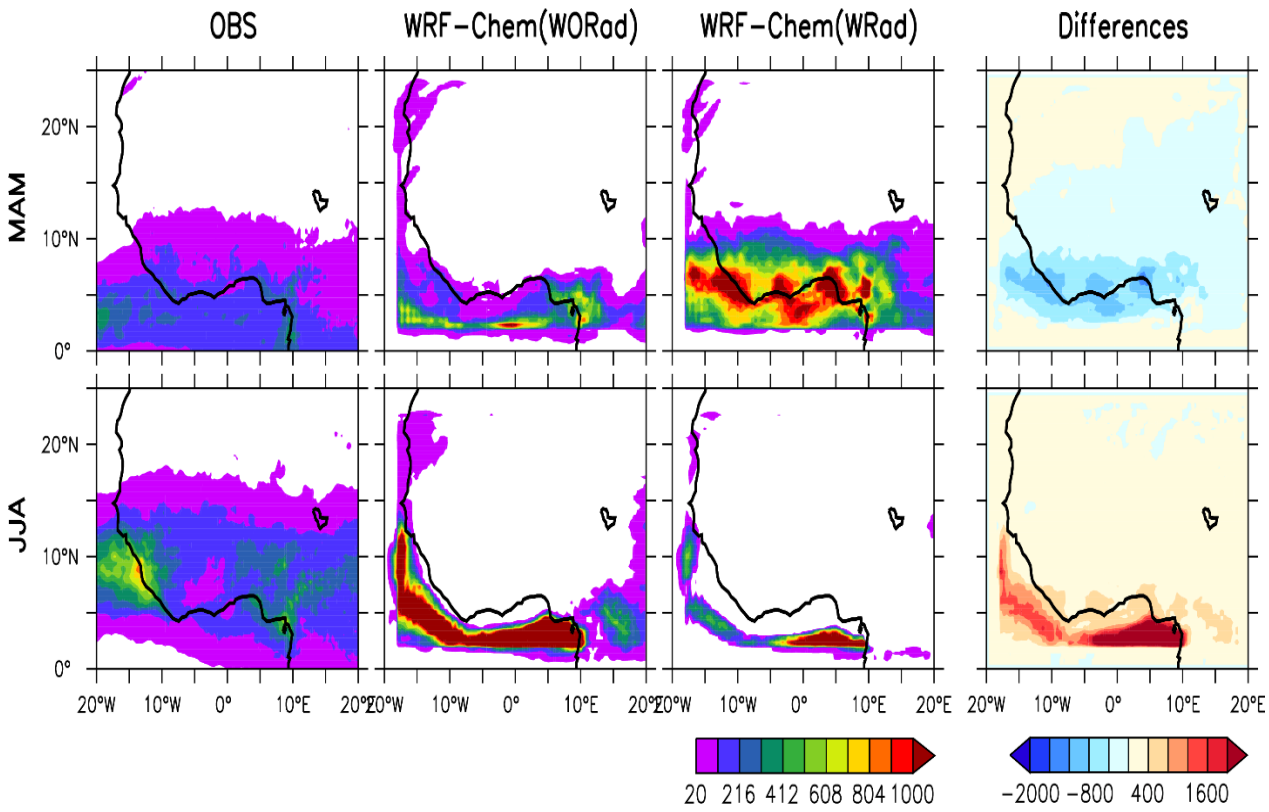

Figure 4.52: Total rainfall distribution from ERA5, WRF-Chem (WORad and WRad) and Differences for MAM and JJA seasons

4.3.7 Comparison of Annual Reanalysis Outgoing Longwave Radiation (OLR) and WRF-Whem Outgoing Longwave Radiation (OLR).

The daily reanalysis OLR from ERA5 (OBS), WRF-Chem OLR output with radiative effects (WRad), and OLR without radiative effects (WORad) for the months of March, April, May, June, July, and August 2012, are presented in figures 4.53 and 4.54. Using a threshold of OLR $\leq$ 220 W m^{-2} is associated with deep convection (Zhang 1993, Krishnan *et al.* 2000), the simulated OLR outputs have shown an overestimation of deep convections throughout the study period.

This deep convection was observed over Nigeria, Cameroon, Niger, Chad, and Central African Republic on the continent and Sierra Leone, Liberia, and some part of Guinea and Ivory Coast under WRad for the month of March. A deep convective over the Coast was observed over the coast of Liberia and Ivory Coast. Deep convection captured under WORad was observed over a similar location as under WRad only that it has not gotten over Niger and Chad. Over the coast, a deep convection was observed over the coast of Cameroon on the Central African Republic axis. Comparing the simulated outputs to the observed that have not recorded any deep convection both over the coast and the continent, the simulated outputs have overestimated the deep convection.

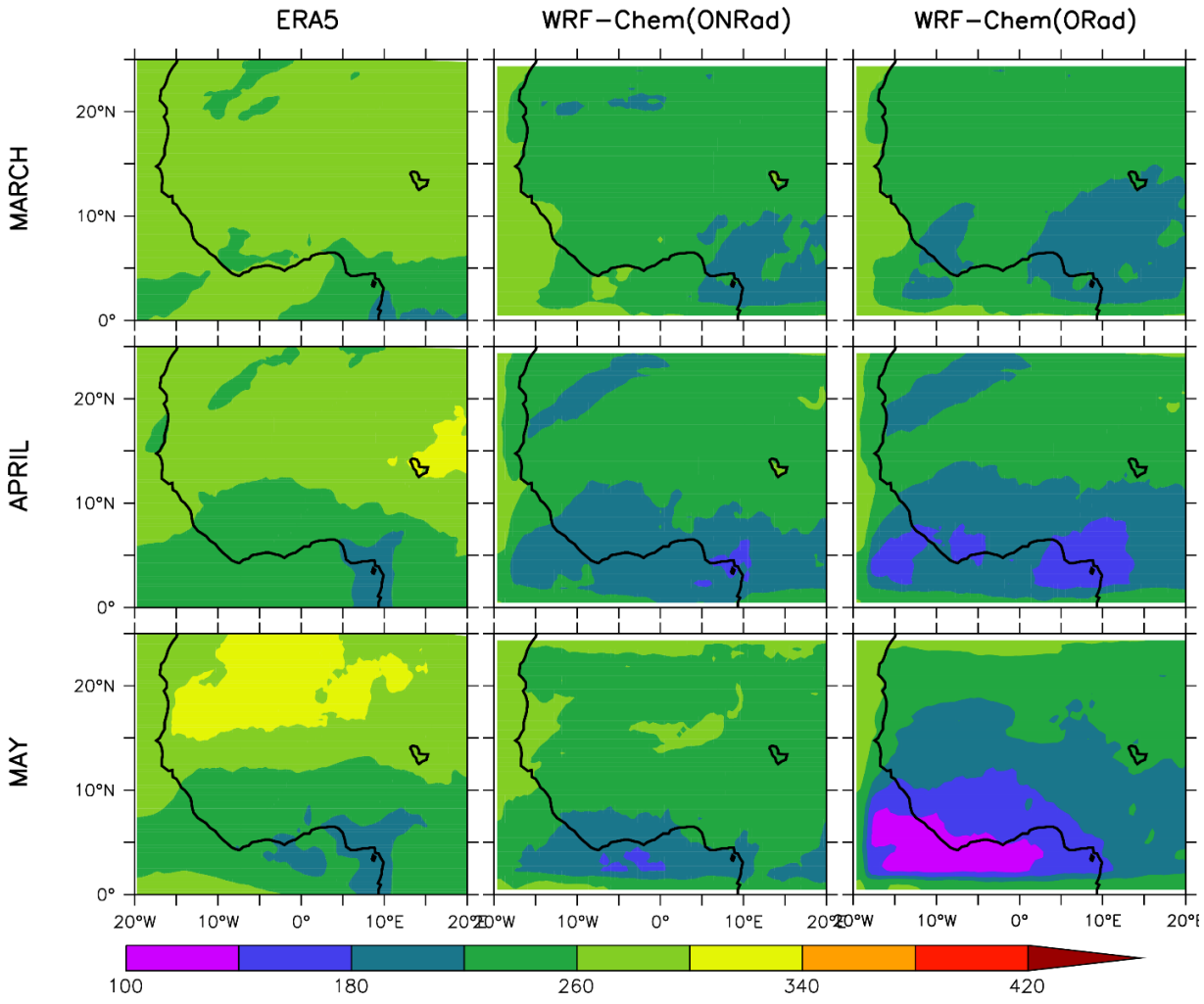

Figure 4.53: Outgoing longwave radiation from ERA5, WRF-Chem OLR (WORad and WRad) for the months of March, April, and May 2012

During the month of April, deep convection was captured over both the Atlantic and the continent south of 15^{o}N under simulated WRad. The activities were also observed across Mauritania. Deep convections under simulated WORad were observed over the coast and the land south of 10^{o}N and across Mauritania but not as strong as the activities under WRad. Comparing them to the observed, in which deep convective was recorded over a portion of Nigeria Cameroon over the coast and the land, the simulated outputs overestimated the deep convection for the month of April 2012. May have observed deep convection under simulated WRad over both the coast and the continent south of 18^{O}N. The activities were heavier over the coast of Liberia and Ivory Coast to Benin but become lighter as it moves inland. Under simulated WORad, deep convections were captured over the coastline of Liberia to Benin and Cameroon. The activities have moved inland from Liberia to Benin. The simulated outputs have overestimated the deep convection when compared to the observed that recorded the activities over the coastline of Nigeria and Cameroon.

Most of the OLR values for both the observed and simulated outputs over the study area in figure 4.54 are above 220W m^{-2}. That means the OLR values needed to form deep convection were less. For the month of June, deep convections captured under the simulated WRad were over the Atlantic on the Sierra Leone axis and the axis of the Central African Republic. There was no deep convection captured over the continent of West Africa, Likewise the simulated WORad. Comparing the simulated outputs with the observed, which recorded deep convection over the coastline of Nigeria and moves a bit inland, there were no similarities, and the simulated outputs overestimated the process. Deep convections for the month of July under OBS, were recorded over the land over Nigeria, Cameroon, and Chad. Over the coast, it was

recorded over the coastline of Guinea. Under the simulated WORad, deep convections were observed over the coast of Guinea and Sierra Leone and the coast of Nigeria and Cameroon.

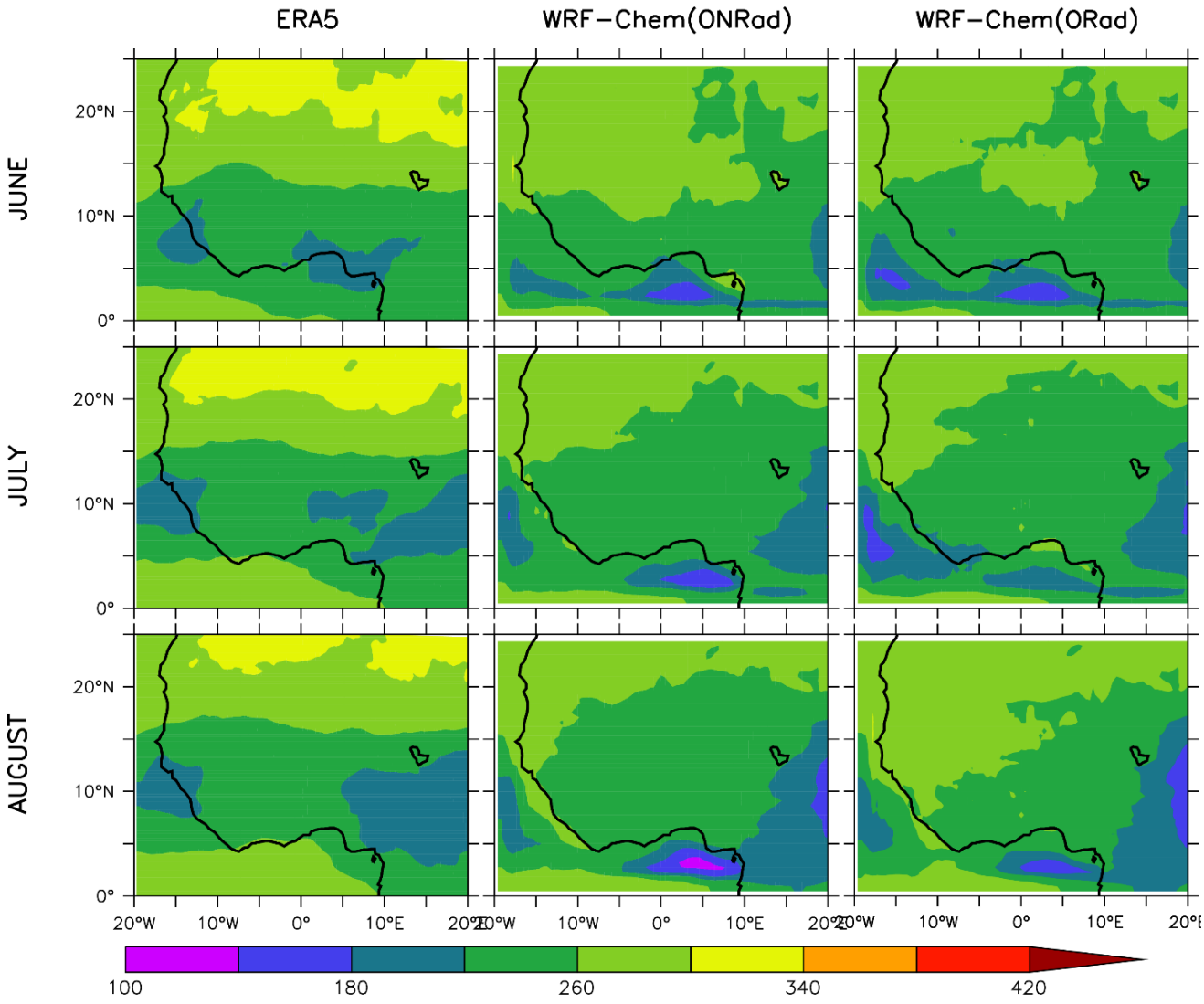

Figure 4.54: Outgoing longwave radiation from ERA5, WRF-Chem OLR (WORad and WRad) for June, July, and August 2012

4.3.8 Comparison of Seasonal Reanalysis Outgoing Longwave Radiation (OLR) and WRF-Chem Outgoing Longwave Radiation (OLR)

Figure 4.55 showed the comparison of the seasonal OLR from ERA5, WRF-Chem outputs (WORad and WRad) for MAM and JJA seasons 2012. In comparing the amount of OLR that leads to deep convection, the MAM season has overestimated the deep convection for both simulations. Deep convection was captured under simulated WRad over both the coast and inland over the south of 15ºN and north of 15º N experiencing the form of a non-precipitation cloud (high values of OLR). The deep convection observed under simulated WORad were not as spread out as under WRad but they were observed over the coast and the inland of Liberia, Ivory Coast to the Central African Republic. When the simulated outputs were compared to the observed, the simulated outputs overestimated the deep convection. The deep convection for the JJA season under the simulation outputs was captured over Central Africa over the land. Over the coast, the activity was captured over the coast of Nigeria and Cameroon, and on the east of Guinea. Under OBS, deep convections were observed over Nigeria and Cameroon.

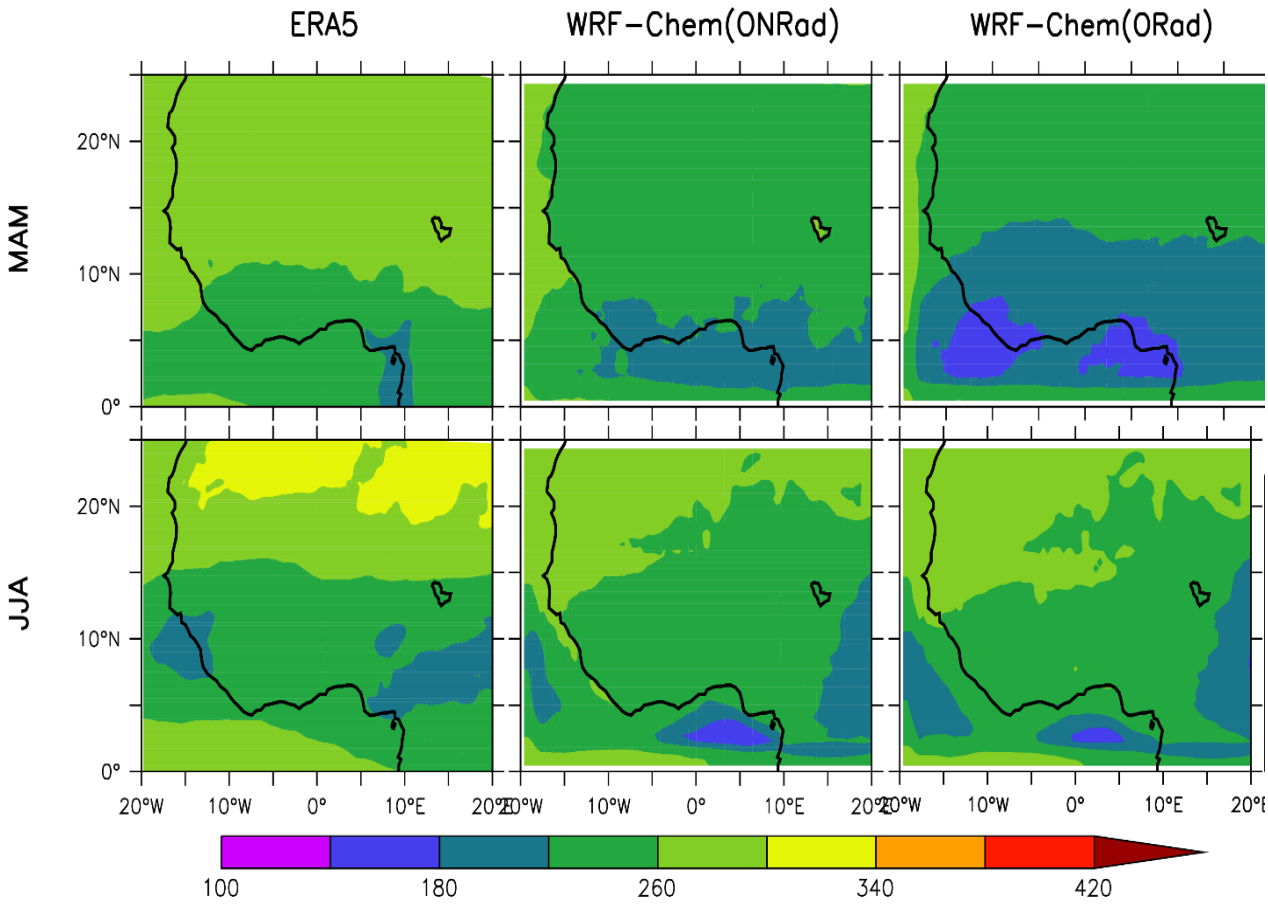

Figure 4.55: Outgoing longwave radiation from ERA5, WRF-Chem OLR (WORad and WRad) for MAM and JJA season 2012

CHAPTER FIVE

5.0 CONCLUSION AND RECOMMENDATIONS

5.1 CONCLUSION

This research successfully evaluates the effects of pre-monsoon biomass burning on rainfall characteristics over West Africa. The specific objectives achieved in the research include estimating the distribution of pre-monsoon biomass burning aerosols (BBA) over the study area; analyzing rainfall characteristics over the study area; evaluating the capability of the regional climate model (WRF-Chem) on capturing the BBA effect on monsoon rainfall and determining the influence of BBA on rainfall characteristics and cloud formation.

5.1.1 Aerosol Distribution over West Africa

The temporal distribution of aerosol properties (AOD, AE) and aerosol classification were studied over five AERONET sites. The period the data covered varies for each site. For temporal distribution of AOD and AE; it was revealed that the highest monthly AOD value occurred during the month of January over the areas south of 10^{o}N and during March, April, May over the areas north of 10^{o}N of the study area. Whereas the minimum AOD value occurred during the month of August over the areas south of 10^{o}N and during the month of December and January over the areas north of 10^{o}N of the study area.

The high values of AE, which reveal dominant fine mode aerosols were observed during the months of December- January (the winter or DJF season) and low AE values which dominate coarse mode aerosol during the months of June- July over the northern part of the study area.

While the southern areas of the region observed a higher AE values during the month of August and a low AE values in April. For the classification of aerosols, the study has shown that desert dust (DD) were the dominant atmospheric aerosol throughout the year in the study area. Even though most BB activities took place during the pre-monsoon (MAM) period, it does not make it the dominant aerosol.

5.1.2: Rainfall Characteristics over West Africa

West Africa exhibited varying rainfall characteristics the analysis showed a high occurrence of normal and wet climatic conditions and low dry (drought) conditions over the sites for the periods under study. The dominant normal and wet climatic conditions were not found only in the annual rainfall but also in the seasonal rainfall for all the sites over the study period. There were high variations for the annual rainfall amount for all the study sites and higher variations for the seasonal rainfall amount for both MAM and JJA for all the sites. There was no trend found in the annual rainfall data (time series data) for all the sites but there were trend (negative) trends observed in the time series for MAM and JJA season. High variation associated with no trend is an indication that rainfall in that area was more dependable. This makes it easier to use the rainfall mean to predict rainfall performance and for farmers to plan their agricultural activities. High variation associated with a negative trend is an indication that rainfall in that area was gradually becoming less dependable. The negative trend makes it difficult to predict rainfall performance.

5.1.3 Model Output

In comparing the model output with ERA5 reanalysis rainfall data, the study has shown that the model outputs have over estimated the amount of rainfall (both convective and total) over the coast and under estimated over the continent for the period under study. for the seasonal

comparism, Wrf-Chem model over estimated the rainfall amounts during MAM, whiles under estimates during the JJA season. From the evaluation of BBA radiative effects on both rainfall types, the study has shown that the model output has increase in the amount of rainfall by 70% to 80% when BBA radiation was introduced in the simulation during MAM season and the amount reduced by 50% to 60% during JJA season.

Comparing the outgoing longwave radiation (OLR) from the model with ERA5 reanalysis OLR, the result has shown more convective cloud under the model output than the observe monthly OLR for all the months under study. The model output under the MAM season has observed more convective clouds than observe. Under the JJA season, there was not much difference between the model outputs and the observed. And comparing the two model outputs (WORad and WRad), it has been observed that the WRad has more convective clouds than the WORad.

From the above observations, it can be concluded that the WRF-Chem model overestimated the rainfall characteristics and the effect of BBA radiation can increase or decrease rainfall amount depending on the period/season over West Africa. The WRF-Chem model also underestimate the values of OLR. However, the effect BBA radiative has increased the rate of convective cloud formation over West Africa

REFRENCES

A. Angstrom, “On the atmospheric transmission of sun radiation and on dust in the air”, *Geografiska Annaler*, vol. **11**, pp. 156–166, 1929.

Ackerman, A. S., Toon, O. B., Stevens, D. E., Heymsfield, A. J., Ramanathan, V., & Welton, E. J. (2000). Reduction of tropical cloudiness by soot. *Science*, *288*(5468), 1042-1047.

Ackerman, F., Ishikawa, M., & Suga, M. (2007). The carbon content of Japan–US trade. *Energy Policy*, *35*(9), 4455-4462.

Ackerman, J. D. (2002). Diffusivity in a marine macrophyte canopy: implications for submarine pollination and dispersal. *American Journal of Botany*, *89*(7), 1119-1127.

Albrecht, B. A. (1989). Aerosols, cloud microphysics, and fractional cloudiness. *Science*, *245*(4923), 1227-1230.

AL-Taie, K., Rajab, J. M., & Al-Salihi, A. M. (2020). Climatology and classification of aerosols based on optical properties over selected stations in Iraq. In *AIP Conference Proceedings* (Vol. 2290, No. 1, p. 050041). AIP Publishing LLC.

AL-Taie, K., Rajab, J. M., & Al-Salihi, A. M. (2020, December). Climatology and classification of aerosols based on optical properties over selected stations in Iraq. In *AIP Conference Proceedings* (Vol. 2290, No. 1, p. 050041). AIP Publishing LLC.

Andreae, M. O., & Gelencsér, A. (2006). Black carbon or brown carbon? The nature of light-absorbing carbonaceous aerosols. *Atmospheric Chemistry and Physics*, *6*(10), 3131-3148.

Andreas, E. L. (1992). Sea spray and the turbulent air-sea heat fluxes. *Journal of Geophysical Research: Oceans*, *97*(C7), 11429-11441.

Andreas, E. L., & Emanuel, K. A. (2001). Effects of sea spray on tropical cyclone intensity. *Journal of the atmospheric sciences*, *58*(24), 3741-3751.

Andreas, E. L., Edson, J. B., Monahan, E. C., Rouault, M. P., & Smith, S. D. (1995). The spray contribution to net evaporation from the sea: A review of recent progress. *Boundary-Layer Meteorology*, *72*, 3-52.

Ångström, A. (1964). The parameters of atmospheric turbidity. *Tellus*, *16*(1), 64-75.

Ault, A. P., Williams, C. R., White, A. B., Neiman, P. J., Creamean, J. M., Gaston, C. J., ... & Prather, K. A. (2011). Detection of Asian dust in California orographic precipitation. *Journal of Geophysical Research: Atmospheres*, *116*(D16).

Ayanlade, A., Atai, G., & Jegede, M. O. (2019). Variability in atmospheric aerosols and effects of humidity, wind and InterTropical discontinuity over different ecological zones in Nigeria. *Atmospheric Environment*, *201*, 369-380

Baker, L. H., Collins, W. J., Olivié, D. J. L., Cherian, R., Hodnebrog, Ø., Myhre, G., & Quaas, J. (2015). Climate responses to anthropogenic emissions of short-lived climate pollutants. *Atmospheric Chemistry and Physics*, *15*(14), 8201-8216.

Bi, H., Peterson, W. T., & Strub, P. T. (2011). Transport and coastal zooplankton communities in the northern California Current system. *Geophysical Research Letters*, *38*(12).

Boers, R., Jensen, J. B., & Krummel, P. B. (1998). Microphysical and short-wave radiative structure of stratocumulus clouds over the Southern Ocean: Summer results and seasonal differences. *Quarterly Journal of the Royal Meteorological Society*, *124*(545), 151-168.

Boiyo, R., Kumar, K. R., & Zhao, T. (2018). Spatial variations and trends in AOD climatology over East Africa during 2002–2016: a comparative study using three satellite data sets. *International Journal of Climatology*, *38*, e1221-e1240.

Bond, T. C., & Bergstrom, R. W. (2006). Light absorption by carbonaceous particles: An investigative review. *Aerosol science and technology*, *40*(1), 27-67.

Boucher, O., Randall, D., Artaxo, P., Bretherton, C., Feingold, G., Forster, P., ... & Zhang, X. Y. (2013). Clouds and aerosols. In *Climate change 2013: the physical science basis. Contribution of Working Group I to the Fifth Assessment Report of the Intergovernmental Panel on Climate Change* (pp. 571-657). Cambridge University Press.

Bristow, C. S., Hudson-Edwards, K. A., & Chappell, A. (2010). Fertilizing the Amazon and equatorial Atlantic with West African dust. *Geophysical Research Letters*, *37*(14).

Cadle, R. D. (1966). Particles in the Atmosphere and Space.

Cahill, A. E., Aiello-Lammens, M. E., Fisher-Reid, M. C., Hua, X., Karanewsky, C. J., Yeong Ryu, H., ... & Wiens, J. J. (2013). How does climate change cause extinction?. *Proceedings of the Royal Society B: Biological Sciences*, *280*(1750), 20121890.

Charlson, R. J., Schwartz, S. E., Hales, J. M., Cess, R. D., Coakley Jr, J. A., Hansen, J. E., & Hofmann, D. J. (1992). Climate forcing by anthropogenic aerosols. *Science*, *255*(5043), 423-430.

Chen, Q., Farmer, D. K., Schneider, J., Zorn, S. R., Heald, C. L., Karl, T. G., ... & Martin, S. T. (2009). Mass spectral characterization of submicron biogenic organic particles in the Amazon Basin. *Geophysical Research Letters*, *36*(20).

Colbeck, I., & Lazaridis, M. (2014). *Aerosol Science*. Wiley Online Library.

Creamean, J. M., Suski, K. J., Rosenfeld, D., Cazorla, A., DeMott, P. J., Sullivan, R. C., ... & Prather, K. A. (2013). Dust and biological aerosols from the Sahara and Asia influence precipitation in the western US. *Science*, *339*(6127), 1572-1578.

d'Almeida, G. A. (1986). A model for Saharan dust transport. *Journal of Applied Meteorology and Climatology*, *25*(7), 903-916

DeMott, P. J., Sassen, K., Poellot, M. R., Baumgardner, D., Rogers, D. C., Brooks, S. D., ... & Kreidenweis, S. M. (2003). African dust aerosols as atmospheric ice nuclei. *Geophysical Research Letters*, *30*(14).

Ding, A. J., Huang, X., Nie, W., Sun, J. N., Kerminen, V. M., Petäjä, T., ... & Fu, C. B. (2016). Enhanced haze pollution by black carbon in megacities in China. *Geophysical Research Letters*, *43*(6), 2873-2879.

Doherty, O. M., & Evan, A. T. (2014). Identification of a new dust-stratocumulus indirect effect over the tropical North Atlantic. *Geophysical Research Letters*, *41*(19), 6935-6942.

Duce, R. A. (1995). Sources, distributions, and fluxes of mineral aerosols and their relationship to climate. *Aerosol forcing of climate*, *6*, 43-72.

Eck, T. F., Holben, B. N., Reid, J. S., Dubovik, O., Smirnov, A., O'neill, N. T., ... & Kinne, S. (1999). Wavelength dependence of the optical depth of biomass burning, urban, and desert dust aerosols. *Journal of Geophysical Research: Atmospheres*, *104*(D24), 31333-31349.

Elbert, W., Taylor, P. E., Andreae, M. O., & Pöschl, U. (2007). Contribution of fungi to primary biogenic aerosols in the atmosphere: wet and dry discharged spores, carbohydrates, and inorganic ions. *Atmospheric Chemistry and Physics*, *7*(17), 4569-4588.

Eshet, A., & Raju, J. P. (2022). Daily and Seasonal Variation of Aerosol Optical Depth and Angstrom Exponent over Ethiopia using MODIS Data. *Pollution*, *8*(1), 315-329.

Falkovich, A. H., Ganor, E., Levin, Z., Formenti, P., & Rudich, Y. (2001). Chemical and mineralogical analysis of individual mineral dust particles. *Journal of Geophysical Research: Atmospheres*, *106*(D16), 18029-18036.

Feingold, G., Jiang, H., & Harrington, J. Y. (2005). On smoke suppression of clouds in Amazonia. *Geophysical research letters*, *32*(2).

Friedlingstein, P., O'sullivan, M., Jones, M. W., Andrew, R. M., Hauck, J., Olsen, A., ... & Zaehle, S. (2020). Global carbon budget 2020. *Earth System Science Data*, *12*(4), 3269-3340.

Gantt, B., & Meskhidze, N. J. A. C. (2013). The physical and chemical characteristics of marine primary organic aerosol: a review. *Atmospheric Chemistry and Physics*, *13*(8), 3979-3996.

Gao, Y., Anderson, J. R., & Hua, X. (2007). Dust characteristics over the North Pacific observed through shipboard measurements during the ACE-Asia experiment. *Atmospheric Environment*, *41*(36), 7907-7922.

Gonçalves, J. A., & Henriques, R. (2015). UAV photogrammetry for topographic monitoring of coastal areas. *ISPRS journal of Photogrammetry and Remote Sensing*, *104*, 101-111.

Greve, P., Orlowsky, B., Mueller, B., Sheffield, J., Reichstein, M., & Seneviratne, S. I. (2014). Global assessment of trends in wetting and drying over land. *Nature geoscience*, *7*(10), 716-721.

Hansen, J., Sato, M., & Ruedy, R. (1997). Radiative forcing and climate response. *Journal of Geophysical Research: Atmospheres*, *102*(D6), 6831-6864.

Hansen, J., Sato, M., & Ruedy, R. (1997). Radiative forcing and climate response. *Journal of Geophysical Research: Atmospheres*, *102*(D6), 6831-6864.

Hartmann, D. L., Tank, A. M. K., Rusticucci, M., Alexander, L. V., Brönnimann, S., Charabi, Y. A. R., ... & Zhai, P. (2013). Observations: atmosphere and surface. In *Climate change 2013 the physical science basis: Working group I contribution to the fifth assessment report of the intergovernmental panel on climate change* (pp. 159-254). Cambridge University Press.

Havers, N., Burba, P., Lambert, J., & Klockow, D. (1998). Spectroscopic characterization of humic-like substances in airborne particulate matter. *Journal of Atmospheric Chemistry*, *29*(1), 45.

Hodnebrog, Ø., Myhre, G., & Samset, B. H. (2014). How shorter black carbon lifetime alters its climate effect. *Nature communications*, *5*(1), 5065.

Hofmann, T., Lowry, G. V., Ghoshal, S., Tufenkji, N., Brambilla, D., Dutcher, J. R., ... & Wilkinson, K. J. (2020). Technology readiness and overcoming barriers to sustainably implement nanotechnology-enabled plant agriculture. *Nature Food*, *1*(7), 416-425.

Holben, B. N., Eck, T. F., Slutsker, I. A., Tanré, D., Buis, J. P., Setzer, A., ... & Smirnov, A. (1998). AERONET—A federated instrument network and data archive for aerosol characterization. *Remote sensing of environment*, *66*(1), 1-16.

Holben, B. N., Tanre, D., Smirnov, A., Eck, T. F., Slutsker, I., Abuhassan, N., ... & Zibordi, G. (2001). An emerging ground-based aerosol climatology: Aerosol optical depth from AERONET. *Journal of Geophysical Research: Atmospheres*, *106*(D11), 12067-12097

Holben, B. N., Tanre, D., Smirnov, A., Eck, T. F., Slutsker, I., Abuhassan, N., ... & Zibordi, G. (2001). An emerging ground-based aerosol climatology: Aerosol optical depth from AERONET. *Journal of Geophysical Research: Atmospheres*, *106*(D11), 12067-12097.

Horowitz, H. M., Jacob, D. J., Zhang, Y., Dibble, T. S., Slemr, F., Amos, H. M., ... & Sunderland, E. M. (2017). A new mechanism for atmospheric mercury redox chemistry: implications for the global mercury budget. *Atmospheric Chemistry and Physics*, *17*(10), 6353-6371.

Ilotoviz, E., Khain, A. P., Benmoshe, N., Phillips, V. T., & Ryzhkov, A. V. (2016). Effect of aerosols on freezing drops, hail, and precipitation in a midlatitude storm. *Journal of the Atmospheric Sciences*, *73*(1), 109-144.

Iqbal, Z., Sarott, F. A., & Veprek, S. (1983). Optical absorption in hydrogenated microcrystalline silicon. *Journal of Physics C: Solid State Physics*, *16*(10), 2005.

Jacobson, M. Z. (2012). *Air pollution and global warming: history, science, and solutions*. Cambridge University Press.

Jankowiak, I., & Tanré, D. (1992). Satellite climatology of Saharan dust outbreaks: Method and preliminary results. *Journal of Climate*, *5*(6), 646-656.

Jirak, I. L., & Cotton, W. R. (2006). Effect of air pollution on precipitation along the Front Range of the Rocky Mountains. *Journal of Applied Meteorology and Climatology*, *45*(1), 236-245.

Jones, A. M., & Harrison, R. M. (2004). The effects of meteorological factors on atmospheric bioaerosol concentrations—a review. *Science of the total environment*, *326*(1-3), 151-180.

Kannel M.(2016) Development of Broadband Aerosol Optical Depth Models. *Dissertationes Geophysicales Universitatis Tartuensis*, vol. **26**,

Kannemadugu, H. B. S., Varghese, A. O., Mukkara, S. R., Joshi, A. K., & Moharil, S. V. (2015). Discrimination of aerosol types and validation of MODIS aerosol and water vapour products using a sun photometer over Central India. *Aerosol and Air Quality Research*, *15*(2), 682-693.

Kaufman, Y. J., & Remer, L. A. (1994). Detection of forests using mid-IR reflectance: an application for aerosol studies. *IEEE transactions on geoscience and remote sensing*, *32*(3), 672-683.

Khain, A. P. (2009). Notes on state-of-the-art investigations of aerosol effects on precipitation: a critical review. *Environmental Research Letters*, *4*(1), 015004.

Knutti, R., & Sedláček, J. (2013). Robustness and uncertainties in the new CMIP5 climate model projections. *Nature climate change*, *3*(4), 369-373.

Koch, D., & Del Genio, A. D. (2010). Black carbon semi-direct effects on cloud cover: review and synthesis. *Atmospheric Chemistry and Physics*, *10*(16), 7685-7696.

Lau, K. M., & Kim, K. M. (2006). Observational relationships between aerosol and Asian monsoon rainfall, and circulation. *Geophysical research letters*, *33*(21).

Lewis, E. R., & Schwartz, S. E. (2004). *Sea salt aerosol production: mechanisms, methods, measurements, and models* (Vol. 152). American geophysical union.

Liu H.(2005) Global scale aerosol properties: implications for surface shortwave radiation budget.

Lowenthal, D. H., Borys, R. D., Cotton, W., Saleeby, S., Cohn, S. A., & Brown, W. O. (2011). The altitude of snow growth by riming and vapor deposition in mixed-phase orographic clouds. *Atmospheric environment*, *45*(2), 519-522.

Lynn, B., Khain, A., Rosenfeld, D., & Woodley, W. L. (2007). Effects of aerosols on precipitation from orographic clouds. *Journal of Geophysical Research: Atmospheres*, *112*(D10).

Malloch, A. J. C. (1972). Salt-spray deposition on the maritime cliffs of the Lizard Peninsula. *The Journal of Ecology*, 103-112.

Mandrioli, P., Negrini, M. G., Scarani, C., Tampieri, F., & Trombetti, F. (1980). Mesoscale transport of Corylus pollen grains in winter atmosphere. *Grana*, *19*(3), 227-233.

Meehl, G. A., Arblaster, J. M., Lawrence, D. M., Seth, A., Schneider, E. K., Kirtman, B. P., & Min, D. (2006). Monsoon regimes in the CCSM3. *Journal of climate*, *19*(11), 2482-2495.

Middleton, N. J. (2017). Desert dust hazards: A global review. *Aeolian research*, *24*, 53-63.

Moulin, C., Lambert, C. E., Dulac, F., & Dayan, U. (1997). Control of atmospheric export of dust from North Africa by the North Atlantic Oscillation. *Nature*, *387*(6634), 691-694.

Myhre, G., Myhre, C. E. L., Samset, B. H., & Storelvmo, T. (2013). Aerosols and their relation to global climate and climate sensitivity. *Nature Education Knowledge*, *4*(5), 7.

Papagiannopoulos, N., Mona, L., & Pappalardo, G. (2016, April). Aerosol classification using EARLINET measurements for an intensive observational period. In *EGU General Assembly Conference Abstracts* (pp. EPSC2016-16026).

Persad, G. G., Samset, B. H., & Wilcox, L. J. (2022). Aerosols must be included in climate risk assessments. *Nature*, *611*(7937), 662-664.

Persad-Clem, R., Hoerster, K. D., Romano, E. F. T., Huizar, N., & Maier, K. J. (2022). Climate to COVID, global to local, policies to people: a biopsychosocial ecological framework for syndemic prevention and response in behavioral medicine. *Translational Behavioral Medicine*, *12*(4), 516-525.

Peters, G. P., Marland, G., Le Quéré, C., Boden, T., Canadell, J. G., & Raupach, M. R. (2012). Rapid growth in CO2 emissions after the 2008–2009 global financial crisis. *Nature climate change*, *2*(1), 2-4.

Pósfai, M., Gelencsér, A., Simonics, R., Arató, K., Li, J., Hobbs, P. V., & Buseck, P. R. (2004). Atmospheric tar balls: Particles from biomass and biofuel burning. *Journal of Geophysical Research: Atmospheres*, *109*(D6).

Praseed, K. M., Nishanth, T., & Kumar, M. K. S. (2012). Spectral variation of AOD and its validation using MODIS: First cut result from Kannur, India. Atmospheric and Climate Sciences, 2, 94–100.

Prospero, J. M. (1981). Arid regions as sources of mineral aerosols in the marine atmosphere. *Geological Society of America Special Paper*, *186*, 71-86.

Prospero, J. M. (1999). Long-term measurements of the transport of African mineral dust to the southeastern United States: Implications for regional air quality. *Journal of Geophysical Research: Atmospheres*, *104*(D13), 15917-15927.

Prospero, J. M., Ginoux, P., Torres, O., Nicholson, S. E., & Gill, T. E. (2002). Environmental characterization of global sources of atmospheric soil dust identified with the Nimbus 7 Total Ozone Mapping Spectrometer (TOMS) absorbing aerosol product. *Reviews of geophysics*, *40*(1), 2-1.

Putaud, J. P., Van Dingenen, R., Alastuey, A., Bauer, H., Birmili, W., Cyrys, J., ... & Raes, F. (2010). A European aerosol phenomenology–3: Physical and chemical characteristics of particulate matter from 60 rural, urban, and kerbside sites across Europe. *Atmospheric Environment*, *44*(10), 1308-1320.

Ravindra, K., Sokhi, R., & Van Grieken, R. (2008). Atmospheric polycyclic aromatic hydrocarbons: source attribution, emission factors and regulation. *Atmospheric environment*, *42*(13), 2895-2921.

Rosenfeld, D., & Givati, A. (2006). Evidence of orographic precipitation suppression by air pollution–induced aerosols in the western United States. *Journal of applied meteorology and climatology*, *45*(7), 893-911.

Rosenfeld, D., Lohmann, U., Raga, G. B., O'Dowd, C. D., Kulmala, M., Fuzzi, S., ... & Andreae, M. O. (2008). Flood or drought: how do aerosols affect precipitation?. *Science*, *321*(5894), 1309-1313.

Rotstayn, L. D., Cai, W., Dix, M. R., Farquhar, G. D., Feng, Y., Ginoux, P., ... & Wang, M. (2007). Have Australian rainfall and cloudiness increased due to the remote effects of Asian anthropogenic aerosols?. *Journal of Geophysical Research: Atmospheres*, *112*(D9).

Rupakheti, D., Kang, S., Rupakheti, M., Cong, Z., Tripathee, L., Panday, A. K., & Holben, B. N. (2018). Observation of optical properties and sources of aerosols at Buddha's birthplace, Lumbini, Nepal: environmental implications. *Environmental Science and Pollution Research*, *25*, 14868-14881

Saikia, J., Sarma, R. K., Dhandia, R., Yadav, A., Bharali, R., Gupta, V. K., & Saikia, R. (2018). Alleviation of drought stress in pulse crops with ACC deaminase producing rhizobacteria isolated from acidic soil of Northeast India. *Scientific reports*, *8*(1), 3560.

Saleeby, S. M., Cotton, W. R., & Fuller, J. D. (2011). The cumulative impact of cloud droplet nucleating aerosols on orographic snowfall in Colorado. *Journal of applied meteorology and climatology*, *50*(3), 604-625.

Saleeby, S. M., Cotton, W. R., Lowenthal, D., & Messina, J. (2013). Aerosol impacts on the microphysical growth processes of orographic snowfall. *Journal of Applied Meteorology and Climatology*, *52*(4), 834-852.

Samset, B. H., Myhre, G., Herber, A., Kondo, Y., Li, S. M., Moteki, N., ... & Zhang, K. (2014). Modelled black carbon radiative forcing and atmospheric lifetime in AeroCom Phase II constrained by aircraft observations. *Atmospheric Chemistry and Physics*, *14*(22), 12465-12477.

Sattler, B., Puxbaum, H., & Psenner, R. (2001). Bacterial growth in supercooled cloud droplets. *Geophysical Research Letters*, *28*(2), 239-242.

Schepanski, K., Tegen, I., & Macke, A. (2009). Saharan dust transport and deposition towards the tropical northern Atlantic. *Atmospheric Chemistry and Physics*, *9*(4), 1173-1189.

Schindelholz, E., Risteen, B. E., & Kelly, R. G. (2014). Effect of relative humidity on corrosion of steel under sea salt aerosol proxies: I. NaCl. *Journal of The Electrochemical Society*, *161*(10), C450.

Schnell, R. C., & Vali, G. (1976). Biogenic ice nuclei: Part I. Terrestrial and marine sources. *Journal of Atmospheric Sciences*, *33*(8), 1554-1564.

Schulz, M., Textor, C., Kinne, S., Balkanski, Y., Bauer, S., Berntsen, T., ... & Takemura, T. (2006). Radiative forcing by aerosols as derived from the AeroCom present-day and pre-industrial simulations. *Atmospheric chemistry and physics*, *6*(12), 5225-5246.

Strong, P. J., Xie, S., & Clarke, W. P. (2015). Methane as a resource: can the methanotrophs add value? *Environmental science & technology*, *49*(7), 4001-4018.

Sylla, M. B., Diallo, I., & Pal, J. S. (2013). West African monsoon in state-of-the-science regional climate models. *Climate Variability—Regional and Thematic Patterns*, *10*(55140), 1805-1817.

Tao, M., Chen, L., Xiong, X., Zhang, M., Ma, P., Tao, J., & Wang, Z. (2014). Formation process of the widespread extreme haze pollution over northern China in January 2013: Implications for regional air quality and climate. *Atmospheric environment*, *98*, 417-425.

Thornhill, G. D., Ryder, C. L., Highwood, E. J., Shaffrey, L. C., & Johnson, B. T. (2018). The effect of South American biomass burning aerosol emissions on the regional climate. *Atmospheric Chemistry and Physics*, *18*(8), 5321-5342.

Tiwari S., Srivastava A., Singh A., and Singh S. (2015) "Identification of aerosol types over Indo-Gangetic Basin: implications to optical properties and associated radiative forcing", *Environmental Science and Pollution Research*, vol. **22**, pp. 12246–12260.

Trochkine, D., Iwasaka, Y., Matsuki, A., Yamada, M., Kim, Y. S., Nagatani, T., ... & Shen, Z. (2003). Mineral aerosol particles collected in Dunhuang, China, and their comparison with chemically modified particles collected over Japan. *Journal of Geophysical Research: Atmospheres*, *108*(D23)

Tsoar, H., & Pye, K. (1987). Dust transport and the question of desert loess formation. *Sedimentology*, *34*(1), 139-153.

Twomey, S. (1977). Atmospheric aerosols.

Twomey, S. J. A. E. (1974). Pollution and the planetary albedo. *Atmospheric Environment (1967)*, *8*(12), 1251-1256.

Tzanis, C., & Varotsos, C. A. (2008). Tropospheric aerosol forcing of climate: a case study for the greater area of Greece. *International Journal of Remote Sensing*, *29*(9), 2507-2517.

Wang, C. (2007). Variability of the Caribbean low-level jet and its relations to climate. *Climate dynamics*, *29*, 411-422

Wu, Z., Dijkstra, P., Koch, G. W., Peñuelas, J., & Hungate, B. A. (2011). Responses of terrestrial ecosystems to temperature and precipitation change: A meta-analysis of experimental manipulation. *Global change biology*, *17*(2), 927-942.

Yadav, A. N., Kumar, V., Dhaliwal, H. S., Prasad, R., & Saxena, A. K. (2018). Microbiome in crops: diversity, distribution, and potential role in crop improvement. In *Crop improvement through microbial biotechnology* (pp. 305-332). Elsevier.

Yu, H., Chin, M., Yuan, T., Bian, H., Remer, L. A., Prospero, J. M., ... & Zhao, C. (2015). The fertilizing role of African dust in the Amazon rainforest: A first multiyear assessment based on data from Cloud-Aerosol Lidar and Infrared Pathfinder Satellite Observations. *Geophysical Research Letters*, *42*(6), 1984-1991

Zhang, H., Wang, Y., Hu, J., Ying, Q., & Hu, X. M. (2015). Relationships between meteorological parameters and criteria air pollutants in three megacities in China. *Environmental research*, *140*, 242-254.

Zhang, J., Lindsay, R., Schweiger, A., & Steele, M. (2013). The impact of an intense summer cyclone on 2012 Arctic sea ice retreat. *Geophysical Research Letters*, *40*(4), 720-726.

Zhang, Q., Streets, D. G., Carmichael, G. R., He, K. B., Huo, H., Kannari, A., ... & Yao, Z. L. (2009). Asian emissions in 2006 for the NASA INTEX-B mission. *Atmospheric Chemistry and Physics*, *9*(14), 5131-5153.

Zhang, Y. H., Hu, M., Zhong, L. J., Wiedensohler, A., Liu, S. C., Andreae, M. O. & Fan, S. J. (2008). Regional integrated experiments on air quality over Pearl River Delta 2004 (PRIDE-PRD2004): overview. *Atmospheric Environment*, *42*(25), 6157-6173.